STUDIES OF NONLINEAR DYNAMICS IN REACTION-DIFFUSION-CONVECTION SYSTEMS

THESIS

SUBMITTED TO THE

UNIVERSITY OF PUNE

FOR THE DEGREE OF

DOCTOR OF PHILOSOPHY

IN PHYSICS

By

Anandamohan Ghosh

Chemical Engineering Division

National Chemical Laboratory

Pune 411008

India

November, 2002

CERTIFIED that the work incorporated in the thesis

Studies of nonlinear dynamics in reaction-diffusion-convection systems

submitted by Shri. Anandamohan Ghosh was carried out by the candidate under my guidance. Such material as has been obtained from other sources has been duly acknowledged in the thesis.

Bhaskar D Kulkarni
(Supervisor)

to dina

Acknowledgement

I would like to thank

my supervisor Dr. B. D. Kulkarni for his guidance, constant encouragement and giving me all the freedom to express myself.

Dr. V. Ravi Kumar for helping me in every possible way: letting me join the group...stimulating scientific discussions...completion of thesis.

Prof. A. D. Gangal for the excellent course on nonlinear dynamics.

Dr. M. V. Badiger for his help in organizing the rheological experiments.

Jainy for being a wonderful colleague and tolerating my programming techniques.

my early colleagues Manojit and Suhita and Somnath, Bhaskar, Joon, Arnab, Mohit(B), Gaurav, Swapnil, Sagar, Sachin, HemC and Sharada for being extremely helpful.

the "B-11 gang" of Ash, Shiva, Kishore, Priyal, Harish, Mahendra, Pratip, Meenal, Mohit, Collins and Navin for being great friends.

Ma, Baba, Dina and Mama and everyone in Kolkata for their loving support.

Department of Science and Technology, India for providing the financial assistance and Chemical Engineering Division, National Chemical Laboratory for providing the necessary facilities during the course of the work.

Contents

List of Tables

List of Figures

Abstract

Nonlinear mechanisms operating in interdisciplinary systems are generally responsible for the observed complex dynamical behavior as has been observed in many physical, chemical, biological, social and financial systems [Str95]. For example, in a physical system of a NH_3-FIR (far-infrared) single mode lasers chaotic pulsing has been observed and the underlying mechanism has been deduced and modeled by a set of nonlinear differential equations [Hub89]. Similarly in reacting systems, nonlinear rates typified by higher order or negative order reactions lead to non-stationary behavior including oscillations, chaos, pattern formation, etc [Sco91].

Systems can be made to operate under conditions far-from-equilibrium by allowing a continuous exchange of mass or energy with its surroundings. A simple chemical example of this situation is the continuous stirred tank reactor (CSTR) which is a well-mixed system operating under the above conditions. It can form a generic model for studying coupled systems by connecting similar such units in parallel or in series. Connecting well-mixed systems operating under far-from-equilibrium conditions form an excellent domain for studying behavior of complex systems taking place in spatial domains with diffusion mechanisms now simultaneously playing an important role. The analysis of reaction-diffusion systems is important due to the fact that many physical, chemical and biological systems are governed by their ubiquitous presence. The study of these systems has important implications in devising methods for control of pattern formation, extracting non-monitored variable information for mechanism interpretation and also in a basic understanding of what-would-happen-when experimental conditions are altered. Apart from diffusion, other transport mechanisms like convection can also occur by imposing external gradients. Reaction-diffusion-convection systems can show turbulence with complicated structures and it is only recently that significant advances in their understanding have been made by taking

into consideration the nonlinear nature of these interactions. The present thesis is devoted to bringing out new methodologies of analysis for reaction-diffusion-convection systems employing a systematic approach beginning from batch to well-mixed coupled stirred tank reactors to spatiotemporal systems involving diffusion and convection mechanisms. The advantages gained over conventional linear analysis is made apparent from a view point of understanding high-dimensional behavior including pattern formation, spatiotemporal chaos and turbulence by studying invariants characterization, inverse problems, formation of coherent structures and importance of noise reduction for feature extraction.

An introduction to these topics pertaining to the thesis along with the background literature is made in Chapter 1. The subsequent Chapters 2-5 present the devised methodologies and results of analysis in carrying out the studies. A summary of the individual Chapters is described below.

Chapter 2: Characterization of Chaotic Dynamics: Dynamical and Topological Invariants from Time Series Analysis

Studies in chaos theory have enhanced the scope of studying irregular time series data obtained from experiments [Aba93]. The studies provide deep connections between empirical observations and theory which has been hitherto lacking. Chapter 2 studies systems that give rise to irregular behavior in time series data for both model and experimental systems with the aim of further understanding this correspondence in terms of system invariants behavior. Experimental observations of stress measurements (using a stress controlled rheometer) as a function of time in a aqueous polymer solution (N-isopropyl acrylamide) and a biopolymer (Carrageenan) showed the presence of sustained dynamic features for identifiable steady shear regions. Liquid movement and transmission of stresses in solutions in which polymer molecules are dissolved are affected by the interaction and entanglement properties of long chain

molecules. The rotation and flexibility of carbon-carbon bonds is curtailed even in dilute solutions due to changes in effective viscosity. It is possible to drive the system to operate away from thermodynamic equilibrium conditions by applying a constant shear. Moreover, viscoelastic surfactant solutions exhibit interesting nonlinear flow properties especially at high shear rates. Chapter 2 discusses the results of studying data obtained by carrying out rheological experiments under non-equilibrium conditions with nonlinear flow properties. In fact, analysis of the obtained data using phase-space reconstruction techniques revealed the presence of low-dimensional chaotic dynamics by evaluating the metric and dynamical invariants, *viz*, correlation dimension, Lyapunov exponents and entropy. Topological analysis [Gil98] of the periodic orbits, extracted suitably from the rheological data, showed that global characterization and classification of dynamics is possible based on evaluation of linking numbers and relative rotation rates. The analysis of these invariants in turn yielded the template and the Markov transition matrix that contained in them valuable topological information about the system dynamics. The results obtained were compared with the topological invariants from a model endo-exothermic reaction in a CSTR. Interestingly, the results showed that both the rheological system and the model systems follow the Horseshoe mechanism in terms of stretching and folding mechanisms of the chaotic dynamics. These results point to the fact that many systems of interest in physical and chemical systems exhibiting chaotic dynamics may be classified and studied on common grounds. The beauty of this analysis is that it can also relate properties of systems even in interdisciplinary areas due to existence of universal properties. The importance of preprocessing the empirical data for noise reduction to make the above inferences has also been brought out in the above study. Traditionally, denoising a signal is done by suitable filtering techniques using moving averages, Kalman filtering, Fourier transforms, etc. Very recently it has been shown that wavelet transforms because of its superior space-time localization prop-

erties can efficiently denoise time series data obtained from nonlinear systems. The noise reduction has been carried out efficiently by differentiating the stress measurement data and subjecting the differentiated data to wavelet transform. This process of noise reduction shifts the power due to noise to the lower wavelet scales which could be identified from the power spectrum. Eliminating the wavelet coefficients in these lower wavelet scales before inverse wavelet transform and integration gave rise to noise free time series measurements which showed very clearly all the signatures of deterministic chaos *via* the invariants behavior.

Chapter 3: Inverse Problem of Parameter Estimation Using Multiple Shooting Boundary Value Approach

The invariant measures analyzed above depend upon the parameter values of the system. A knowledge of these parameter values is essential for studying the system properties. Thus it is important to estimate the unknown parameters of the system by tuning an appropriate nonlinear model to fit the observed chaotic data [Boc83]. The first step would be to consider a simpler situation of well-mixed systems whose dynamics can be described by ordinary differential equations. It may be noted that for chaotic dynamics estimating parameters and system states is not a trivial task even for simple model descriptions. The aim here is to simultaneously estimate the unknown parameters and non-monitored system states from available transient data. The results obtained focus on this practically important aspect of modeling and show the advantages gained by applying a boundary-value shooting approach to stringent nonlinear situations when the system exhibits low-dimensional chaotic dynamics. We exemplify the analysis by also adapting the method to tune empirical mathematical models in case phenomenological descriptions are not available and using scalar time series with noisy data. The results of analysis are presented for model system, namely, the endo-exothermic CSTR and hydroxylation of benzene to phenol, where, it is

shown that identification of all intrinsic kinetic constants and operation parameters is possible from even small data sets obtained. Ways to make the multiple shooting boundary value method robust have been devised *viz.* curtailing error propagation for chaotic dynamics, stopping at local minima during optimization, using, nonlinear quadrature minimization techniques, parallelization and convergence rates are also dealt in Chapter 3.

Chapter 4: Feature Extraction in Spatially Extended Reaction-Diffusion-Convective Systems

A widely studied class of complex systems are spatially extended systems describing the dynamics of reaction-diffusion-convection systems in one, two or three space dimensions. Unlike the above systems that could be modeled as ordinary differential equations (representing the dynamics at any one point in space), spatially extended systems are modeled using partial differential equations. Under suitable conditions the above system can show pattern forming features including highly sensitive spatiotemporally chaotic and turbulent dynamics [Cro93]. It would be desirable to formulate suitable strategies for parameter and state variable estimation for these situations when the dimensionality of the system is much higher due to the consideration of the spatial domain. It would be first necessary to devise appropriate strategies whereby the high dimensional dynamics can be studied in an optimal lower dimensional subspace by suitable projection [Hol96]. The advantages of employing Karhunen-Loève (KL) transformations for the above purpose for spatiotemporal data obtained from autocatalytic, activator-inhibitor systems, etc., have been studied and the results discussed in this Chapter. Importantly, we also consider situations when incomplete spatiotemporal information is only available, where, the aim is to reconstruct masked portions of the data while carrying out the projection. The method would find applications in a number of situations when experimental data is not re-

solved well due to effects such as noise or marring in snapshots and yield unbiased estimates using empirical eigenfunctions. The empirical eigenfunctions are related to the spatial properties of the system dynamics and can be further used to characterize the coherent structures present in the data. The formulations for projecting data on a lower-dimensional subspace and the results on characterization are presented in Chapter 4.

Chapter 5: Inverse Problem and Model Reduction for Reaction-Diffusion-Convective Systems

It would be desirable to appropriately design ways of using the low-dimensional analysis to arrive at mathematical models which are reduced descriptions of the original high-dimensional model. This can be achieved by projecting the governing equations onto relevant modes by KL decomposition alongwith Galerkin projection (KLG). The use of empirical eigenfunctions as spatial basis functions are advantageous because of their orthogonal properties which lead to considerable simplification of the original high-dimensional model. Chapter 5 discusses the ways for model reduction using the above approach. We also show a new use of this approach for parameter estimation employing reduced model descriptions of spatiotemporal systems and which advantageously uses subsystem data for the identification. Here we develop the Karhunen-Loève and Galerkin multiple shooting (KLGMS) approach and exemplify it for a discrete time continuous variable coupled map lattice (CML) systems representative of a reaction-diffusion-convective process exhibiting turbulent dynamics. Subsequently we apply the methodology to continuous time domain multi-variable systems such as the autocatalytic reaction-diffusion, exhibiting chaos. The resulting advantages in estimating parameters from small amounts of data from subsystems, availability of only scalar and noisy time series data, effects of space time parameter variations and in the presence of multiple time scales have been discussed. Apart

from empirical eigenfunctions, the use of wavelet basis functions have been studied because they are known to have superior space-time localization properties. The results of analysis show that wavelet basis functions can be used to further simplify the reduced model, whereby, the higher order derivatives can be estimated analytically using connection coefficients in conjunction with the wavelet transforms. The use of wavelet basis functions is also advantageous in terms of studying snapshots of system dynamics for long evolutions, synchronization properties of spatiotemporal dynamics, parameter estimation and multi-time scale features.

Chapter 6: Conclusion and Future Scope

In the concluding Chapter 6 a summary of the results is presented and future scope of work indicated.

Chapter 1

Introduction

Nonlinear dynamics, in the guise of planetary motions, has some claim to be the most ancient of scientific problems. Celestial motion, regarded as the mathematical realization of harmony in the universe, yields complex orbits whose behavior is impossible to predict when more than three celestial bodies are involved. In terms of antiquity, studies of celestial dynamics is closely followed by geometry. It therefore seems surprising that geometric methods in nonlinear dynamics were not earnestly pursued until the early 20^{th} century. The founder of geometric dynamics is universally acknowledged to be Henri Poincaré (1854-1912), who saw the usefulness of studying topological structure in the phase space of dynamical trajectories and was also the first person to glimpse the possibility of chaos, whereby a deterministic system exhibits aperiodic behavior that depends sensitively on initial conditions to an extent which renders long-term prediction impossible. The theoretical foundations laid by Poincaré were strengthened by G. D. Birkhoff (1884-1944), but, apart from a few instances such as the stability analysis of Lyapunov, Poincaré's ideas seemed to have little effect on dynamical problems in physics for almost half a century. The reasons may be that Poincaré and Birkhoff, motivated by problems in celestial mechanics, concentrated on energy conserving Hamiltonian systems for which Liouville's theorem holds. On the other hand, volume contraction in a dissipative system, in the

long term, has a strong tendency to simplify trajectories in phase space. This often mean that a complex dynamical system with even an infinite-dimensional phase space - governed for example by partial differential equations - can settle to final behavior in a subspace of only a few dimensions. Recent experimental observations of such low-dimensional behavior, for example in Couette flow [Dip81], chemical kinetics [Gra90], and solid-state plasma, suggest that a better understanding of *a priori* low-dimensional mathematical models of dynamics would be helpful guide to behavior in more complex dissipative systems.

To present the necessary background for topics studied in this thesis we shall broadly classify the subject area into two, namely, development of analysis with respect to *temporal dynamics* – the analysis of measurements at a point in space – and analysis with respect to *spatiotemporal dynamics* where the dimensionality of temporal system becomes high due to consideration of spatial domains. Within these two classes we introduce systematically the topics under consideration. The extensive studies in the subject area of nonlinear science has been well reviewed by a number of peers [Aba93, Arg94, Bal01, Cro93, Cru87, Dau92, Fie85, Gea71, Gen79, Gil98, Gra84, Guc83, Hol96, Kau93, Kan93, Kan97, Koc81, Kur84, Lum71, Ott93, Sco91, Str95, Ton90, Tuf92, Vos00, Wit98] and therefore the emphasis in the introduction is to reference the literature pertinent to the research topics handled (*viz.* dynamical invariants, topological invariants, signal separation, wavelet transform, parameter estimation, pattern formation, coherent structures, model reduction, etc.).

1.1 Temporal dynamics

The rise in the study of chaos itself was not realized until the 1960's when Edward Lorenz (1963) with the aid of newly invented high-speed computers experimented on nonlinear equations to discover chaotic motion on a strange attractor. Lorenz

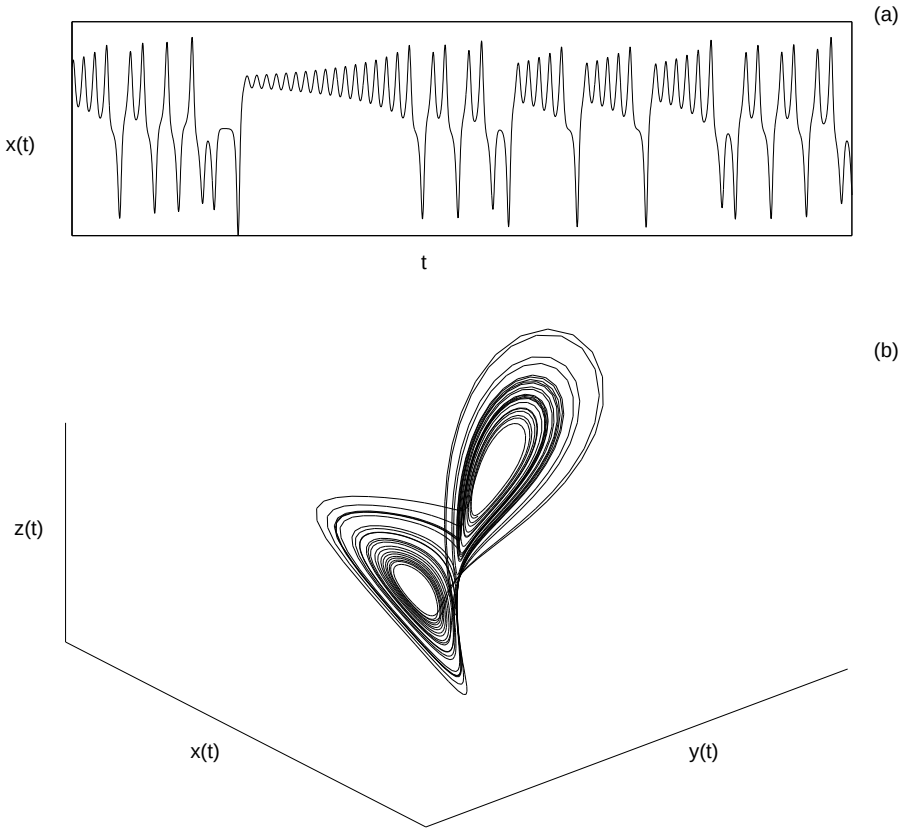

Figure 1.1: (a) Time series $x(t)$ obtained from Lorenz equations for $\sigma = 10$, $r = 30$ and $b = 8/3$. (b) The Lorenz attractor.

studied a simplified model of convection rolls in the atmosphere, to gain insight into the predictability of the weather, given by the set of equations:

$$\begin{aligned} \frac{dx}{dt} &= -\sigma x + \sigma y \\ \frac{dy}{dt} &= rx - y - xz \\ \frac{dz}{dt} &= -bz + xy \end{aligned} \tag{1.1}$$

Simulations show that the solution to these simple ordinary differential equations never settles to equilibrium and continues to oscillate in an aperiodic irregular fashion Fig. 1.1(a). Moreover, simulations started from two slightly different initial conditions resulted in completely different behavior implying that the system is inherently unpredictable and chaotic. However, the solution to the set of equations falls on a butterfly-shaped set of points, revealing an underlying structure in chaos Fig. 1.1(b).

At one point in time, as recently as late 80's, during the development of chaos theory, it was considered that chaotic dynamics is an extremely rare phenomenon but now a multitude of experiments revealing chaotic phenomenon have been reported in literature in the past two decades. Examples of nonlinear systems exhibiting complex chaotic dynamics is often encountered in physics, e.g., lasers [Wed84]; electric circuits [Boc84a]; a bouncing ball [Tuf92]; optics [Are91]. Periodically forced single degree of freedom oscillators had been originally proposed by van der Pol (1927) and Duffing (1918) as models in electric circuit theory and solid mechanics. These simple systems with nonlinear damping exhibit chaos and have been extensively studied but still open questions remain to be answered [Guc83, Kau93, Sma91]. Another such well studied physical system exhibiting periodic and chaotic self-pulsing is NH_3 FIR (far-infrared) single-mode lasers [Hub89]. The typical spiral type pulsing of the laser intensity varies irregularly in time as shown in Fig. 1.2. Chaotic pulsing corresponds to motion on a strange attractor and can be modeled by a set of simple differential equations, known as Lorenz-Haken model, and validates the existence of

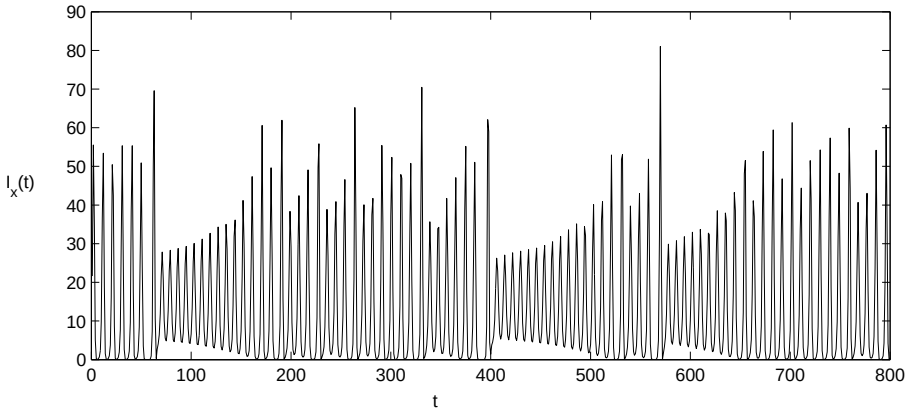

Figure 1.2: Spiral type pulsing of laser intensity.

low-dimensional chaos. It is now established that chaotic dynamics is an universal phenomenon and is ubiquitous. The observations and results of analysis have firmly established the notion that erratic time series may be explained by low-dimensional deterministic dynamics. Investigators have indeed concentrated on modeling physical systems by simple differential equations with the purpose of using chaotic dynamics profitably for improvements in forecasting, control and communication.

Nonlinearity is by no means unusual in chemical systems. In fact, it is the linear reactions, with strictly first-order kinetics, that are rare ones. Typically, the rate of an elementary reaction depends on concentration of more than two species and is naturally nonlinear and various 'empirical' rate laws can emerge with varying powers of concentration dependence. Aperiodic oscillatory behavior in chemical systems due to self-acceleration or self-inhibition can arise through, say, chain branching, auto-catalysis or self-heating and do not require very complex and unusual reaction mechanisms but only require nonlinearity with feedback mechanism [Kur84, Gra90, Sco91, Sli94, Kap95]. Analysis and simulation of the experimental observations have lead to direct understanding of the underlying reaction mechanisms in the past decade especially due to the direct observation of catalytic surfaces made

possible with the help of modern techniques in studying surface science [Chen93]. The very rich dynamic behavior observed in heterogeneous catalytic processes can be considered as a prototype chemical system exhibiting chaos. Numerous studies of CO oxidation over Pd zeolite catalysts have established that appearance of kinetic oscillations in this system occurs due to periodic oxidation and reduction of the Pd [Pes00, Sli01]. Simple mechanistic models based on Lamgmuir-Hinshelwood adsorption-reaction-desorption steps

$$\begin{aligned} CO + M &\Leftrightarrow MCO \\ O_2 + 2M &\Rightarrow 2MO \\ MCO + MO &\Rightarrow CO_2 + 2M \\ MO + M_v &\Rightarrow M_vO + M \\ M_vO + MCO &\Rightarrow CO_2 + M_v + M \end{aligned} \tag{1.2}$$

when mathematically modeled can describe the appearance of oscillations and complex dynamical behavior. Here M denotes vacant sites on the metal catalytic surface, MCO and MO absorbed CO and O atoms, respectively, M_v indicates free sites and M_vO sites occupied by O. The dynamic behavior of the observed species is shown in Fig. 1.3 for adsorbed species CO in (a) and O in (b).

Open non-equilibrium chemical systems with a continuous supply of reactants and removal of products are aplenty in nature and designed processes. Simple kinetics like autocatalator or endo-exothermic reaction carried out in coupled stirred tank reactor can exhibit oscillatory and chaotic behavior [Kah81]. Unlike equilibrium processes, the oscillatory behavior in these systems can be sustained depending on system mechanism and operating conditions. To study the basic features of systems operating under such conditions a number of theoretical and experimental studies on systems like the Belousov-Zhabotinskii reaction have been extensively undertaken [Bel58, Zha87, Kap95]. Apart from chaotic dynamics in reaction kinetics irregular

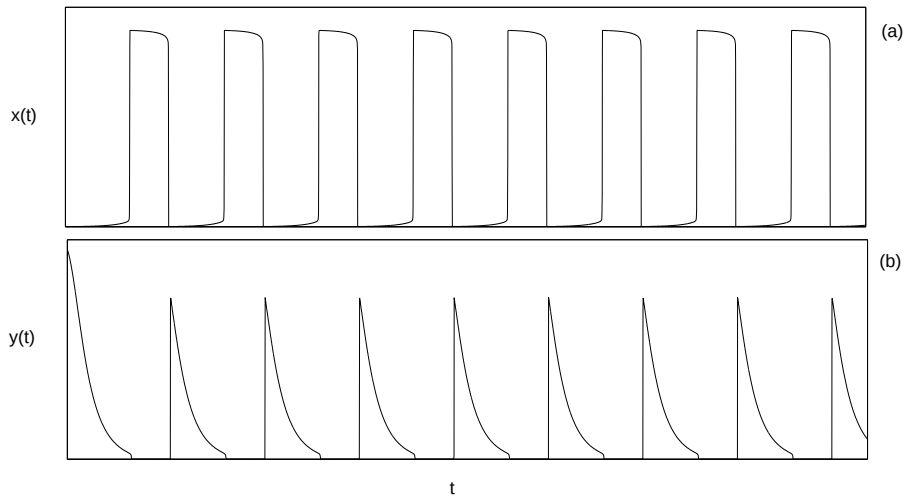

Figure 1.3: Oscillations in the adsorbed species (a) CO and (b) O, for CO oxidation over Pd zeolite.

flow pattern in macromolecular polymer systems have been intriguing physicists and chemists for the past few decades [Gen79]. Polymers are merely larger than usual molecules and are in the form of chains of small subunits which interact in a way unmatched in other forms of matter. The study of polymers over the last decades has forced us to broaden our notions of how it can organize itself in space, how it can flow and how it can transmit forces. These new behaviors arise from unique features of the polymer molecule's structure and the possibility of understanding these phenomenon have been aided with ability of synthetic chemists to control the molecular structure. The spatial distribution of atoms may be described by scaling properties and strong thermodynamic and hydrodynamic properties could be attributed to the same [Wit98]. Liquid movement and transmission of stresses in solutions in which polymer molecules are dissolved are affected by their interactions and entanglement properties and interesting dynamic behavior has been observed [Mun00, Bal01].

Actual observations of irregular evolution in the experimental systems are typically measurements of a single scalar observable at a fixed spatial location. This observation could be voltage or current in a nonlinear circuit, plasma dynamic exper-

iment, densities or velocities in fluid dynamics, or temperature variations at different locations in a chemical reactor, etc. The very first job in analyzing the data is identifying the signal of interest in the observation, that is probably contaminated by the environment, by perturbations on the source of the signal or by properties of the measuring device [Aba93]. The problem of isolating a signal in a linear process is much simpler in the sense that the source may be assumed to emit spectrally monochromatic signals contaminated by broadband interference. On the other hand, in the case of chaotic signals obtained from nonlinear processes both the signal of interest and the background are broadband as indicated by Fourier analysis. Therefore, in order to carry out an effective signal separation we must establish some difference between the information-bearing signal and the interference. The task of preprocessing the empirical data for noise reduction has been traditionally done by suitable filtering techniques using moving averages, Kalman filtering [Jaz70], Fourier transforms [Coh95] and of late using the recently developed wavelet transforms [Dau92, Hol95].

Wavelets are mathematical tools for analyzing time series and have introduced a new way of thinking in signal processing aided with elegant mathematics and efficient computational algorithms. Wavelet analysis is in some cases complementary to existing analysis techniques (e.g., correlation and spectral analysis) and in other cases capable of solving problems with their superior time-frequency localization properties [Per00]. Wavelet transform essentially correlates a signal with "dilated" versions of a wavelet function and yields a multiresolution representation of the signal which can be profitably used for the purpose of signal identification.

On finding the signal of interest we would like to establish the correct space to visualize the signal. In the case of nonlinear processes where the chaotic behavior is fundamentally multivariate, we can embed the scalar data in an optimum d-dimensional space using the geometrical and dynamical ideas based on an information-theoretic approach [Kan97]. With a clean signal and the proper phase-space one can there-

fore address the problem of classifying the underlying processes. Much of the work in nonlinear dynamics in the past has concentrated on learning how to classify the nonlinear systems by analyzing the output from known systems. These efforts have provided significant insights into behavior of nonlinear dynamical systems in terms of quantities termed as invariant measures. The set of chaotic orbits is not simply characterized by geometric objects such as points, lines or planes. As in the case of Lorenz attractor, orbits are observed to exist on a transcendental structure consisting of an uncountably infinite number of finite two-dimensional domains. The orbits have infinitely recurring self-similar structure in the direction in which phase volume decreases. Thus the geometric nature of chaos is not characterized by integers but rather by self-similarity. Mathematically, this characterization is measured by the Hausdroff dimension, practically calculated as nonintegral correlation or fractal dimension [Gra83a, Gra83b]. The degree with which two infinitesimally separated orbits move away or approach each other is measured by the Lyapunov exponents, and is calculated by taking long-time evolution averages of the logarithm of the amplification/reduction rate of the differences arising between the two orbits [Kan97]. Topological methods have recently been developed for the analysis of dissipative dynamical systems that operate in chaotic regime [Gil98, Tuf92]. Topological analysis procedures depend on identifying the unstable periodic orbits in the attractor and represent the stretching and folding mechanisms by a characteristic caricature (a branched manifold), which becomes a template, a two-dimensional representation of the dynamical system in the limit of infinite dissipation. The topological structure is identified by a set of integer invariants and can be extracted from the chaotic time series [Min90].

When experimental measurements are available one would naturally like to address the problem of building models of the physical processes. One approach is to make empirical models using the observed variables and its derived quantities but

invariably the description of the system turns out to be different from the original differential equations, one would have written down from first principles based on Newton's laws or from arguments about the physics of the experiment. An alternative approach would be to consider the usual variables of the process and attempt to develop phenomenological models of the system. In cases when information on the model structure is available, usually from conservation equations and transport phenomena principles, what is then required is accurate estimation of the parameters in the model such that the model outputs can be matched as closely as possible to the experimental data [Boc83]. The job of the physicist would be to explore the robustness of these models for various invariant measures under the dynamics for validation. Because of the intrinsic instability, an experimental orbit and a computed orbit will be uncorrelated, but, what defines their commonality is the statistical properties. Topological invariants are particularly useful in determining the underlying dynamics of the system as they do not involve any distance or metric computation of the points on an orbit and are robust even in the presence of noise and reasonable changes in system parameters.

1.2 Spatiotemporal dynamics

A widely studied class of complex systems are spatially extended systems describing the dynamics of reaction-diffusion-convection system or turbulent hydrodynamics of a flow. Unlike the low-dimensional systems that could be modeled as ordinary differential equations (representing the dynamics at any one point in space), spatially extended systems are modeled using partial differential equations. Under suitable conditions the spatiotemporal systems can show pattern forming features including high-dimensional chaotic and turbulent dynamics [Cro93]. The study of pattern formation in fluids has greatly benefited from recent careful and controlled experiments

as well as the development in the mathematical study of dynamical systems in one hand [Dip81] and progress in statistical mechanics of condensed matter on the other. Systems under non-equilibrium external conditions exhibit macroscopic spatial structures even under stationary states, a phenomenon that goes under the name of dissipative structures, synergetics and self-organization [Kri84]. The general connection between spatiotemporal patterns and linear instabilities was first emphasized by Turing (1952). The mechanism of pattern formation can be attributed to existence of constraints and conservation laws as in Rayleigh-Benard convection of a fluid placed between horizontal plates, where the buoyancy force attempts to lift the whole mass of the fluid and the top plate provides the constraint against motion. Another mechanism for instabilities is provided by the competing interaction between elementary units as seen in magnetic materials leading to antiferromagnetism [Cha95] and is also ubiquitous in chemical and biological systems [Kau93]. From a theoretical point of view, since we are far from equilibrium there is no *a priori* reason to assume that minima in the free energy functional gives rise to patterns. We must therefore discuss the system in terms of larger sets of "microscopic" equations. For fluid systems these are generally the Navier-Stokes equation and for chemical systems they are the reaction laws. In order to explain the irregular behavior often observed in these deterministic equations the above sets of equations have to be appropriately formulated. By spatiotemporal chaos one means a finite correlation in both space and time domain while turbulence is used in the context of fluid dynamics to signify disordered flow involving generation and transport of vorticity. The chaos that occurs in models such as Ginzburg-Landau or Kuramoto-Shivashinsky equations are termed "weak" turbulence [Kur84] while "strong" turbulence is associated with real flows [Shr92].

In perturbative analyses of the microscopic equations for various systems one encounters complex partial differential equations which go under the name of "amplitude equations" and are popularly known as Ginzburg-Landau equations [Saa92]. A basic

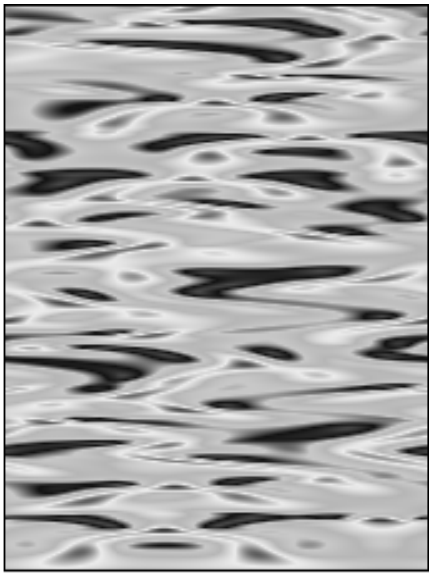

Figure 1.4: Evolution of the amplitude field for the CGL equation for $D = 0.0035$, $c_1 = -2$ and $c_2 = 2$.

source of chaos in the complex Ginzburg-Landau (CGL) equation is the instability arising due to interplay between spatial and temporal dispersion properties. Many properties of non-equilibrium systems are encountered in these equations and many difficult problems such as existence and interaction of defects and coherent structures and chaos may be profitably addressed within a simple framework [Cro93]. The ordinary diffusively (*i.e.* locally) coupled complex Ginzburg-Landau equation [Kur84] is given by

$$\frac{dW(x,t)}{dt} = W - (1 + ic_2)|W|^2 W + D(1 + ic_1)\delta^2 W \tag{1.3}$$

which can be derived, for example, from equations of oscillatory media in the vicinity of their Hopf bifurcation points by the center-manifold reduction technique, where, W is the complex amplitude of an oscillator at a given time t and location x. The spatially uniform solution is unstable and the system exhibits spatiotemporal chaos

for appropriate parameter values as shown in Fig. 1.4 [1]. A two-dimensional Ginzburg-Landau model of plasma turbulence, which has added forcing and dissipation acting at different scales, has been studied with primary focus on the role of coherent structures in turbulent transport and dissipation [New88].

Nonlinear reaction-diffusion systems are also capable of spontaneously forming a wealth of spatiotemporal patterns ranging from Turing patterns, spiral waves and "chemical turbulence". In the case of heterogeneous catalytic reaction discussed earlier carried out on polycrystalline Pt and on Pt(110) single crystals under ultra-high vacuum conditions revealed a surprisingly large variety of structures like spirals, standing waves and chemical turbulence Fig. 1.5. In order to describe the formation and properties of spatiotemporal patterns, the model of the reaction kinetics Eq. (1.3) have been extended to partial differential equations by incorporating the surface diffusion of the adsorbed CO [Bar94]. The model equations for the CO coverage and the degree of (1×1), reconstruction denoted by u and v, respectively, are

$$\begin{aligned} \frac{\partial u}{\partial t} &= -\frac{1}{\epsilon}u(u-1)(u-\frac{b+v}{a}) + D \bigtriangledown^2 u \\ \frac{\partial v}{\partial t} &= h(u) - v \\ h(u) &= \begin{cases} 0, & 0 \leq u < 1/3 \\ 1 - 6.75u(u-1)^2, & 1/3 \leq u \leq 1 \\ 1, & 1 < u. \end{cases} \end{aligned} \tag{1.4}$$

The physical parameters, *viz.*, temperature T, partial pressures p_{CO}, p_{O_2} are present in the model parameters a, b and ϵ.

Any partial differential equation can be discretized into a system of coupled maps where the system is already chaotic even in the absence of coupling. The ensuing spatiotemporal dynamics of the coupled map lattices display enormous variety,

[1] Black in the gray scale image indicates lowest concentration while white corresponds to highest concentration and this is being consistently used in all the spatiotemporal images presented in the thesis.

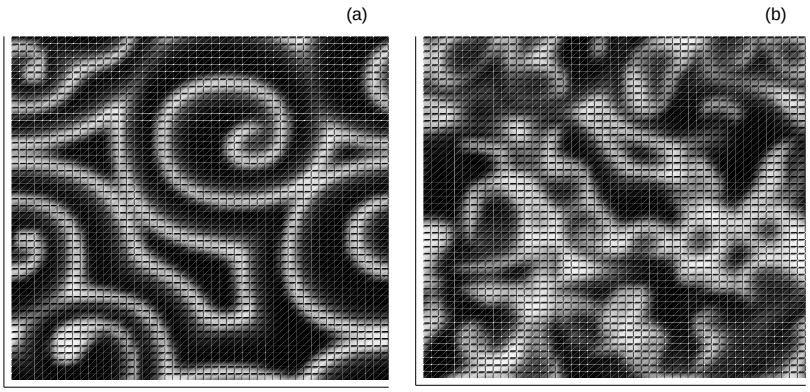

Figure 1.5: Snapshots showing CO-coverage for CO oxidation on Pt(110) for $a = 0.84$ and $b = 0.07$ (a) stable spirals ($\epsilon = 0.07$) (b) turbulent state ($\epsilon = 0.1$)

and these models have been widely studied due to relative ease of generating large amounts of data and studying complex phenomenon for unraveling their properties. The coupled logistic maps have been particularly popular since the chaotic behavior of the individual elements has been well understood. Kaneko [Cru87, Kan89, Kan93] has identified different phases in these systems ranging from ordered patterns, to disordered frozen ones and what he calls "fully turbulent" phases. Interesting spatiotemporal behavior can emerge from these simplistic models by various choice of local dynamics and strength of coupling and many notions in pattern formation in spatially extended systems are better understood. Models consisting of coupled oscillators have attracted growing attention due to their relevance to chemical and biological phenomenon [Kur84a, Str88, Som91].

For turbulent flows the mathematical model exist in the form of incompressible Navier-Stokes equations but since these "microscopic" equations are nonlinear partial differential equations and are mathematically so complex that only limited information can be extracted from them. It would be desirable to appropriately design ways of using low-dimensional analysis to arrive at mathematical models which are reduced descriptions of the original high-dimensional model. Traditionally physicists

in all disciplines tend to study complex natural phenomenon by reducing to several simple processes and comprehending the whole on superposition. This strategy is often referred as "Ockham's razor" and favors a minimum number of assumptions and descriptors. A typical way for implementation of reductionism is by decomposition into several modes and subsequent superposition as is done by the method of Fourier transformation. This reductionism approach based on the principle of superposition holds true only for linear systems but fails in nonlinear systems exhibiting chaos. However, recent developments have lead to a revolution in the concept of reductionism in turbulent systems [Hol96]. The discovery of coherent structures have played an important role in the research of turbulence. In many visualizations of turbulence one can see coherent structures to develop, move or merge. We define a coherent structure by the proper orthogonal decomposition involving Karhunen-Loéve expansion schemes [Kar46, Loe55, Lum71]. Karhunen-Loéve decomposition provides a basis for the modal decomposition of an ensemble of functions. The most striking property of this is the optimality as it captures most effectively the dominant components of an infinite-dimensional process with only a finite number of "modes". Indeed, the relevant set of basis functions provides a low-dimensional sub-space on which the reduced models can be formulated. This can be achieved by projecting the governing equations onto relevant modes by KL decomposition along with Galerkin projection (KLG). The use of empirical eigenfunctions as spatial basis functions are advantageous because of their orthogonal properties that lead to considerable simplification of the original high-dimensional model.

Recently there has been a great deal of interest in forecasting spatiotemporal time series and model identification using polynomial and mixed functions [Bar99, Par00, Vos98]. Short-term prediction of spatiotemporal dynamics by reconstruction of local states [Par00], and KL decomposition using empirical basis functions by training amplitude coefficients using genetic algorithms for optimization [Lop00] have been

studied and assessed. Rather than phase space reconstruction models, identification using some knowledge of the system structure, along with nonlinear parametric regression [Vos98, Vos00], has also been used for modeling spatially extended systems.

1.3 Outline

As seen from the discussion in Section 1.2, reaction-diffusion-convection mechanisms cover a broad class of natural as well as designed systems. Further, the examples bring out the fact that a variety of complex behavior and patterns can be observed even when mathematical model are high-dimensional due to consideration of the spatial domains but are not exceedingly complex. It would then be desirable to develop ways of studying the high-dimensional system behavior in quantitative terms so that a deeper understanding of the factors responsible for the patterns and dynamics observed can be elucidated. The Introduction has also brought out the fact that low-dimensional systems (with no spatial considerations) can also exhibit complex dynamical behavior. The factors responsible for their observance in low-dimensional systems have also been much better understood. Under these circumstances, it would be worthwhile to see the connections that are possible between the behavior of high-dimensional and low-dimensional systems and use the valuable experience that has been gained while studying the latter class. The general aim of the studies presented in this thesis is to realize this difficult aim [Aba93] to a reasonable extent by developing suitable methodologies. The advantages gained is made apparent from a point of understanding spatial pattern formation, analyzing for coherent structures, spatiotemporal chaos and turbulence by studying system invariants and their scaling relationships, inverse problems of parameter estimation, importance of noise reduction for feature extraction, etc.

The focus of the studies presented in Chapter 2 is to first bring out the under-

standing of complex behavior in low-dimensional systems and show its applications to systems of practical interest. By presenting new results the interdisciplinary nature of the approach and its utility will also be validated. For purposes of exemplifying behavior of low-dimensional systems, we choose to study an excellent paradigm exhibiting the varied dynamics of nonlinear systems without any spatial effects, namely, that of a continuous stirred tank reactor (CSTR). The CSTR with its finite volume but well-mixed assumption with nonlinear kinetics provides the necessary phenomenology for complex behavior to be observed. As stated above, it would be interesting to show the generality and usefulness of the methodologies to practical systems. For this purpose we shall apply the analysis to rheological data of polymer solutions which interestingly showed complex dynamics when carrying out experiments. By simultaneously analyzing both model and experimental data (using phase-space reconstruction; metric and dynamical invariants, *i.e.*, correlation dimension, Lyapunov exponents, entropy; topological invariants, *i.e.*, linking numbers and relative rotation rates) a better understanding of the distinct and general characteristics is likely to be revealed. Experimental data however is likely to be contaminated with noise and it would be necessary to ascertain its effects on the analysis. As discussed in Section 1.1, wavelet transforms provide a powerful tool to develop filtering aids that extract out the true complex dynamical signal. It was therefore thought necessary to apply a suitably developed wavelet transform based noise reduction methodology to bring out true system features if noise was present in the data. The results did validate the above conjecture and the discussion highlights this feature.

Apart from quantitatively characterizing the complex dynamics, it is also desirable that mathematical models involving system parameters be evaluated accurately from the data collected from experiments. This would make it possible to use the mathematical model for predicting system behavior. It may also be possible to gain valuable information about unmonitored system variables and their state values. In

Chapter 3 we show a robust method of parameter estimation which possesses many significant advantages when applied to low-dimensional systems exhibiting complex dynamics including chaos. This way of parameter estimation employs a multiple shooting boundary value approach that curtails error propagation for chaotic dynamics, stops at local minima during nonlinear optimization, employs quadrature minimization techniques, parallelization, etc. The usefulness of the multiple shooting approach is seen on analyzing model CSTR data exhibiting chaotic dynamics and also in model development.

The analysis in Chapters 2 and 3 provide the necessary background for characterizing and modeling the dynamics of spatiotemporal systems. Thus ways to reformulate the methodologies for low-dimensional systems presented in Chapters 2 and 3 have been developed for high-dimensional systems by suitable reformulation. For this purpose, we first employ the Karhunen-Loève (KL) decomposition to spatiotemporal data as it provides a convenient way for obtaining optimal reduction in the dimensionality of the system. In this way considerable model reduction of the spatiotemporal system under study is likely to be possible. The effectiveness of this approach for coupled map lattices and reaction dynamics is studied in Chapter 4. The results can also be assessed for developing the method further for application to continuous time systems described by partial differential equations in an easier fashion. It would also be interesting to use these reduced models to retrieve information about partially hidden (missing) data which may arise either in spatial or temporal domain. Once again it is likely that the data collected is noisy. It would then be useful to retrieve noise free information from the spatial snapshots and the results obtained analyzed. All the above issues are addressed in Chapter 4 sequentially.

The difficult but commonly encountered situation of recovering all intrinsic and operating parameters of spatiotemporal dynamics and recovering unmonitored system information in terms of variable behavior is attempted in Chapter 5 using the

formalisms developed in Chapters 3 and 4. More specifically, we show the results of developing the Karhunen-Loève Galerkin Multiple Shooting (KLGMS) and the Wavelet Galerkin Multiple Shooting (WGMS) approaches for realizing the above aims for CML and continuous time domain models. The advantages of these methods are studied in terms of parameter and state variable estimation from few / extended snapshots in one, two or three spatial dimensions, synchronization properties of spatiotemporal dynamics, multi-time scale features, missing and noisy data, data availability from local regions, etc.

In the conclusion, Chapter 6 summarizes the results obtained and discuss the future scope of work.

Chapter 2

Characterization of Chaotic Dynamics: Dynamical and Topological Invariants from Time Series Analysis

Nonlinear mechanisms in low dimensional systems often result in complex dynamical behavior. Irregular behavior in many such physical, chemical and biological systems can be attributed to deterministic chaos. Studies in deterministic chaos have enhanced the scope of exploring irregular time series and its analysis provide a connection between empirical observations and chaos theory. Non-periodic signals have usually been modeled as arising from a linear stochastic process, but, it has been established that dynamical systems without random inputs can also lead to irregularity in dynamical properties. However, data procured in most experimental systems is generally contaminated with noise and as a prerequisite to time series analysis denoising is of primary importance. Traditionally denoising a signal is done by suitable filtering techniques using Fourier transform [Coh95], etc. Wavelet transform [Dau92] provides superior space-time localization properties and efficient denoising algorithms have been proposed using wavelet transform based techniques [Roy99]. Experimental data, when suitably denoised, can be further subjected to characterization for signatures of its stationary/dynamical behavior. Time series data can be characterized

through computation of metric and dynamical invariants [Aba93]. Metric invariants involve statistical characterization of distribution of points in phase space while dynamical invariants like the Lyapunov exponents are based on evolution properties of the trajectories. However, the determination of both types of invariants has limitations in the sense that they provide little information on the mechanism governing the nonlinear system. On the other hand, topological invariants are based on the stretching and folding mechanisms present in the dynamics and has many advantages to offer besides complementing that gained by dynamical invariant analysis [Gil98].

Robustness of the metric, dynamical and topological invariant analysis have been studied and shown here for a model endo-exothermic reacting system and subsequently applied to time series data of shear measurements in aqueous polymer solution. Liquid movement and transmission of stresses in solutions in which polymer molecules are dissolved are affected by the interaction and entanglement properties of long chain molecules. The rotation and flexibility of carbon-carbon bonds is curtailed even in dilute solutions with changes in effective viscosity. It is possible to drive the system to operate away from thermodynamic equilibrium conditions by applying a constant shear. Moreover viscoelastic surfactant solutions exhibit interesting nonlinear flow properties especially at high shear rates. Rheological studies were carried out with aqueous polymer solutions subject to shear, which after denoising showed the presence of interesting dynamical features including oscillations and chaotic dynamics with features of a strange attractor. The results of analysis with respect to behavior of system invariants showed meaningful inferences can be drawn. In fact, it is shown that topological analysis provides a global characterization in the form of template and that an interesting correspondence between a model low-dimensional chaotic system and experimental system may be made.

The organization of the chapter is as follows: In Section 2.1 we discuss the background studies of aqueous polymer systems and our experimental setup to obtain the

rheology data. In Section 2.2 we introduce wavelet transform and show its application to the experimental rheology data. In Section 2.3 we characterize the dynamics of the model endo-exothermic CSTR and experimental rheology data in terms of the dynamical invariants (Section 2.3.1) and the topological invariants (Section 2.3.2). We conclude the chapter by discussions in Section 2.4.

2.1 Aqueous Polymer Systems

2.1.1 Background

Viscoelastic surfactant solutions exhibit interesting nonlinear flow properties especially at high shear rates. For example, shear thickening at high shear rates forming gel like structures with a large increase in birefringence and first normal stress difference properties have been seen. The mechanism for these effects are attributed to the shear induced structure (SIS) formation and breaking in solution. Flow induced phase transition in surfactant solutions [Reh88], causing periodic oscillations in the birefringence has also been reported. Studies of instabilities in viscoelastic fluids [Lar92] have also shown that for critical stress, large fluctuations in the shear rates could occur.

Rheological studies carried out by us with aqueous polymer solutions subject to shear do seem to further validate the above observations and we have in the course of experiments seen the presence of interesting dynamical features including oscillations and chaotic dynamics with features of a strange attractor. Here our aim is to bring out the methodology to extract these nonlinear features from the complex data and study its dynamical characterization by extracting invariant measures such as the entropy and Lyapunov dimensions. Here we report the results of study with two types of polymer solutions whose properties are interesting and show application potential. The first type of aqueous polymer solution studied is thermosensitive and shows

thermodynamic *lower critical solution temperature* (LCST) behavior. These polymer solutions can undergo reversible phase separation [Eli62] and the cross-linked gels exhibit volume transition effects [Hof95]. In these polymers, at higher temperatures, the entropy associated with mixing increases over the enthalpy of hydrogen bonding between the polymer molecules and water. This makes the polymer to phase separate at higher temperatures – contrary to what is normally observed in normal solutions. Thermosensitive polymers are therefore, attracting considerable attention in various fields such as biotechnology [Gal95], flocculation [Sno94], enhanced oil recovery [Sno95], water treatment [Sno93] etc., as smart materials. Their properties show extreme sensitivity and in view of their potential practical applications, understanding their rheological behavior is necessary. For our studies the choice of the thermosensitive polymer is poly *N*-isopropyl acrylamide (PNIPAm) which shows remarkable LCST and phase separation properties. In the recent past rheological studies on PNIPAm based on intrinsic viscosity measurements have been carried out by Fujishige [Fuj87] and Eliassaf [Eli78]. The latter has reported a four-fold increase in the intrinsic viscosity of PNIPAm solution in the presence of 1% surfactant, sodium dodecyl sulfate. Tam et al.[Tam92] have reported the effects of polymer concentration, temperature and surfactant on the rheological properties of PNIPAm. Recently, Zeng et al.[Zen98] have reported on the network formation in PNIPAm-water system studied by dynamic viscoelastic measurements. For deforming solutions it has been suggested that the stored elastic energy of the flowing polymer solution brings about an increase in free energy and this leads to altering the phase equilibrium from that of a stagnant solution [Naf84]. Experiments and theories have also shown that the critical properties of a binary mixture can be changed when exposed to shear [Cha90].

The second aqueous polymer solution is carrageenan, a plant biopolymer obtained from sea weeds [Whi73]. Plant biopolymers, known as hydrocolloids, usually comprise complex mixtures of long chains of sugar molecules, together with minor amounts of

protein. Biopolymers display a vast range of functional properties and depending on their chemical composition alter liquid properties. They do this by thickening or gelling the liquid, or by emulsifying components which would not normally disperse in liquid. The rheological behavior of this solution is important to study because the above properties find applications in food, cosmetics and pharmaceutical industries [Chr64].

2.1.2 Experimental Setup

The *N*-isopropyl acrylamide (NIPAm) monomer was obtained from Polyscience, USA, and was recrystallized from a benzene/hexane mixture prior to use. The polymerization was carried out in benzene (analytical grade) at 60^0C for 24 hours (under nitrogen atmosphere) with a monomer concentration of 1.104 mol l^{-1} and 0.289 mol% azo-bis (isobutyronitrile) as initiator. After polymerization, benzene was decanted and the polymer was dissolved in acetone and precipitated in hexane twice and finally vacuum dried in oven at 40^0C. The ^{1}H NMR spectrum was obtained in D_2O using Bruker spectrometer operating at a proton frequency of 200 MHz. The proton signal assignments were made as follows, δ : 1.126 ppm ($C\underline{H})_3$, 3.88 ppm $(CH_3)_2 - C\underline{H}$, 1.573 ppm ($C\underline{H}_2$) and 1.99 ppm ($C\underline{H}$). No vinyl protons were detected which indicates the sample to be pure. The molecular weight of the polymer was determined by intrinsic viscosity and found to be 1.2×10^6 gm/mole. All the solutions were prepared by dissolving a known amount of the polymer (3.0 wt %) in water (filtered by means of millipore filters) with a gentle stirring. The samples were kept for homogenization in the refrigerator for two weeks before taking them for the experiments.

Experiments with aqueous solutions were similarly carried out using carrageenan (HiMedia Laboratories Pvt. Ltd., Mumbai) (2.0 wt %) in the presence of potassium sorbate (K-sorbate) (0.2 wt%) and potassium chloride (KCl) (1.0 wt %). The presence of these salts are known to influence the solubility characteristics of carrageenan.

The solutions were prepared using double distilled water and allowed to equilibrate for at least 10 days before the experiments.

All the rheological experiments were carried out on a stress controlled rheometer (BOHLIN CVO-50 of Bohlin Instruments, UK) with a double gap geometry fixture with inner and outer cylinder diameters measuring 40 mm and 50 mm, respectively. The measuring unit was connected to a Julabo (KTB-30) thermostat bath, interfaced with a computer controlled temperature program that maintained accuracy within $\pm 0.1^0$C. A solvent evaporation jacket prevented any loss of solvent from the sample. Steady shear experiments were carried out as a function of time in the ranges of shear rates ($\dot{\gamma} = 5$ to 50 s^{-1}) and temperatures 25^0 to 45^0C (Table 2.1). These ranges correspond to the conditions when the dynamics showed fluctuating and oscillating behavior in shear stress. In order to eliminate sample time history effects, each experiment used a fresh sample. The stress measurements obtained from the rheometer was collected after the initial transient phase was over. Normally data was collected for 5000 s and corresponds to 2024 data points.

2.2 Wavelet Transform and Denoising

The wavelet transform is the mathematical tool to resolve a given signal into different frequency components locally in time [Dau92, Hol95]. The standard Fourier transform $(\mathcal{F}f)(\omega)$ of any function $f(x)$ given by

$$(\mathcal{F}f)(\omega) = \frac{1}{\sqrt{2\pi}} \int f(x) e^{-i\omega x} dx \tag{2.1}$$

gives a representation of the frequency content (ω) but information concerning time-localization is lost. In a sense time localization may be achieved by first windowing the signal $f(x)$ and then taking its Fourier transform

$$(\mathcal{F}^{win}f)(\omega, x) = \int f(y) g(y - x) e^{-i\omega y} dy \tag{2.2}$$

where g is the window function well concentrated in both time and frequency.

The wavelet transform $(\mathcal{W}f)(a,b)$

$$(\mathcal{W}f)(a,b) = \frac{1}{|a|}\int f(x)\Phi\left(\frac{x-b}{a}\right)dx. \tag{2.3}$$

provides a similar time-frequency description where by restricting a, b to take only discrete values: $a = a_0^j$, $b = kb_0a_0^j$ with $j,k \in \mathbb{Z}$, denoting the scale and translation indices respectively, and $a_0 > 1$, $b_0 > 0$ it can be more suitably written as

$$(\mathcal{W}f)(j,k) = \frac{1}{a_0^{-m/2}}\int f(x)\Phi(a_0^{-m}x - nb_0)dx. \tag{2.4}$$

The construction of $\Phi(x)$ the orthonormal wavelet basis function satisfies some conditions [Dau92] and is conveniently chosen from a set of dyadically rescaled and translated functions

$$\{\Phi_{jk}(x)\} = \{2^{j/2}\Phi(2^jx - k)\}. \tag{2.5}$$

$\{\Phi_{jk}(x)\}$ forming an orthonormal basis in $L^2(\mathbb{R})$ with, $j,k \in \mathbb{Z}$ the scale and the translation indices respectively. In particular, we require the wavelet basis functions to satisfy

$$\int_{-\infty}^{\infty}\Phi(x)dx = 0, \quad \int_{-\infty}^{\infty}\Phi^2(x)dx = 1, \quad \int_{-\infty}^{\infty}\Phi(x)\Phi(x+n)dx = \delta_{n,0}$$

where $\delta_{n,0}$ is the Kronecker delta. The family of basis functions $\{\Phi_{jk}(x)\}$ can be used to construct a family $\Psi_{jk}(x)$ of zero mean, 1-periodic functions on a domain of length one as

$$\Psi_{jk}(x) = 2^{j/2}\sum_n \Phi(2^j(x+n) - k), \quad x \in [0,1]. \tag{2.6}$$

Associated with the wavelet functions $\Phi(x)$ and 1-periodic functions $\Psi(x)$ we can define a family of scaling functions as $\phi(x)$ and $\psi(x)$ respectively. The family of wavelets thus defined is better understood in the context of a multiresolution analysis

of $L^2(\mathbb{T})$, where $\mathbb{T} = \mathbb{R}/\mathbb{Z}$ is the unit circle. The multiresolution analysis consists of a sequence of nested subspaces $\{V_j\}_{j\geq 0}$, permitting increasingly close approximation of any given function and including increasingly fine detail and fluctuations. The spaces V_j satisfy

- $V_0 \subset V_1 \subset V_2 \subset \cdots \subset V_j \subset \cdots \subset L^2(\mathbb{T})$
- $\overline{\cup_{j\geq 0} V_j} = L^2(\mathbb{T})$
- V_0 consists of constant functions

  $f(x) \in V_j \Rightarrow f(2x) \in V_{j+1}$

  $f(x) \in V_{j+1} \Rightarrow f(\frac{x}{2}) + f(\frac{x}{2} + \frac{1}{2}) \in V_j$
- dim $V_j = 2^j$

If we denote by W_j the orthogonal complement of V_j in V_{j+1},

$$V_{j+1} = V_j \oplus W_j, \qquad (L^2(\mathbb{T}) = V_0 \oplus W_0 \oplus W_1 \oplus W_2 \cdots \oplus W_j \oplus \cdots) \tag{2.7}$$

then dim $W_j = 2^j$ and the functions $\Psi_{jk}(x)$ form an orthonormal basis for W_j. When we impose the condition of zero mean the space of constant functions becomes $V_0 = \{0\}$ and we need only the wavelet $\Psi_{jk}(x)$ as our basis. It follows from the above definitions that varying j, which implies compression or dilation, allows one to zoom in or out, while changes in k correspond to horizontal translations. For notational simplicity it may be noted that wavelet basis functions $\Psi_{j,k}$ can be alternatively represented ψ_α. The index α represent the multi-index (j, k) and the equivalence in the notation can be given by $\alpha = 2^j + k$. The wavelet basis functions for Daubechies-4 are shown in Figure 2.1.

Filtering of data employing a noise reduction algorithm using wavelet transform is known to possess distinct advantages in treating signals with a high degree of non-linearity such as chaotic dynamics which has a broad range of frequencies with a only

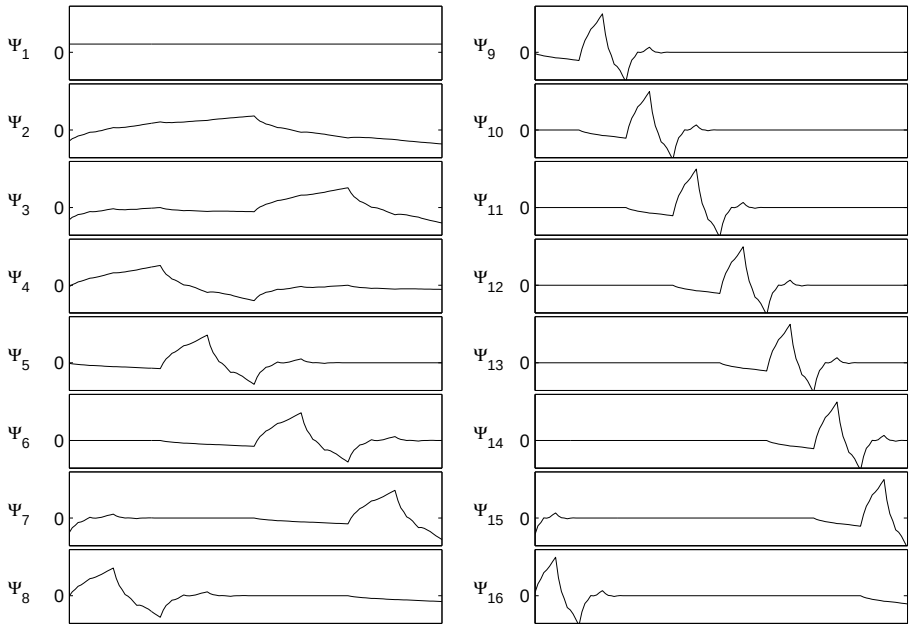

Figure 2.1: The Daubechies-4 wavelet basis functions.

short-time correlations. Wavelet transform methods study properties of the data at varying scales and has superior time localization features when compared to Fourier transform techniques. The noise reduction algorithm we use [Roy99] is advantageous, because, the degree to which noise is present in the data can be inferred and filtered even for signals exhibiting chaotic dynamics and non-stationary behavior in an efficient manner without taking into consideration the statistical properties of the signal for thresholding the wavelet coefficients. The algorithm consists of the following steps and is briefly summarized below. The noisy data $y(t)$ is numerically differentiated to obtain $y_d(t)$, using central finite differences with fourth order correction [Con87]. We then take the WT of the differentiated time series $y_d(t)$ and obtain wavelet coefficients $\mathcal{W}_d(j,k)$ at dyadic scales j and $k,\ k = 1, 2, \cdots, N$ displacements for the N data points. A dyadic scale is the scale whose numerical magnitude is equal to 2 (two) raised to an integer exponent, and is labeled by the exponent. Thus, the dyadic scale j refers to a scale of magnitude 2^j. In other words, it indicates studying the data with

using a resolution of 2^j. A lower value of j implies analyzing data at a finer resolution when compared to a coarser resolution for a higher j value. For the WT, we use the discrete analog of continuous WT [Hol95] with the popular Daubechies compactly supported orthogonal function having four filter coefficients [Dau92, Pre92] as the wavelet basis function. We may estimate the power P_j contained in different dyadic scales j, *via*,

$$P_j \quad = \quad \sum_{k=1}^{2^{(p-j)}} |\mathcal{W}_d(j,k)|^2 \qquad (j = 0, 1, 2, \cdots, p) \tag{2.8}$$

where $p = \log N / \log 2$ is the total number of analyzable wavelet scales for the N data points.

The basis on which the noise reduction algorithm functions is that the power due to noise shifts to the finer scales on WT of the differentiated data $y_d(t)$. Using fluctuating data (generated synthetically by model studies as well as experimental data monitored by instruments) studies show that a clean separation in the scales covered by the differentiated signals and white noise (if present) is possible.

The fluctuations in the stress data seen here Figure 2.2 therefore suggests that it would be worthwhile to test for the presence of noise in the data and if present filter it.

Figure 2.3 shows the calculated values of P_j with j, for a typical experimental condition and it is possible to identify in an automated fashion the scale j_m upto which power due to noise resides in the differentiated data. Therefore by resetting all wavelet coefficients $\mathcal{W}_d(j,k)$ up to scale j_m to zero, *i.e.*, $\mathcal{W}_d(j,k) = 0$, for $j = 1, 2, \cdots, j_m$ and taking an inverse WT (using the modified $\mathcal{W}_d(j,k)$) we obtain differentiated data $y'_d(t)$ with noise effects minimized. This differentiated data $y'_d(t)$ when integrated back yields the denoised signal $y'(t)$ which captures the true system dynamics in its dominant scales with its local features in time truly enhanced (Figure 2.4a) as compared to the noisy data $y(t)$ in Figure 2.2.

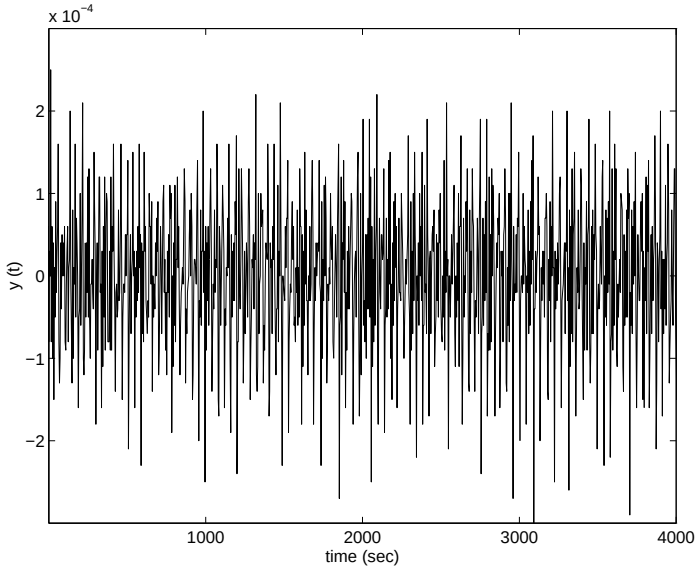

Figure 2.2: Fluctuations in the standardized data for shear stress in PNIPAm solution at $T = 25^0C$, $\dot{\gamma} = 5\ s^{-1}$.

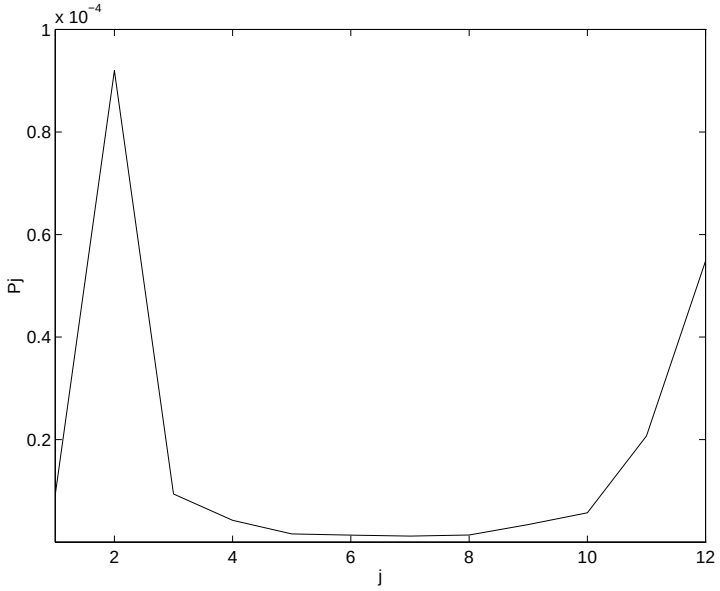

Figure 2.3: Estimated power P_j in dyadic wavelet scales j for shear stress data for PNIPAm solution at $T = 25^0C$, $\dot{\gamma} = 5\ s^{-1}$.

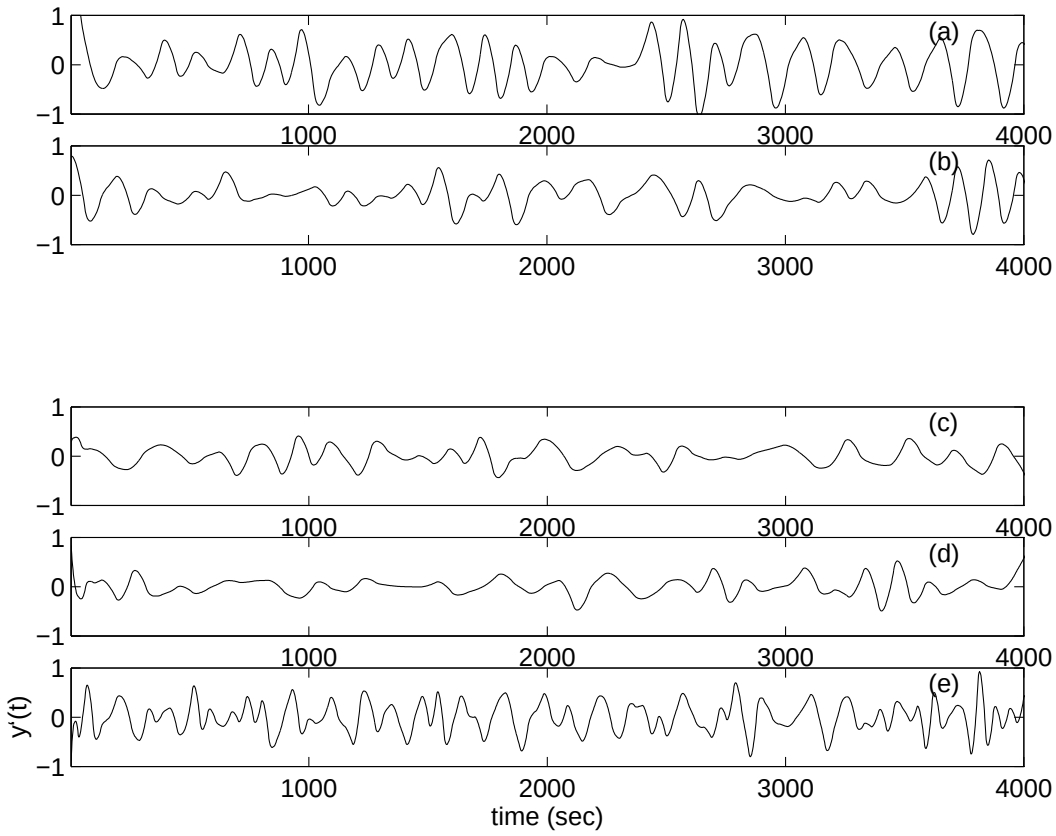

Figure 2.4: The denoised and standardized time series for shear stress. For PNIPAm solutions (a) $T = 25^0C$, $\dot{\gamma} = 5\ s^{-1}$ (b) $T = 30^0C$, $\dot{\gamma} = 10\ s^{-1}$; and for Carrageenan solutions (c) $T = 25^0C$, $\dot{\gamma} = 20\ s^{-1}$ (d) $T = 45^0C$, $\dot{\gamma} = 20\ s^{-1}$ (e) $T = 45^0C$, $\dot{\gamma} = 50\ s^{-1}$.

2.3 Characterization of complex dynamics

Chaotic dynamical systems have been the concern of numerous studies and the effort has proved significant insight into the unpredictable but still deterministic behavior of these systems. It is interesting to study whether any observed fluctuations arise from a deterministic process and if so assessing its complexity. Here we study various facets of time series analysis based on data obtained by numerically integrating a model endo-exothermic reaction. The model assumes that the process considered is a jacketed CSTR where an irreversible, first order, endo-exothermic and consecutive reaction $A \rightarrow B \rightarrow C$ takes place. The dimensionless equations describing this system consist of mass and energy balances and may be written as,

$$\frac{dx}{dt} = 1 - x - D_a\ x\ \exp\left[\frac{z}{1+\epsilon z}\right] \tag{2.9}$$

$$\frac{dy}{dt} = -y + D_a\ x\ \exp\left[\frac{z}{1+\epsilon z}\right] - D_a\ S\ y\ \exp\left[\frac{\kappa z}{1+\epsilon z}\right] \tag{2.10}$$

$$\frac{dz}{dt} = -z + D_a\ B\ x\ \exp\left[\frac{z}{1+\epsilon z}\right] - D_a\ B\ \alpha\ y\ \exp\left[\frac{\kappa z}{1+\epsilon z}\right] - \beta z \tag{2.11}$$

where x and y represent dimensionless concentrations of species A and B, while z denotes the dimensionless temperature. The other dimensionless groupings are listed below and defined elsewhere [Ban93]; B, adiabatic temperature rise; D_a, Damkohler number; S, ratio for rate constants for series reaction; κ, ratio of activation energies for series reaction; α, ratio of heat effects for series reaction; β, heat transfer coefficient. Extensive studies [Kah81] reveal that there exists a strongly contracting flow and there is a sequence of period doubling bifurcations to chaos for realistic ranges of parameter values, i.e., $D_a = 0.26$, $S = 0.5$, $B = 57.77$, $\kappa = 1.0$, $\beta = 8.0$ and $\alpha = 0.426$.

The presence of the nonlinear exponential terms renders these model equations highly stiff and have been integrated using an adaptive step-size method [Gea71] with sampling time $\Delta t = 0.001$. The attractor generated for above mentioned parameter values is shown in Figure 2.5 as a phase plane plot.

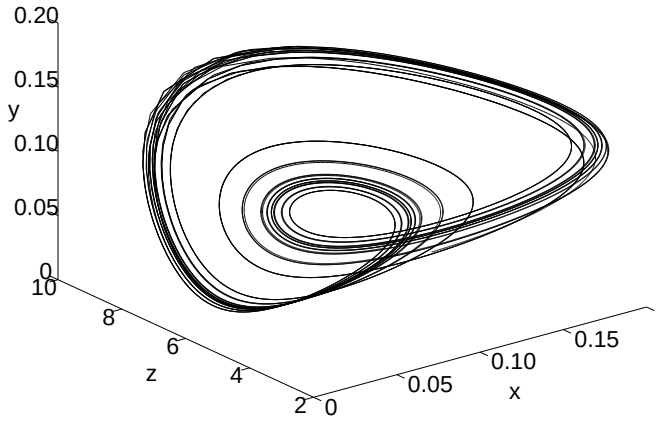

Figure 2.5: Three dimensional attractor for endo-exothermic CSTR.

2.3.1 Characterization by Dynamical Invariants

If we consider a completely deterministic system, knowledge of the present state in entirety means all future states are determined as well. Thus establishing a vector space or phase space for the system and hence specifying a point in this space specifies the state of the system. Thus dynamics of the system can be studied by studying the dynamics of the phase space points.

Mutual Information and Choice of Delay Time

What we observe typically in an experiment is not the phase space points but time series points. Thus it is important to reconstruct the state vector from the observed time series. Let x_n be the observed time series sampled at time-steps of Δt and by delay reconstruction in m dimensions using the embedding theorem of Takens [Tak81] the vector $\mathbf{x}(n)$ is formed as

$$\mathbf{x}(n) = (x_{n-(m-1)\nu}, x_{n-(m-2)\nu}, \cdots, x_n). \tag{2.12}$$

The delay vectors differ by $\tau = \nu\Delta t$ in time known as the lag or delay time where μ is the integer index corresponding to time.

The delay time τ is obtained from the mutual information method developed by Fraser and Swinney [Fra86]. Let A be the ensemble of values $x(n)$ and B be the ensemble of values $x(n+\tau)$ and let $P_A(a)$ and $P_B(b)$ be the probability of choosing a and b when making a selection from the set A and B, respectively. Let Y be a vector chosen from the set of time delayed evolution vectors $y(n)$ and the joint probability $P_{A,B}(a,b)$ is the probability of getting a as the first component and b as the second component of Y. The method estimates the average mutual information, $I_{AB}(\tau)$ between the measurements of elements of the ensemble A and B as a function of the lag τ. The mutual information is defined by

$$I_{AB}(\tau) = \sum_{a\in A, b\in B} P_{A,B}(a,b)\log_2\left[\frac{P_{A,B}(a,b)}{P_A(a)P_B(b)}\right]. \tag{2.13}$$

$I(\tau)$ is a measure of how much one knows about the numerical value of the second component of the evolution vector y, when one knows the numerical value of the first component. $I(\tau)$ vanishes or is minimum when the ensembles A and B are independent. The first minima of the plot of $I(\tau)$ vs. τ gives the delay time required to embed the scalar data Figure 2.6.

Correlation Dimension

There are several ways to quantify the self-similarity of a geometrical object by a dimension. The definition coincides with the usual notion of dimension associated with non fractal objects and is called correlation dimension [Gra83a, Far83].

Let us first define the correlation sum of a collection of points $\mathbf{x}(n)$ in Eq. (2.12) in the reconstructed vector space to be the fraction of all possible pairs of points closer

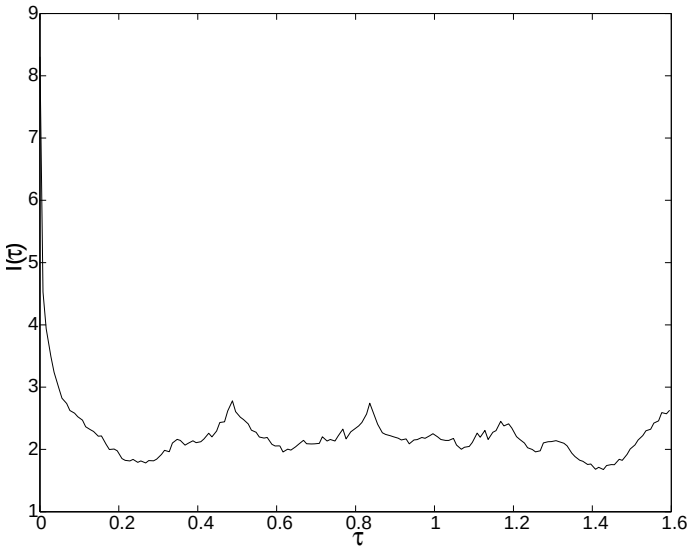

Figure 2.6: The average mutual information for endo-exothermic CSTR.

than a distance ϵ as

$$C(\epsilon, N) = \frac{2}{(N - n_{min})(N - n_{min} - 1)} \sum_{i=1}^{N} \sum_{j=i+n_{min}}^{N} \Theta(\epsilon - ||\mathbf{x}(i) - \mathbf{x}(j)||). \quad (2.14)$$

Here, Θ is the Heaviside step function; $\Theta(x) = 0$ if $x \leq 0$ and $\Theta(x) = 1$ if $x > 0$. The sum counts the pair of points $(\mathbf{x}(i), \mathbf{x}(j))$ whose distance is smaller than ϵ. The above formula takes care of spurious correlation sums due to temporal coherence by considering the second summation after a correlation time $t_{min} = n_{min}\Delta t$ [The86]. In the limit of the number of data points $N \to \infty$ and small ϵ, the correlation sum scales as power law, $C(\epsilon) \propto \epsilon^D$. Thus correlation dimension D is defined by

$$D = \lim_{\epsilon \to 0} \lim_{N \to \infty} \frac{\partial \ln C(\epsilon, N)}{\partial \ln \epsilon}. \quad (2.15)$$

The typical plot of correlation sum for varying embedding dimension m is shown in Figure 2.7. The correlation dimension D evaluated using Eq.(2.15)is seen to converge for higher embedding dimension Figure 2.8.

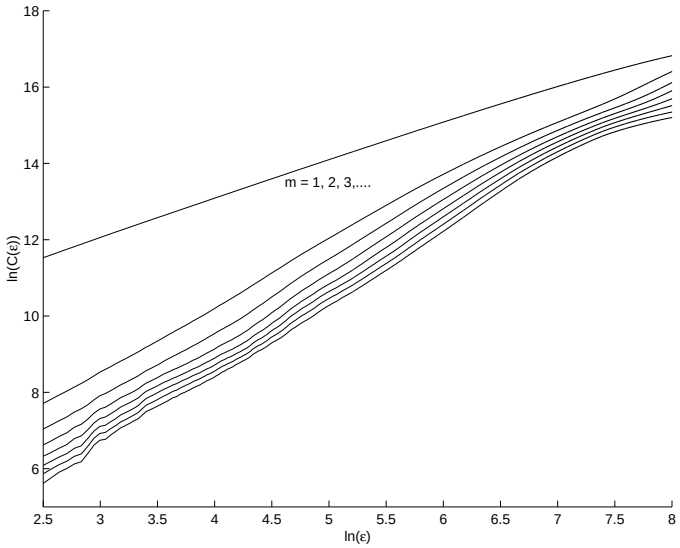

Figure 2.7: The correlation sum for endo-exothermic CSTR.

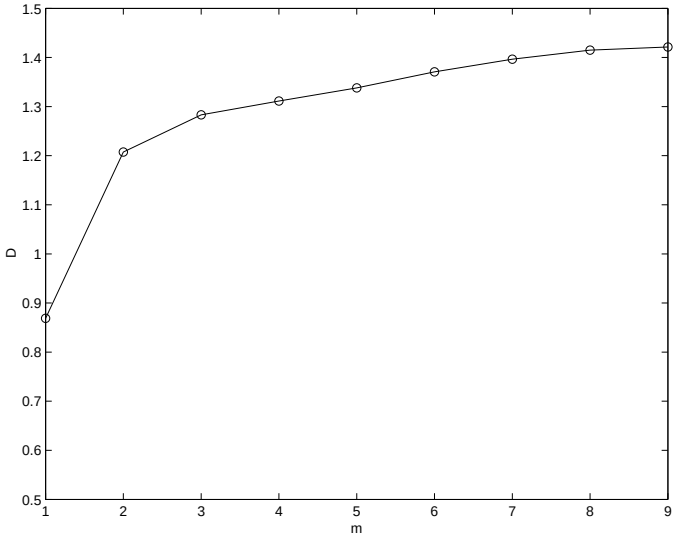

Figure 2.8: The correlation dimension for endo-exothermic CSTR.

Lyapunov exponent

The stability behavior of a reference trajectory subjected to small perturbations in the initial conditions can be quantified in terms of Lyapunov exponents [Arg94]. Let $\mathbf{x}_r(t)$ be the reference trajectory satisfying $\dot{\mathbf{x}}_r = \mathbf{F}(\mathbf{x}_r)$ and we observe a neighboring trajectory subject to an initial perturbation $\tilde{\mathbf{x}}(t_0)$. Expanding $\mathbf{F}(\mathbf{x})$ into a Taylor series in the neighborhood of $\mathbf{x}_r(t)$ and neglecting higher order terms we get

$$\dot{\tilde{\mathbf{x}}}(t) = \frac{\partial \mathbf{F}}{\partial \mathbf{x}} \mid_{\mathbf{x}_r(t)} \tilde{\mathbf{x}}(t) \tag{2.16}$$

The solution of the above equation can be represented in terms of the fundamental matrix $\phi(t, t_0)$ as

$$\begin{aligned} \tilde{\mathbf{x}}(t) &= \phi(t, t_0)\tilde{\mathbf{x}}(t_0) \\ \tilde{\mathbf{x}}(t) &\approx \mathrm{e}^{t\lambda}\tilde{\mathbf{x}}(t_0) \end{aligned} \tag{2.17}$$

which can be considered as mapping taking tangent vector $\tilde{\mathbf{x}}(t_0)$ of the flow at point $\tilde{\mathbf{x}}_r(t_0)$ onto the image vector $\tilde{\mathbf{x}}(t)$ associated with the tangent space at $\tilde{\mathbf{x}}_r(t)$. The Lyapunov exponents are given by

$$\lambda_{\mathbf{x}_r}(\tilde{\mathbf{x}}) = \lim_{t\to\infty} \sup \frac{1}{t} \log \frac{|\tilde{\mathbf{x}}(t)|}{|\tilde{\mathbf{x}}(t_0)|}. \tag{2.18}$$

The convergence of Lyapunov exponents with time t for the endo-exothermic CSTR is shown in Figure 2.9 indicating that $\lambda_1 > 0$, $\lambda_2 \simeq 0$ and $\lambda_3 < 0$.

Another important invariant measure is the Kolmogorov-Sinai (KS) entropy which measures the information production per unit time for a series of consecutive measurements [Far82, Sha81]. For n-dimensional dynamical systems it is seen that a relation exists between the KS entropy (h) and the positive Lyapunov exponents as

$$h = \sum_{i}^{+} \lambda_i. \tag{2.19}$$

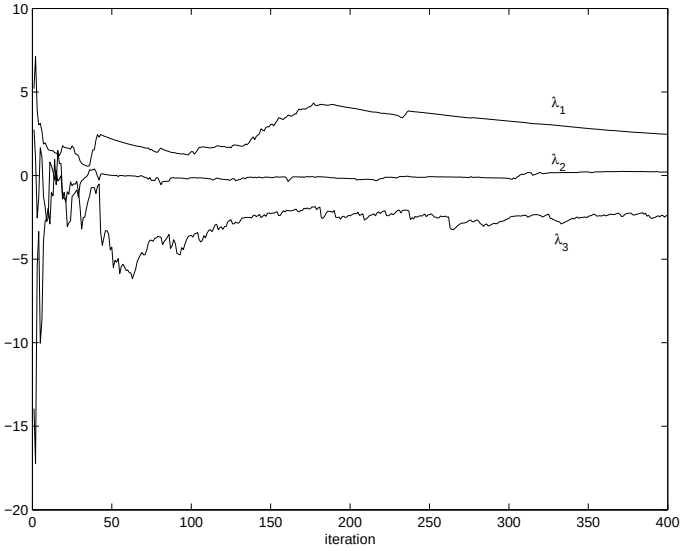

Figure 2.9: The Lyapunov exponents for endo-exothermic CSTR.

Strange attractors are characterized by a positive finite value of the KS entropy, *viz.*, $h > 0$. The entropy calculated from the Lyapunov exponents, estimated earlier, is 2.3484.

Kaplan and Yorke [Kap79] have conjectured that there exists a link between the values of the Lyapunov exponents and dimensionality of the attractor as

$$d_L = K + \frac{\sum_{i=1}^{K} \lambda_i}{|\lambda_{K+1}|}, \tag{2.20}$$

where, K is the number of positive Lyapunov exponents λ_i. Estimating the Lyapunov dimension d_L is consequently useful from the point of view of estimating the reduced dimensionality of the system after it has stabilized on the attractor manifold [Gra84, Tem88]. The Lyapunov dimension estimated for the endo-exothermic system is 2.9051.

The dynamical invariants discussed so far have been estimated for experimental shear measurements in aqueous polymer solutions. The analysis of the post-transient time-series data, reveals the presence of low-dimensional chaotic dynamics. Interestingly, the results obtained from different types of polymer solutions, *viz.*, thermosensi-

Table 2.1: Dynamical invariants of the sheared polymer solutions for different experimental conditions.

System	$T(^0C)$	$\dot{\gamma}(s^{-1})$	D	λ_1	h	d_L
PNIPAm	25	5	4.9 ± 0.01	0.13 ± 0.001	0.142	2.62
	30	10	5.2 ± 0.04	0.18 ± 0.006	0.200	2.33
Carrageenan	25	20	4.3 ± 0.03	0.12 ± 0.001	0.125	2.32
	45	20	5.8 ± 0.04	0.18 ± 0.005	0.210	2.44
	45	50	7.4 ± 0.02	0.24 ± 0.006	0.276	2.90

tive polymers poly n-isopropyl acrylamide (PNIPAm) and biopolymers Carrageenan, show similar complex dynamical features and suggest that mechanism responsible are common. The experimental data, obtained for different temperature (T^0C) and shear rates $\dot{\gamma}(s^{-1})$, have been analyzed with a view to characterize the strange attractor in terms of invariant measures such as the correlation, embedding, Lyapunov dimensions and entropy and are listed in Table 2.1.

2.3.2 Characterization by Topological Invariants

Topological invariants are based on 'stretching' and 'folding' mechanisms present in the dynamics and has many advantages to offer besides complementing that gained by metric and dynamical invariants analysis [Bou97, Gil98]. Topological invariants being stable under parametric variations allow system features to be verified independently. Indeed, a global characterization of system dynamics may be obtained in the form of templates that allow different systems to be proven equivalent or otherwise. Also, bifurcation selection rules, for creation and annihilation of unstable periodic orbits [Lat89], in chaotic dynamics can be studied. Topological analysis can also be used to validate models created by parameter estimation from chaotic time series data [Let98]. However, absence of topological invariants in dimensions greater than three limits the application of this procedure to low dimensional chaotic systems. A sufficient condition for the template identification by topological analysis is then $d_L < 3$

suggesting the presence of a strongly contracting flow [Gil98]. Topological invariants have been used for analysis of physical systems showing chaotic dynamics and have been well studied over the years.

As complex as it may appear, a strange attractor is a highly organized geometrical object. In particular, it contains an infinite number of unstable periodic orbits, densely embedded in it. Unstable periodic orbits have been recognized as a major tool to analyze chaotic systems as they provide a hierarchical approximation of a strange attractor. In three dimensional phase space periodic orbits are closed curves and can be characterized by computing topological invariants using the mathematical framework of knot theory [Kau91]. The main feature of topological analysis is that any set of periodic orbits embedded in an attractor has one-to-one correspondence with set of orbits, having same topological invariants, on a two dimensional manifold called template or knot-holder [Bir83]. Thus the template completely describes the global organization of the flow.

Here we exemplify the methodology of topological analysis on the observed dynamics for the model endo-exothermic system as well as the experimental shear data collected by rheology measurements discussed earlier.

Detection of unstable periodic orbits

The extraction of periodic orbits can be done from the three dimensional attractor, constructed from x, y, z data or constructed with any one variable by suitable embedding, in the following way: A Poincaré section, the plane $z = 0.6$, was constructed on the attractor shown in Figure 2.5 and x_n and y_n can be considered as iterates of the Poincaré map.

The plot of first return maps *i.e.* x_{n+1} vs. x_n and y_{n+1} vs. y_n (shown in Figure 2.10 for y) are unimodal in nature having a single critical point. This suggests that two symbols are sufficient to uniquely label the periodic orbits and that the template

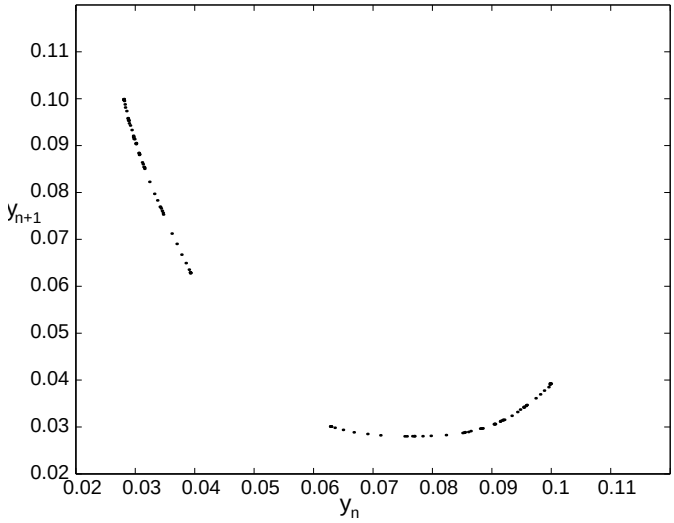

Figure 2.10: The first return map for the variable y in endo-exothermic CSTR.

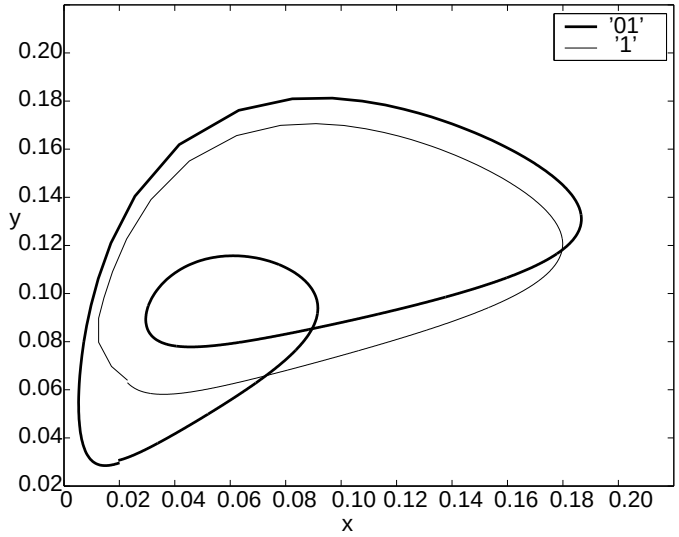

Figure 2.11: The periodic orbits '1' and '01' extracted for endo-exothermic CSTR.

has two branches one orientation preserving (0) and the other orientation reversing (1) [Gil98]. All values of i for which $((x_{i+p} - x_i)^2 + (y_{i+p} - y_i)^2)^{1/2} < \varepsilon$ are initial conditions for a period-p orbit. Depending on which side of the critical point of the first return map, with sides labeled '0' and '1', a period-p orbit visits it and crosses the Poincaré section determines the symbolic representation of the orbit.

Thus a period 5 orbit symbolically represented by '00111' means '0' branch is visited twice and '1' branch is visited thrice. In Figure 2.11 the period one orbit '1' and the period two orbit '01' extracted from the endo-exothermic CSTR attractor is shown. Once the periodic orbits are extracted and their symbolic representation determined, their topological invariants can be computed.

Computation of topological invariants

Topological invariants, namely, relative rotation rates and linking numbers, were proposed to understand the organization of periodic orbits [Sol88]. Let, A and B be two periodic orbits in three dimensional space with periods p_A and p_B. For any pair of initial conditions (i, j) on the Poincaré section, the relative rotation rate $R_{ij}(A, B)$ is given by,

$$R_{ij}(A, B) = \frac{1}{2\pi p_A p_B} \oint \frac{\mathbf{n} \cdot (\triangle \mathbf{r} \times \mathbf{d}(\triangle \mathbf{r}))}{\triangle \mathbf{r} \cdot \triangle \mathbf{r}} \tag{2.21}$$

The integral spreads over $p_A \cdot p_B$ periods, and $\mathbf{n}$ is the unit vector orthogonal to the plane spanned by vectors $\triangle \mathbf{r}$ and $\mathbf{d}(\triangle \mathbf{r})$. It is to be noted that relative rotation rates are symmetric $R_{ij}(A, B) = R_{ji}(B, A)$ and that the self rotation rate is well defined subjected to the convention $R_{ii}(A, A) = 0$. The linking number $L(A, B)$ can be computed from the relative rotation rates $R_{ij}(A, B)$ as

$$L(A, B) = \sum_{i,j} R_{ij}(A, B) \tag{2.22}$$

Table 2.2: Relative rotation rates for endo-exothermic CSTR.

	0	1	01	011	001	0111	0011	0001
0	0							
1	0	0						
01	0	0	$0,\frac{1}{2}$					
011	0	0	$\frac{1}{6}$	$0,(\frac{1}{3})^2$				
001	$\frac{1}{3}$	0	0	$0,\frac{1}{3}$	0			
0111	0	0	0	$\frac{1}{6}$	$\frac{1}{12}$	$0,(\frac{1}{4})^3$		
0011	$\frac{1}{4}$	0	0	$\frac{1}{12}$	$\frac{1}{12}$	$0,(\frac{1}{4})^2$	$0,\frac{1}{4}$	
0011	$\frac{1}{4}$	0	$(\frac{1}{2})^2$	$\frac{1}{12}$	$\frac{1}{6}$	$0,\frac{1}{4}$	$0,(\frac{1}{4})^2$	$0,\frac{1}{4}$

Table 2.3: Linking numbers for endo-exothermic CSTR.

	0	1	01	011	001	0111	0011	0001
0	0							
1	0	0						
01	0	0	1					
011	0	0	1	2				
001	1	0	0	1	0			
0111	0	0	0	2	1	3		
0011	1	0	0	1	1	2	1	
0011	1	0	2	1	2	1	2	1

and the self linking numbers of orbit A is given by $SL(A)$. The relative rotation rates computed are tabulated in Table 2.2 and the linking numbers are evaluated as

$$L(0111, 011) = 4 \times 3 \times \frac{1}{6} = 2 \tag{2.23}$$

$$L(0111, 0111) = 4 \times 3 \times \frac{1}{4} = 3 \tag{2.24}$$

are given in Table 2.3 for the extracted periodic orbits.

Determination of the template

To gain insight into the global structure of the flow the organization of periodic orbits is modeled by the branched two dimensional manifold, the template. The relation of above mentioned topological invariants with the template can be achieved by defining

two matrices, the $n \times n$ template matrix $\mathcal{T}$ and $1 \times n$ insertion matrix $\mathcal{I}$, where n is the number of branches in the template [Min90].

In the present analysis as suggested from the unimodal map we need a two symbol representation so $n = 2$ and the template matrix is written as

$$\mathcal{T} = \begin{pmatrix} t_0 & 2L \\ 2L & t_1 \end{pmatrix} \tag{2.25}$$

where t_0 and t_1 is the local torsion of '0' and '1' orbit and $L = L(0,1)$ is the linking number of orbit '0' and '1'. The insertion matrix is

$$\mathcal{I} = \begin{pmatrix} 0 & m \end{pmatrix} \tag{2.26}$$

where $m = 1$ if the '1' branch is above '0' branch or $m = -1$ if the '1' branch is below '0'. Determination of the template structure from the topological invariants amounts to solving the following equations for the unknowns t_0, t_1, L and m [Bou97]:

$$\begin{aligned} SL(01) &= 2L + m = 1 && (2.27)\\ L(1,01) &= L + \frac{1}{2}[t_1 + o(t_1)m] = 0 && (2.28)\\ L(1,011) &= L + t_1 = 0 && (2.29)\\ L(1,0111) &= L + \frac{1}{2}[3t_1 + o(t_1)m] = 0 && (2.30)\\ L(01,001) &= 3L + m + t_0 + \frac{1}{2}[t_1 + o(t_1)m] = 0 && (2.31) \end{aligned}$$

Where $o(t)$ indicates parity of t: $o(t) = 1$ if t is odd and $o(t) = 0$ if t is even. Solving the above equations the template and insertion matrix may be obtained as

$$\begin{aligned} \mathcal{T} &= \begin{pmatrix} -1 & 0 \\ 0 & 0 \end{pmatrix} && (2.32)\\ \mathcal{I} &= \begin{pmatrix} 0 & 1 \end{pmatrix} && (2.33) \end{aligned}$$

For the purpose of template determination a few of the topological invariants that had been computed is used, remaining ones thus can be used to validate the template

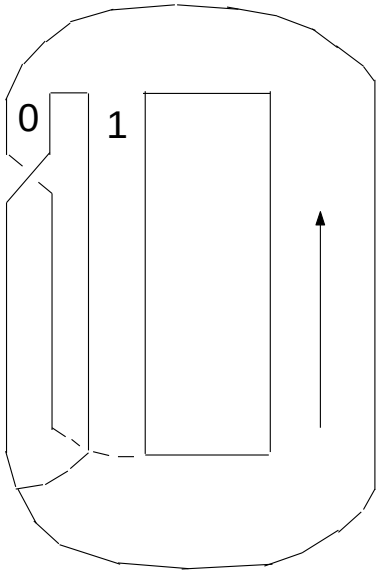

Figure 2.12: Endo-exothermic CSTR template.

[Tuf92] by verifying that they are correctly predicted as reported in Table 2.2 and 2.3.

The template matrix depicting the dynamics of the flow can be geometrically represented as shown in Figure 2.12. The two dimensional caricature of the three dimensional attractor has two branches '0' and '1', with branch '0' having a twist.

Entropy estimation

A careful examination of the points on the Poincaré section reveals that points in '0' map only to points in '1' while points in '1' map to points in '0' $\cup$ '1'. This rule is represented in the form of transition matrix $\mathcal{M}$ [Gil98]:

$$\mathcal{M} = \begin{array}{c} \\ 0 \\ 1 \end{array} \begin{array}{c} \begin{array}{cc} 0 & 1 \end{array} \\ \begin{bmatrix} 0 & 1 \\ 1 & 1 \end{bmatrix} \end{array}$$

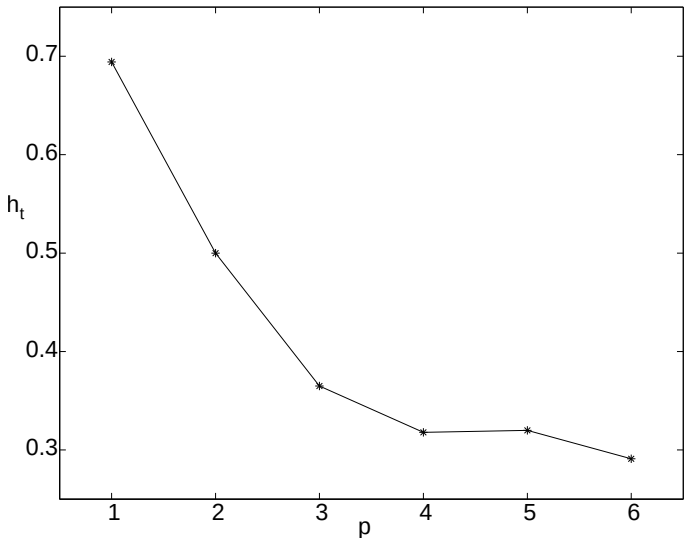

Figure 2.13: Convergence of topological entropy h_t with period p.

Similar examination of the data for 2-digit strings yields

$$\mathcal{M} = \begin{array}{c} \\ 01 \\ 10 \\ 11 \end{array} \begin{array}{c} \begin{array}{cccc} 01 & 10 & 11 & \end{array} \\ \begin{bmatrix} 1 & 0 & 1 \\ 0 & 1 & 1 \\ 1 & 1 & 0 \end{bmatrix} \end{array}$$

Assuming that the dynamics is described by $\mathcal{M}$ then the topological entropy h_t is given by [Lat89]

$$h_t = \lim_{p\to\infty} \frac{1}{p} \log_2 \mathrm{tr}\mathcal{M}^p \tag{2.34}$$

and in this case as $p \to \infty$ we have $h_t \to \log_2 \lambda_{\max}$. Thus topological entropy estimated for different periods (*i.e.* p) is shown in Figure 2.13. The topological entropy converges to a value ≈ 0.297 by considering orbits upto period six and is comparable to entropy estimated form Lyapunov spectrum in preceding Section 2.3.1.

Chaotic dynamics has been observed in stress experiments performed at constant shear rates on poly N-isopropyl acrylamide (PNIPAm) solution at varying temperatures as stated in previous section. We have carried out the topological analysis on a

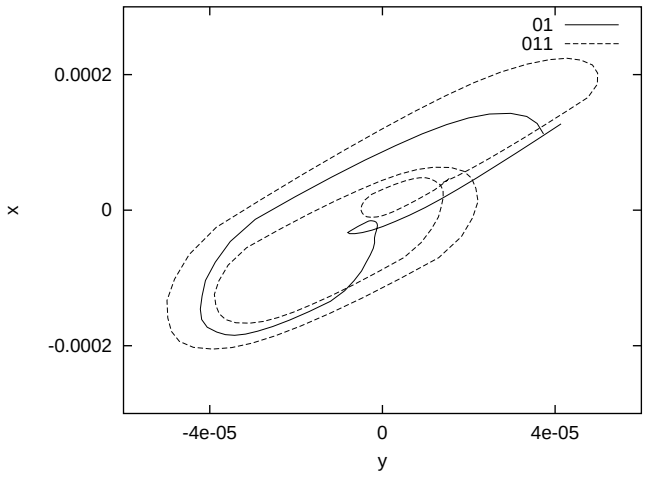

Figure 2.14: Linking number calculations for the period-2 orbit '01' and period-3 '011' extracted from sheared polymer solution.

typical PNIPAm sheared data shown in Figure 2.4. The linking number calculation for the '01' and '011' orbits from their projection on the $x - y$ plane is illustrated in Figure 2.14.

We observed that the linking numbers obtained from the period-1, 2 and 3 orbits was sufficient to obtain the template as shown in Figure 2.15.

The procedure when implemented for the other data sets obtained on different experimental conditions of sheared polymer solutions yielded the same template showing a commonality in the global dynamical features.

2.4 Conclusions

Shear stress experiments of polymer solutions having differing properties show low-dimensional chaos over a range of experimental conditions. The experimental data has been analyzed to obtain dynamical invariant measures such as dimensions and entropies. These invariants help to characterize the dynamical properties of the observed strange attractor. The presence of low-dimensional chaotic dynamics is suggested by

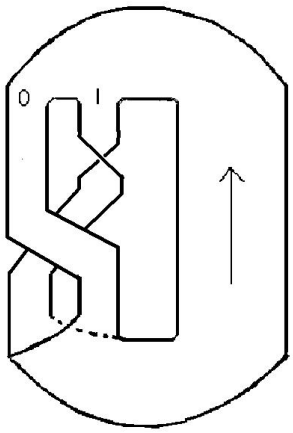

Figure 2.15: Template for sheared polymer solution.

the Lyapunov dimension d_L to be less than three. This is particularly advantageous because it suggests that topological studies of the strange attractor is feasible. The results of studying topological invariants is presented and interestingly draws similarities between the nature of the chaos arising due to shear with that observed in a commonly studied nonlinear model reacting systems exhibiting chaotic dynamics.

The observance of instability with chaotic dynamics in dilute sheared solutions suggests that the study of more viscous systems where diffusion and convection mechanisms play more dominant roles may be well worth-the-while. It is known that presence of instabilities can affect polymer processing operations [Gra99]. The additional degrees of freedom that arise due to introduction of spatial considerations could lead to interesting analyses of the occurrence of pattern formation and even turbulence [Gro00] in these systems as will be studied in Chapter 4.

Chapter 3

Inverse Problem of Parameter Estimation Using Multiple Shooting Boundary Value Approach

The invariant measures analyzed in Chapter 2 depend upon the parameter values of the system. A knowledge of these parameter values is essential for studying the system properties. Thus it is important to estimate the unknown parameters of the system by tuning an appropriate nonlinear model to fit the observed chaotic data [Boc83, Boc84]. The first step would be to consider a simpler situation of well-mixed systems whose dynamics can be described by ordinary differential equations. It may be noted that for chaotic dynamics estimating parameters and system states is not a trivial task even for simple model descriptions. The aim here is to simultaneously estimate the unknown parameters and non-monitored system states from available transient data. The results obtained focus on this practically important aspect of modeling and show the advantages gained by applying a boundary-value shooting approach to stringent nonlinear situations when the system exhibits low-dimensional chaotic dynamics. We exemplify the analysis by also adapting the method to tune empirical mathematical models in case phenomenological descriptions are not available and using noisy scalar time series data. The results of analysis are presented for model system, the endo-

exothermic CSTR, and experimental data obtained for hydroxylation of benzene to phenol. In all cases, it is shown that identification of all intrinsic kinetic constants and operation parameters is possible from even small data sets. Ways to make the multiple shooting boundary value method robust for parameter estimation have been devised *viz.* curtailing error propagation for chaotic dynamics, stopping at local minima during optimization, using, nonlinear quadrature minimization techniques, parallelization, etc., have been implemented in the algorithm.

The organization of the Chapter is follows: In Section 3.1 we outline the parameter estimation techniques and introduce the improved multiple shooting algorithm. The methodology is demonstrated for a model system (Section 3.2.1) and the experimental system of hydroxylation of benzene to phenol (Section 3.2.2).

3.1 Parameter Estimation Techniques

Parameter estimation is a discipline that provides tools for the efficient use of data in mathematical modeling of phenomena so that estimation of constants and unknown system states appearing in these models can be tracked. It can thus be visualized as a study of inverse problems. Much of parameter estimation can be related to four optimization problems:

- **criterion**- the choice of the best function to optimize (minimize or maximize)
- **estimation**- the optimization of the chosen function
- **design**- optimal design to obtain the best parameter estimates
- **modeling**- the mathematical model which best describes the system from which data are measured.

Let p be the (state/parameter) vector containing the parameters to be estimated. The dimension of p, say m, is the number of parameters to be estimated. Let z be

the (measurement) vector which is the output of the system to be modeled. The system is described by a vector function f which relates z to p such that

$$f(p, z) = 0. \tag{3.1}$$

Often the observed measurements y are only available for the true system state z corrupted with noise ϵ, *i.e.*

$$y = z + \epsilon. \tag{3.2}$$

We usually make a number of measurements for the system, say y_i $(i = 1, \cdots, n)$ and we want to estimate p using y_i. As the data are noisy, the function $f(p, y_i) = 0$ is not valid anymore. In this case, we write down a function

$$\mathcal{F}(p, y_1, \cdots, y_n) \tag{3.3}$$

which is to be optimized (without loss of generality, we will minimize the function). This function is usually called *the cost function* or *the objective function*. If there are no constraints on p and the function $\mathcal{F}$ has first and second partial derivatives defined everywhere, necessary conditions for a minimum are

$$\frac{\partial \mathcal{F}}{\partial p} = 0 \qquad \text{and} \qquad \frac{\partial^2 \mathcal{F}}{\partial p^2} > 0 \tag{3.4}$$

By the second condition we mean that the $m \times m$-matrix is positive definite.

3.1.1 Least Square Fitting

The problem of parameter estimation can be considered as fitting a conic section to a set of n data points $\{x_i, y_i\}, (i = 1, \cdots, n)$. A conic section can be described by the following equation

$$Q(x, y) = Ax^2 + 2Bxy + Cy^2 + 2Dx + 2Ey + F = 0 \tag{3.5}$$

where, A and C are not simultaneously zero. In practice, we encounter data contaminated with noise and it is unlikely to find a set of parameters such that $Q(x_i, y_i) = 0, \forall i$. Instead, we will try to estimate the parameters by minimizing some objective function. A common practice is to directly minimize the algebraic distance, *i.e.* to minimize the following function

$$\mathcal{F} = \sum_{i=1}^{n} Q^2(x_i, y_i). \tag{3.6}$$

Note that there exists a trivial solution $A = B = C = D = E = F = 0$ and so in order to avoid it, we should normalize the $Q(x, y)$ approximately.

Normalization with $A + C = 1$

Since the trace $A + C$ can never be zero for an ellipse, the arbitrary scale factor in the coefficients of the conic equation can be naturally removed by the normalization $A + C = 1$. An ellipse can then be described by a 5-vector

$$p = [A, B, D, E, F]^T \tag{3.7}$$

and the system equation $Q(x_i, y_i) = 0$ becomes:

$$f_i \equiv a_i^T - b_i = 0, \tag{3.8}$$

where

$$a_i = [x_i^2 - y_i^2, 2x_iy_i, 2x_i, 2y_i, 1]^T \quad \text{and} \quad b_i = -y_i^2. \tag{3.9}$$

Given n points, we have the following vector equation:

$$Ap = b, \tag{3.10}$$

where

$$A = [a_1, a_2, \cdots, a_n]^T \quad \text{and} \quad b = [b_1, b_2, \cdots, b_n]^T. \tag{3.11}$$

The function to minimize becomes

$$\mathcal{F}(p) = (Ap - b)^T (Ap - b). \tag{3.12}$$

Obtaining the partial derivative with respect to p and setting it to zero yield:

$$2A^T(Ap - b) = 0. \tag{3.13}$$

The solution is readily given by

$$p = (A^T A)^{-1} A^T b. \tag{3.14}$$

This method is known as *pseudo inverse* technique.

Normalization with $F = 1$

Let p be the vector of parameters of which the last element $p_6 = F = 1$. In general, if A is a $n \times m$ matrix, p is m-vector of which p_m is the last element. Thus the function to minimize is

$$\mathcal{F}(p) = (Ap)^T (Ap) \equiv p^T B p \quad \text{subject to} \quad p_m = 1. \tag{3.15}$$

The symmetric matrix B can be decomposed as $B = UEU^T$, with

$$E = \text{diag}(v_1, v_2, \cdots, v_m)$$
$$U = [e_1, e_2, \cdots, e_m].$$

The eigenvector and eigenvalue are normalized with respect to e_{im} the last element of the eigenvector e_i and we obtain

$$B = U' E' u'^T. \tag{3.16}$$

The original problem now translates to finding $a_1, a_2, \cdots, a_m$ such that $p^T B p$ is minimized with $p = a_1 e'_1 + a_2 e'_2 + \cdots + a_m e'_m$ subject to $a_1 + a_2 + \cdots + a_m = 1$. The

problem now becomes to minimize the following unconstrained function:

$$\begin{aligned}\mathcal{F} &= p^T B p \\ &= a_1^2 v_1' + a_2^2 v_2' + \cdots + a_m^2 v_m' + \lambda(a_1 + a_2 + \cdots + a_m), \end{aligned} \tag{3.17}$$

where, λ is the Lagrange multiplier. Setting the derivatives of $\mathcal{F}$ with respect to a_is and λ to zero yields:

$$\begin{aligned} & 2a_1 v_1' + \lambda = 0 \\ & 2a_2 v_2' + \lambda = 0 \\ & \cdots \\ & 2a_m v_m' + \lambda = 0 \\ & a_1 + a_2 + \cdots + a_m - 1 = 0 \end{aligned} \tag{3.18}$$

The unique solution to the above set of equations is given by

$$a_i = \frac{1}{v_i} S, \quad \text{for} \quad i = 1, \cdots, m, \quad \text{where} \quad S = \frac{1}{\sum_{j=1}^{m} \frac{1}{v_j'}}$$

The parameters p can be obtained as

$$p = \sum_{i=1}^{m} a_i e_i' = \frac{\sum_{i=1}^{m} \frac{1}{v_j'} e_i'}{\sum_{j=1}^{m} \frac{1}{v_j'}} \tag{3.19}$$

It is to be noted that this normalization procedure has singularities for all conics going through origin and such conics can not be fitted as it requires setting $F = 0$. However, this singularity problem can be overcome by shifting the data so that they are centered on the origin.

3.1.2 Gradient Weighted Least Square Fitting

In general we are given n equations:

$$f_i \equiv a_i^T p - b_i = \epsilon_i \tag{3.20}$$

where ϵ_i is the additive error in the i-th equation with mean zero: $E(\epsilon_i) = 0$ and variance $\Lambda_{\epsilon_i} = \sigma_i^2$. Above equation written in matrix form yields

$$Ap - b = e. \tag{3.21}$$

The least square estimator described in Section 3.1.1 tries to estimate p by minimizing the following sum of squared errors:

$$\mathcal{F} = e^T e = (Ap - b)^T (Ap - b), \tag{3.22}$$

of which the solution obtained as

$$p = (A^T A)^{-1} A^T b \tag{3.23}$$

is "optimal" in the sense that it assumes error ϵ_i are uncorrelated, $E(\epsilon_i, \epsilon_j) = \sigma_i^2 \delta_{ij}$, and variances are constant, $\Lambda_{\epsilon_i} = \sigma^2, \forall i \in [1, \cdots, n]$. We now compute the variance Λ_{ϵ_i} of function f_i from point (x_i, y_i). Let $(\hat{x}_i, \hat{y}_i)$ be the true position of the point, and we have certainly

$$\hat{f}_i = (\hat{x}_i^2 - \hat{y}_i^2)A + 2\hat{x}_i\hat{y}_i B + 2\hat{x}_i D + 2\hat{y}_i E + F + \hat{y}_i^2 = 0. \tag{3.24}$$

We now expand f_i into Taylor series at $x = \hat{x}_i$ and $y = \hat{y}_i$, *i.e.*,

$$f_i = \hat{f}_i + \frac{\partial f_i}{\partial x_i}(x_i - \hat{x}_i) + \frac{\partial f_i}{\partial y_i}(y_i - \hat{y}_i) + \mathcal{O}((x_i - \hat{x}_i)^2) + \mathcal{O}((y_i - \hat{y}_i)^2). \tag{3.25}$$

Ignoring the high order terms, we can now compute the variance of f_i, *i.e.*

$$\begin{aligned} \Lambda_{\epsilon_i} &= E(f_i - \hat{f}_i)^2 \\ &= \left(\frac{\partial f_i}{\partial x_i}\right)^2 E(x_i - \hat{x}_i)^2 + \left(\frac{\partial f_i}{\partial y_i}\right)^2 E(y_i - \hat{y}_i)^2 \\ &= \left[\left(\frac{\partial f_i}{\partial x_i}\right)^2 + \left(\frac{\partial f_i}{\partial y_i}\right)^2\right] \sigma^2 \equiv \bigtriangledown f_i^2 \sigma^2. \end{aligned} \tag{3.26}$$

It is obvious that the gradient of f_i with respect to x_i and y_i

$$\frac{\partial f_i}{\partial x_i} = 2Ax_i + 2By_i + 2D \qquad \frac{\partial f_i}{\partial y_i} = 2Ay_i + 2Bx_i + 2E + 2y_i$$

and hence the variance of each equation is not same and thus the least square estimator does not yield an optimal solution. In order to obtain a constant variance function, it is sufficient to divide the original function by its gradient, *i.e.*

$$f_i' = \frac{f_i}{\bigtriangledown f_i}. \tag{3.27}$$

We can now try to find the parameters p by minimizing the function

$$\begin{aligned} \mathcal{F} &= \sum f_i'^2 = \sum \frac{f_i^2}{\bigtriangledown f_i^2} \\ &= (Ap-b)^T W^{-1}(Ap-b), \end{aligned} \tag{3.28}$$

where, $W = \text{diag}(\bigtriangledown f_1^2, \bigtriangledown f_2^2, \cdots, \bigtriangledown f_n^2)$. This method is called gradient weighted least square and the solution can be obtained by setting $\partial\mathcal{F}/\partial p = 0$, which yields

$$p = (A^T W^{-1} A)^{-1} A^T W^{-1} b. \tag{3.29}$$

It is to be noted that the gradient weighted least square is in general a nonlinear minimization problem and a close form solution does not exist. In the above derivation, a closed form solution is given as dependence of W on p is ignored in computing $\partial\mathcal{F}/\partial p$. In reality, W depends on p and the above solution is an approximation. In practice one runs the following iterative procedure:

- **step 1**: $k = 0$. Compute $p^{(0)}$ using least squares.
- **step 2**: Compute the weight matrix $W^{(k)}$.
- **step 3**: Compute $p^{(k)}$ using gradient weighted least squares.
- **step 4**: If $p^{(k)}$ is very close to $p^{(k-1)}$, stop; else go to **step 2**.

3.1.3 The Multiple Shooting Boundary Value Approach

Parameter estimation in ODE's may also be carried out with significant robustness by a multiple shooting algorithm formulated as a multi-point boundary value problem

with nonlinear constraints for optimization [Boc83, Baa92]. That is, an interval of observation $[t_a, t_b]$ may be covered by a grid of m multiple shooting nodes ($\tau_1 < \tau_2 < \cdots < \tau_m$) which requires solving $m-1$ initial value problems for the state variables $\mathbf{y} = \{y_1, y_2, \cdots, y_n\}$, whose evolution depends on system parameters $\mathbf{p} = \{p_1, p_2, \cdots, p_k\}$, *i.e.*,

$$\dot{\mathbf{y}} = \mathbf{f}(\mathbf{y}, \mathbf{p}, t) \quad \mathbf{y}(\tau_j) = \mathbf{s}_j, \quad j = 1, 2, \cdots, m \tag{3.30}$$

where, $\mathbf{s}_j$ denote the respective state variable for j^{th} node. Initial guesses for solving Eq.(3.30) are taken to be the available data values η_{ij} for i,j, indicating the component and node index, respectively. The objective of parameter estimation can be achieved by piecewise integration of Eq.(3.30) and simultaneously minimizing a least square functional, analogous to Eq.(3.22), so that the final trajectories are made continuous. An augmented vector is constructed out of variables and parameters $(\mathbf{s}_1, \mathbf{s}_2, \cdots, \mathbf{s}_m, p_1, p_2, \cdots, p_k)$ and an objective functional, written as L_2 norm,

$$\mathcal{L} = \parallel r(\mathbf{s}_1, \mathbf{s}_2, \cdots, \mathbf{s}_m, p_1, p_2, \cdots, p_k) \parallel_2^2 \tag{3.31}$$

is minimized by making

$$\mathbf{y}(\tau_{j+1}; \tau_j, \mathbf{s}_j, \mathbf{p}) - \mathbf{s}_{j+1} \rightarrow 0, \tag{3.32}$$

for $j = 1, 2, \cdots, m-1$. Here the least square objective function takes the form

$$\mathcal{L} = \sum_{i=1}^{m} \sum_{j=1}^{n} \frac{1}{\sigma_{ij}^2} \left[\eta_{ij} - g_j(\mathbf{y}(\tau_i), \mathbf{p}, t_i)\right]^2 \tag{3.33}$$

where, g_j is j^{th} component solution of state variables obtained by integrating the ODEs in Eq.(3.30). The η_{ij} is the observed value of g_j at an instant τ_i and σ_{ij} is its standard deviation if repeated experiments for the same run are performed and data obtained. For easier discussion, let,

$$\mathcal{L}(\mathbf{s}_1, \mathbf{s}_2, \cdots, \mathbf{s}_m, p_1, p_2, \cdots, p_k) = \mathbf{u}_1(\mathbf{z})$$
$$\mathbf{y}(\tau_{j+1}; \tau_j, \mathbf{s}_j, \mathbf{p}) - \mathbf{s}_{j+1} = \mathbf{u}_2(\mathbf{z}).$$

Then the formal problem for parameter estimation and continuity in state variables require

$$\| \mathbf{u}_1(\mathbf{z}) \|_2^2 \rightarrow \text{minimized} \quad ; \quad \mathbf{u}_2(\mathbf{z}) \rightarrow 0. \tag{3.34}$$

The above set of equations may be solved by starting from initial guesses $\mathbf{z}^0$ and iterating the variable $\mathbf{z}$ by

$$\mathbf{z}^{k+1} = \mathbf{z}^k + \omega^k \Delta \mathbf{z}^k \tag{3.35}$$

where, $\omega^k \in [0, 1]$ are damping factors. The correction to the augmented vector $\mathbf{z}$, *i.e.*, $\Delta \mathbf{z}^k$, is obtained by solving for the linearized problem

$$\begin{aligned} \| \mathbf{u}_1(\mathbf{z}^k) + \frac{\partial \mathbf{u}_1(\mathbf{z}^k)}{\partial z} \Delta \mathbf{z}^k \|_2^2 &\rightarrow \text{minimized} \\ \mathbf{u}_2(\mathbf{z}^k) + \frac{\partial \mathbf{u}_2(\mathbf{z}^k)}{\partial z} \Delta \mathbf{z}^k &\rightarrow 0 \end{aligned}$$

by using suitable nonlinear programming techniques as outlined in Section 3.1.2 or by successive quadratic programming algorithm with a finite difference gradient [Sto85]. Computation of the Jacobian elements $\partial \mathbf{u}_1 / \partial z$ and $\partial \mathbf{u}_2 / \partial z$, say $\mathcal{J}_1$ and $\mathcal{J}_2$ are computationally intensive because the sensitivity matrices, $\mathbf{G}$ and $\mathbf{H}$ are simultaneously evaluated for each shoot for varying initial conditions and parameters, *i.e.*,

$$\begin{aligned} \mathbf{G} &= \frac{\partial \mathbf{y}(t; t^0, \mathbf{y}^0, \mathbf{p})}{\partial \mathbf{y}^0} \\ \mathbf{H} &= \frac{\partial \mathbf{y}(t; t^0, \mathbf{y}^0, \mathbf{p})}{\partial \mathbf{p}}. \end{aligned}$$

Thus, $\mathbf{G}$ and $\mathbf{H}$ together form an augmented sensitivity matrix for the variables and parameters. Significant advantages and simplification in problem formulation may be realized by numerical evaluation of these sensitivity matrices and for this purpose we have employed Ridder's differentiation scheme [Pre92] in our numerical coding.

Table 3.1: Estimated parameter values for endo-exothermic CSTR, I - chaotic data, II - chaotic data with noise, III - chaotic data with noise and missing data

Parameter	I	II	III
β	8.000 ± 0.001	7.998 ± 0.003	8.003 ± 0.006
Da	0.259 ± 0.002	0.258 ± 0.004	0.259 ± 0.009
S	0.498 ± 0.001	0.493 ± 0.002	0.491 ± 0.011
B	57.77 ± 0.015	57.75 ± 0.027	57.81 ± 0.031
κ	1.000 ± 0.001	1.001 ± 0.001	1.001 ± 0.002

3.2 Applications of Multiple Shooting Approach

3.2.1 Endo-exothermic CSTR

The method of multiple shooting algorithm has been exemplified for a model of the process in a CSTR where an irreversible, first-order, endo-exothermic and consecutive reaction $A \rightarrow B \rightarrow C$ takes place (Eq.(2.11)). Extensive studies reveal that there exists a sequence of period doubling bifurcations to chaos for realistic ranges of parameter values, i.e., $Da = 0.26$, $S = 0.5$, $B = 57.77$, $\kappa = 1.0$, $\beta = 8.0$ and $\alpha = 0.426$ with sampling time $\Delta t = 0.01$. An attempt has been made to estimate the above mentioned parameters and the results have been tabulated in Table 3.1.

The robustness of the method is evident as estimation with reasonable accuracy is possible even in presence of noise in the chaotic data and in cases of missing data. The convergence of parameter values with iterations is shown in Figure 3.1 where different cases are shown for different initial guesses. The iterative scheme of multiple shooting algorithm can be improved upon by simultaneously considering segments of data and applying the code in a parallelized fashion. Smaller subsets of data are subjected to multiple shooting and on satisfaction of suitable convergence criteria the converged values are put in as guess values for bigger segments to obtain better estimates. Finally, the algorithm employed on the entire data with already improved guesses ensures continuity on integration and better convergence. This methodology

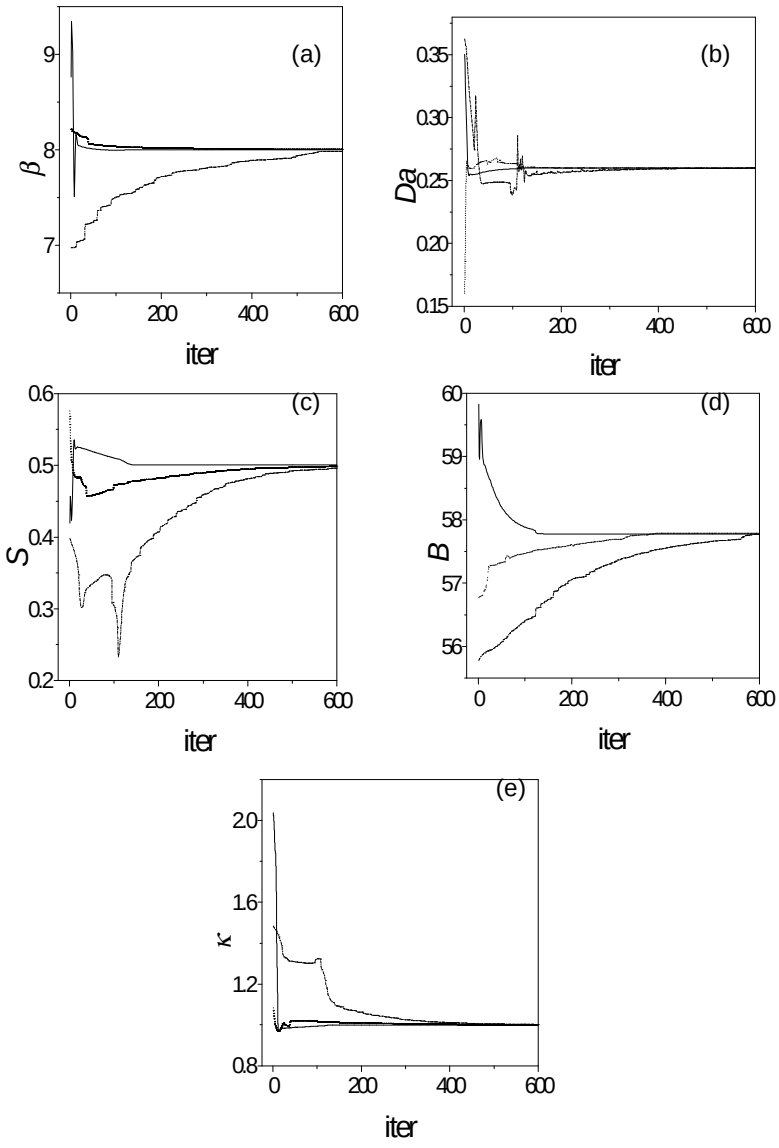

Figure 3.1: (a-e) Simultaneous estimation of the respective parameter values, for the CSTR exhibiting chaotic dynamics. Case III (Table 3.1) takes more iterations to converge while case I, II take less.

facilitates the model equations to fit the data starting from local neighborhoods and finally satisfying the conditions globally.

3.2.2 Benzene Hydroxylation

Data was analyzed from experiments obtained [Bha98] during the oxidation of benzene under solvent free conditions using a triphase system of i) titanium silicate zeolite catalyst sieves ii) organic substrate, and iii) aqueous H_2O_2. The results showed a significant enhancement in reaction rate (of the order of 15-25 times) was possible when compared to that obtained under conventional biphase conditions using an organic solvent. The data from triphase system were obtained from experiments conducted under vigorous stirring (≈ 800 $r.p.m.$) in a glass batch reactor, where, benzene and H_2O_2 were reacted in a 2:1 ratio (wt/wt) over the catalyst. The benzene and phenol concentrations were monitored in time to obtain the H_2O_2 selectivity and phenol selectivity values. For a sequential reaction mechanism

$$C_6H_6 + H_2O_2 \rightarrow Parabenzoquinone \rightarrow Phenol, \tag{3.36}$$

with hydrogen peroxide decomposition written as a parallel step $H_2O_2 \rightarrow H_2O + O_2$, a realistic empirical power law model may be formulated as

$$\begin{aligned} -V\frac{dC_B}{dt} &= k_1[C_B][C_H] + k_2[C_B][C_H] \\ -V\frac{dC_H}{dt} &= k_1[C_B][C_H] + k_2[C_B][C_H] + k_3[C_H]^2 \\ V\frac{dC_P}{dt} &= k_1[C_B][C_H] \\ V\frac{dC_D}{dt} &= k_3[C_H]^2 \end{aligned} \tag{3.37}$$

where, C_B, C_H, C_P, C_D are the concentrations of benzene, H_2O_2, phenol and water. If C_B^0 and C_A^0 are initial concentrations of benzene and phenol, we may define the

following:

$$\begin{aligned} \text{benzene concentration} &= A = (C_B^0 - C_B)/C_B^0, \\ H_2O_2 \text{ selectivity} &= B = 1 - C_D/(C_H^0 - C_H), \\ \text{phenol selectivity} &= C = C_P/(C_B^0 - C_B). \end{aligned}$$

From the balance equations we observe that

$$(-[dC_B/dt] + [dC_D/dt])/(-[dC_H/dt]) = 1 \tag{3.38}$$

which on integration gives

$$C_D = (C_H^0 - C_H) - (C_B^0 - C_B). \tag{3.39}$$

Substituting Eq.(3.39) in Eq.(3.37)we have the model equations for parameter estimation from data as:

$$\begin{aligned} \frac{dA}{dt} &= \frac{1}{C_B^0 V}(p+q) \\ \frac{dB}{dt} &= \frac{B^2}{C_B^0 V A}[(p+q)(\frac{1}{B} - r)] \\ \frac{dC}{dt} &= \frac{1}{C_B^0 V A}[p(1-C) - qC] \end{aligned} \tag{3.40}$$

with simplification of notation by: $p = k_1[C_B][C_H]$, $q = k_2[C_B][C_H]$, $r = k_3[C_H]^2$.

We now attempt to estimate the kinetic parameters k_1, k_2, k_3 for the experimentally obtained benzene hydroxylation data. The benzene hydroxylation in presence of cosolvent is very slow and only $\approx$ 20% selectivity could be obtained after 8 hours. However, for triphase condition the reaction was fast, reaching maximum conversion levels ($\approx$ 80% selectivity) in about 2 hours. The decomposition $H_2O_2 \rightarrow H_2O + O_2$ is a standard reaction [Lai65] and the reaction constant calculated is given by $k_3 = 10^{18} exp[-45000/RT]$. The multiple shooting algorithm employed on the experimental data and minimization of the least square optimization function gave the following best estimates as $k_1 = 0.001008$ and $k_2 = 0.000475$. The excellent fit obtained by the transient data and empirical model is shown in Figure 3.2.

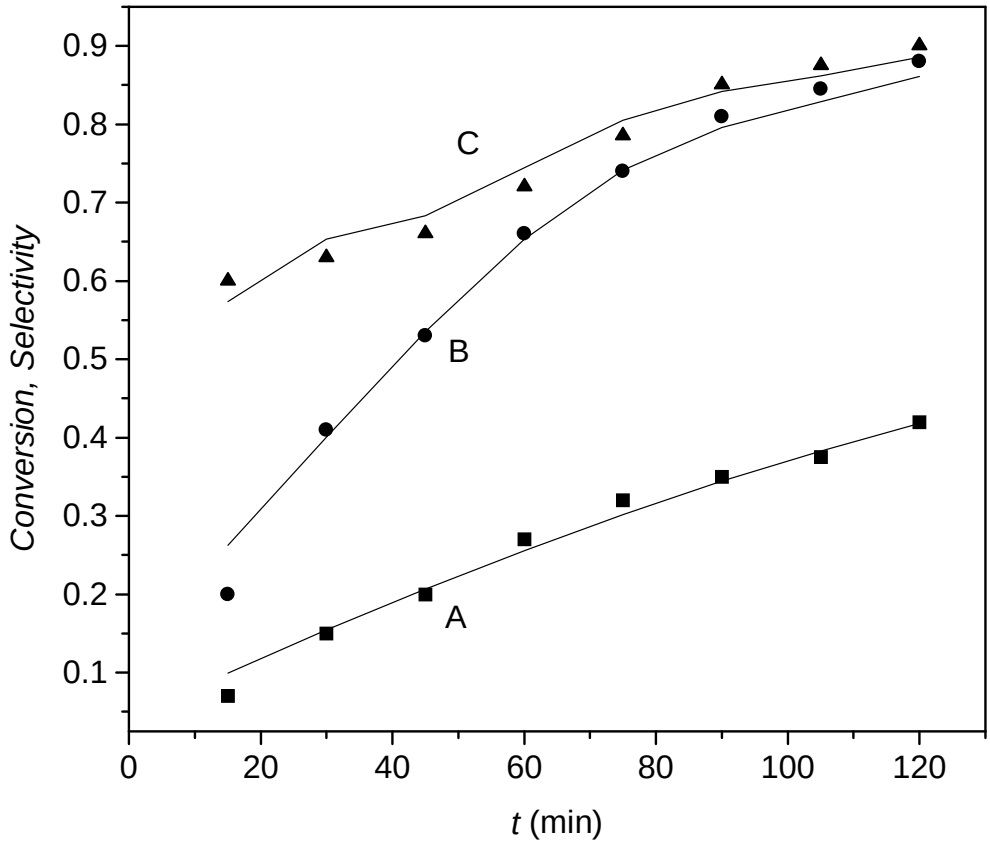

Figure 3.2: Fitted transient curve (solid line) using estimated kinetic constants for A, B, C from the shown experimental data.

3.3 Conclusion

Here, we have shown applications of the multiple-shooting boundary value algorithm for parameter estimation in examples of nonlinear chemically reacting systems. The simulation, control and monitoring of processes with complex dynamics benefit substantially from the derivation and availability of reliable mathematical models. Model simplification and reduced model descriptions of more complex processes can now be attempted. The above methodology may be tailored to situations when online parameter estimation is required. Alternatively stated, online multi-variable control strategies *via* control parameter estimation for nonlinear dynamical systems becomes feasible by this methodology. The applicability of the methodology to noisy data can be further exploited in estimating parameters from reduced description of spatially extended system where the unaccounted modes in the system domain can be treated as noise, as will be revealed in Chapter 5.

Chapter 4

Feature Extraction in Spatially Extended Reaction-Diffusion-Convective Systems

A widely studied class of complex systems are the spatially extended systems where the methodologies for analysis of one point time-series has to be built-up to incorporate the spatial extent of the system. These systems are described by partial differential equations involving nonlinearities along with diffusive and/or convective coupling and can show intricate and complex patterns including turbulence [Cro93]. The most prominent examples are autocatalytic reaction-diffusion in chemical systems [Gra90], Navier-Stokes equation of hydrodynamics [Hol96], complex Ginzburg-Landau equation [Kur84], heterogeneous catalytic reaction on Pt catalyst [Bar94], etc. Analysis of the dynamics of these systems is not an easy task because of the large attractor dimensions involved and extension of approaches designed for low dimensional systems to high dimensional cases is not straightforward [Kan97]. For this reason, identification of pattern forming mechanisms and their characterization techniques is a contemporary research topic. In fact, it would be desirable to develop ways of studying spatiotemporal systems using reduced model descriptions in terms of fewer degrees of freedom. The method can be used in conjunction with subsystem dynamics especially

when it is known that extensive scaling relationships in dynamics exist as a function of subsystem size [Car99, Par98]. The Karhunen-Loève decomposition captures the most energetic coherent structures by projecting the spatiotemporal data on a optimum set of empirical basis functions. Thus it is possible to condense complex spatiotemporal data in terms of few significant eigenfunctions leading to appreciable degree of data reduction in many cases. Here, the methodology has been developed for coupled map lattices (CML), a discrete prototype that possesses the basic reaction-diffusion and convection mechanisms that give rise to complex patterns including spatiotemporal chaos and convective turbulence [Kan93], and suitably extended to systems governed by partial differential equations having one or two spatial dimensions. Moreover, it will be illustrated that given such a set of empirical eigenfunctions the method can give an unbiased estimate of marred (*i.e.* partially masked images as appears in cloud covered satellite images) spatiotemporal data in a reasonable manner.

The organization of the Chapter is as follows: In Section 4.1 we exemplify the Karhunen-Loève decomposition and demonstrate the methodology in Section 4.2 for a discrete system (Section 4.2.1), and continuous systems in one and two spatial dimensions in Section 4.2.2 and Section 4.2.3 respectively. We further extend the KLD procedure for analyzing image processing and show the application in Section 4.3.

4.1 Karhunen-Lòeve Decomposition

The Karhunen-Lòeve decomposition (KLD) provides a basis of ensemble of functions for decomposing data collected in course of experiments. The superiority of such basis functions lie in the fact that they are optimal and an infinite-dimensional process can be represented in terms of very few "modes". KLD, originally introduced by Karhunen, Lòeve, is popular in various fields and forms the basis for the methods like proper orthogonal decomposition, principal component analysis. KLD can be

used to analyze experimental data in order to extract dominant coherent structures and in case of spatiotemporal fields to study patterns in space and time. Here, the emphasis is on identifying key spatial features of spatiotemporal data forming patterns and obtaining a low-dimensional accurate dynamical model of the spatially extended system. The starting point for KLD is in obtaining the fluctuating components $v(t,x)$ by subtracting the time-averaged mean from the field variables $u(t,x)$,

$$v(t,x) = u(t,x) - \lim_{T\to\infty} \frac{1}{T}\int_0^T u(t,x)dt. \tag{4.1}$$

The general idea of KLD is to obtain a *separable* series expansion scheme for $v(t,x)$ in the form,

$$v(t,x) = \sum_{k=1}^{\infty} a_k(t)\phi_k(x), \tag{4.2}$$

where by truncating the index k to a suitable order it is possible to achieve reduction with required accuracy. Here $\phi(x)$ are the coherent structures present in the system and $a(t)$ are time dependent coefficients. Keeping in mind the fact that experimental measurements yield only a discrete and finite set of data, from now on $v(t,x)$ will be represented as an ensemble of snapshots $\{v_n(x)\}$ where $n = 1, 2, \cdots, M$, M is the total number of snapshots. To get efficient reduction, one projects $v_n(x)$ onto an optimal subspace which captures maximum information of the system. ϕs are orthonormal empirical basis functions which contain maximum projection of $v_n(x)$ and maximizes

$$\lambda = \langle (v_n, \phi)^2 \rangle. \tag{4.3}$$

Here, $\langle\cdot\rangle$ represents averaging while $(,)$ is the inner product in infinite dimensional Hilbert space

$$(f,g) = \int f(x)g^{\star}(x)dx \tag{4.4}$$

Then extremising $\langle (v,\phi)^2 \rangle$, subjected to the constraint $||\phi||^2 = 1$, can be treated as a problem of calculus of variations and let the functional be

$$J[\phi] = \langle (v,\phi)^2 \rangle - \lambda(||\phi||^2 - 1) \tag{4.5}$$

and a necessary condition for extrema is that the functional derivative vanish for all variations $\phi + \delta\psi$, *i.e.*,

$$\frac{d}{d\delta} J[\phi + \delta\psi]|_{\delta=0} = 0 \tag{4.6}$$

From Eq. (4.5) and (4.6) we have,

$$\begin{aligned} \frac{d}{d\delta} J[\phi + \delta\psi]|_{\delta=0} &= \frac{d}{d\delta}[\langle (u, \phi + \delta\psi)(\phi + \delta\psi, u)\rangle - \lambda(\phi + \delta\psi, \phi + \delta\psi)]|_{\delta=0} \\ &= 2\mathrm{Re}[\langle (u, \psi)(\phi, u)\rangle - \lambda(\phi, \psi)] = 0 \end{aligned} \tag{4.7}$$

where, we use the property $(f, g) = (g, f)^\star$ Since, $\psi(x)$ is an arbitrary variation and noting the commutativity of $\langle\cdot\rangle$ and $\int \cdot dx$, our condition reduces to

$$\int_0^1 \langle u(x)u^\star(x')\rangle \phi(x')dx' = \lambda\phi(x). \tag{4.8}$$

Thus the optimal basis is given by the eigenfunctions $\{\phi_j\}$ of the integral equation Eq. (4.8) whose kernel is the averaged autocorrelation function $\langle u(x)u^\star(x')\rangle = R(x, x')$. The above optimization problem is equivalent of solving the eigenvalue problem for the spatial correlation matrix $R(x, x')$

$$\int R(x, x')\phi(x')dx' = \lambda\phi(x). \tag{4.9}$$

Eigenvalue spectrum $\{\lambda_i\}$ determine the importance of basis functions and eigenfunctions corresponding to the largest eigenvalue is the most important and so on. A factor may be defined as

$$\eta_N = \frac{\sum_{l=1}^{N} \lambda_l}{\sum_{k=1}^{M} \lambda_k} \tag{4.10}$$

to quantify the energy content for increasing mode index k and decides an index $N < M$ for which the series in Eq. 4.2 may be truncated. From a practical point of view most often one deals with a very large spatial domain for $\mathbf{x}$, and computation

of $R(\mathbf{x}, \mathbf{x}')$ becomes quite an involved procedure. The *method of snapshots* enables to get over this practical difficulty [Sir87]. Eq.(4.9) gives us

$$\int R(\mathbf{x}, \mathbf{x}')\phi(\mathbf{x}')d\mathbf{x}' = \frac{1}{M}\sum_{n=1}^{M} v_n(\mathbf{x}) \int v_n(\mathbf{x}')\phi(\mathbf{x}')d\mathbf{x}' = \sum_{n=1}^{M} \gamma_n v_n(\mathbf{x}). \tag{4.11}$$

Thus the span of the eigenspace of R is restricted to M dimensional space. Combining Eq.(4.9) and (4.11) empirical eigenfunctions can be written as

$$\phi(\mathbf{x}) = \sum_{n=1}^{M} \Gamma_n v_n(\mathbf{x}), \tag{4.12}$$

for some constants $\Gamma_1, \Gamma_2, \cdots, \Gamma_M$ and Eq.(4.9) takes the form

$$C\Gamma = \lambda\Gamma \tag{4.13}$$

where,

$$C = \frac{1}{M}\int v_n(\mathbf{x})v_m(\mathbf{x}')d\mathbf{x}'. \tag{4.14}$$

Thus the computation of eigenvalues and eigenfunctions of a spatial correlation matrix can be replaced by calculating that from the matrix C which has a dimension $(M \times M)$ and is independent of the spatial extent. It is to be noted that C and R are not identical even though they have same eigenvalues.

4.2 Illustrative Examples

4.2.1 Discrete System: Coupled Map Lattice

Because of their computational simplicity, CMLs are a popular and convenient paradigm for studying fully developed turbulence [Kan93, Wil95, Hil99], chaos [Kan89], and pattern formation [Cro93] in spatially extended systems. A CML model is a discrete space-time system with continuous state space and studies the effects of local nonlinear reaction dynamics, the coupling arising from diffusion due to state space gradients

as well as convective effects by asymmetric coupling[Wil95]. Here, we consider a CML involving a single spatial dimension and incorporating these mechanisms as

$$u(n+1,j) = (1 - D_d - D_c)f(u(n,j)) + D_c f(u(n,j-1)) + \frac{D_d}{2}[f(u(n,j+1)) + f(u(n,j-1))], \quad (4.15)$$

where, $u(n,j),\ j = 1, 2, \cdots, L$ is the state of the variable located at site j at time n for a lattice of size L, D_d the nearest neighbor diffusive coupling strength and D_c denoting the asymmetric coupling constant. For $D_c = 0$ the system represents a reaction-diffusion system while for $D_c \neq 0$ mimics one with convective effects included. We assume the reaction dynamics on the lattice sites is governed by the nonlinear logistic function $f(u) = 1 - Fu^2$, where, F is the nonlinearity parameter. Thus, depending on the parameter values for F, D_d and D_c, a variety of dynamical patterns may be observed in Eq. (4.15) and characterized as in [Wil95]. We bring out the methodology for Karhunen-Loéve decomposition for selected dynamics covering a broad range of complexity, *viz.*,

- weak chaos
- traveling wave
- fully developed chaos
- convective turbulence

Spatiotemporal data for the different cases are obtained by evolving Eq. (4.15). All the sites are given random initial conditions at $n = 0$ and snapshots are stored after eliminating initial transients. Cases *(a,b,c)* are evolved with periodic boundary conditions, *i.e.,* $u(n,1) = u(n,L)$ while for the convective case *(d)* the left boundary is assumed fixed, *i.e.,* $u(n,1) = 1$, with the right boundary open. The gray-scale

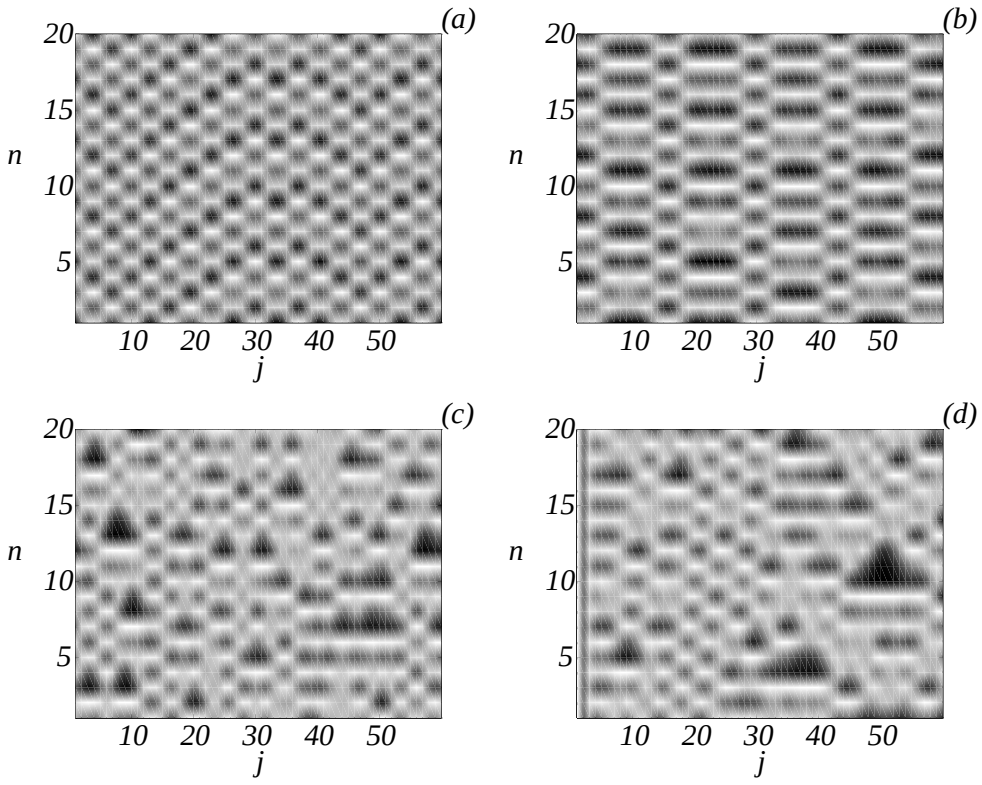

Figure 4.1: Evolved spatiotemporal data $u(n, j)$ for the CML (j spatial grid with $L = 60$; $M = 20$ snapshots. *(a)* Weak chaos ($F = 1.73$, $D_d = 0.4$, $D_c = 0.0$); *(b)* Traveling wave ($F = 1.5$, $D_d = 0.5$, $D_c = 0.0$); *(c)* Fully developed chaos ($F = 2.0$, $D_d = 0.4$, $D_c = 0.0$); *(d)* Convective turbulence ($F = 2.0$, $D_d = 0.4$, $D_c = 0.3$).

Table 4.1: Significance of KL modes in CML.

case		Mode no. k	λ_k	η_k
(a)	Weakly chaotic	1	10.5467	0.9408
		2	0.3639	0.9733
		3	0.2862	0.9988
(b)	Traveling wave	1	13.2207	0.9337
		2	0.3712	0.9600
		5	0.1098	0.9957
(c)	Fully chaotic	1	3.8130	0.2690
		15	0.0661	0.9912
		19	0.0217	0.9999
(d)	Convective turbulence	1	4.0071	0.2950
		15	0.0458	0.9929
		19	0.0106	0.9999

images of the spatiotemporal data along with the parameter values yielding the data for a lattice size of $L = 60$ and for $M = 20$ snapshots, is shown in Figure 4.1.

We obtain a KL decomposition for the spatiotemporal data $v(n, j)$ and Table 4.1 shows the corresponding eigenvalues λ_k, and the energy content η_k, for the data shown in Figure 4.1 *(a-d)*. The results show that for the CML exhibiting weak chaos and traveling wave, a smaller number of basis modes $N = 3$ and $N = 5$, respectively, are required to capture and reconstruct 99% of the data. For the more complex patterns, *viz.*, fully developed chaos and convective turbulence the number of basis modes significantly rise to 15 for $\approx 99\%$ and 19 for $\approx 100\%$ accuracy.

4.2.2 One-dimensional Reaction-Diffusion System: Gray-Scott Model

Pattern formation in reaction-diffusion systems has been extensively studied both theoretically and experimentally [Kur84, Fie85]. Now we undertake a prototype reaction-diffusion model where one chemical species grows autocatalytically on another species [Gra90, Maz96]. This model is a simplification of the model of glycolysis proposed

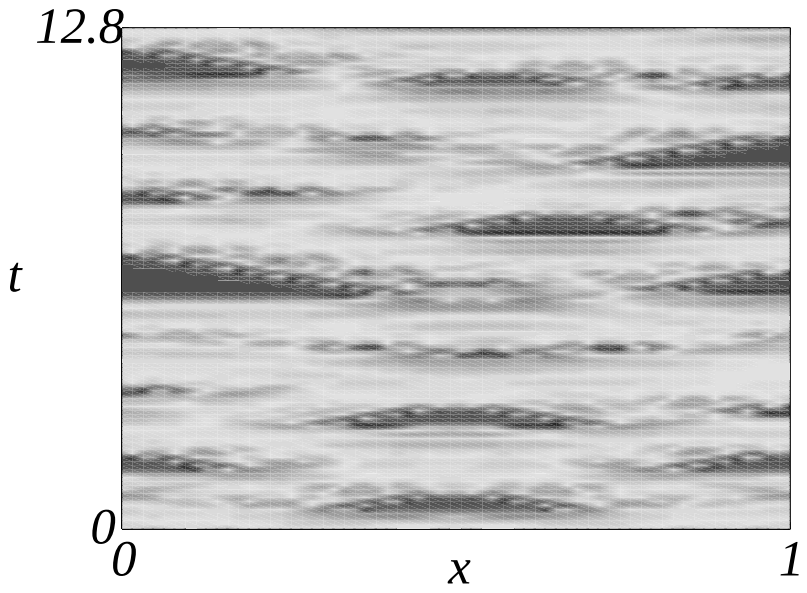

Figure 4.2: Spatiotemporal data for the variable $u^{(1)}(t,x)$ in the autocatalytic reaction-diffusion system with parameter values $f = 0.029$, $k = 0.0535$, $D_u = 0.00002$, $D_v = 0.0001$ with spatial length $L = 1$ spanning 160 spatial sites and $M = 128$ snapshots recorded at a time step $\Delta t = 0.1$ is shown.

by Selkov [Sel68]. It follows the reaction mechanism $U + 2V \rightarrow 3V$; $V \rightarrow P$ with a continuous supply of the reactant U and removal of product P.

A two variable PDE model for a spatially linear system (1-D) involving concentrations $u_1(t,x)$, $u_2(t,x)$ of U, V respectively, may be written as:

$$\begin{aligned} \frac{\partial u_1(t,x)}{\partial t} &= D_u \nabla^2 u_1(t,x) - u_1(t,x)u_2^2(t,x) + f[1 - u_1(t,x)] \\ \frac{\partial u_2(t,x)}{\partial t} &= D_v \nabla^2 u_2(t,x) + u_1(t,x)u_2^2(t,x) - [f+k]u_2(t,x) \end{aligned} \tag{4.16}$$

where, D_u and D_v are diffusion coefficients of U and V respectively. Parameters f and k are related to the flow of reactant into the system and the kinetic rate constant. The parameters f,k form a set of bifurcation parameters for studying spatiotemporal dynamics of the system. In a particular bifurcation parameter space and for unequal diffusion coefficients, a host of spatiotemporal patterns have been identified and char-

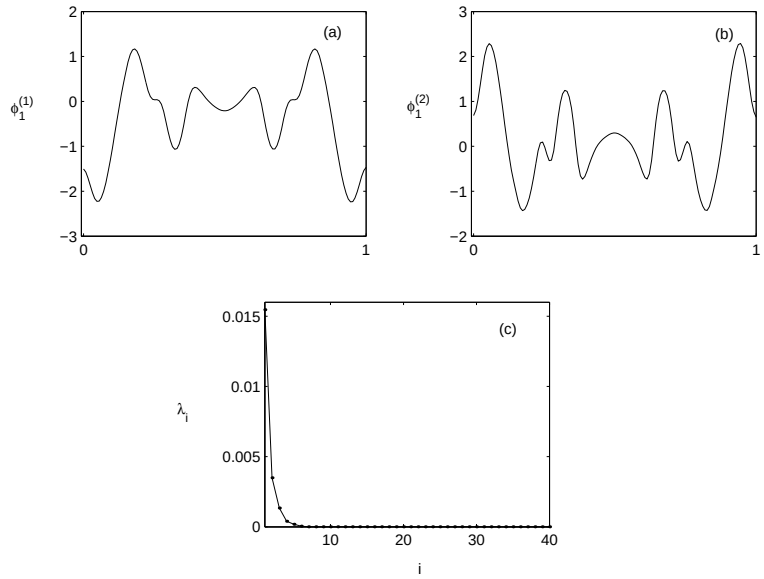

Figure 4.3: The empirical eigenfunctions for the Gray-Scott model (a) $\phi_1^{(1)}$ and (b) $\phi_1^{(2)}$. (c) The eigenvalue spectra λ_i vs. KL-modes i.

acterized, for our study we consider that corresponding to spatiotemporal chaos as shown in Figure 4.2.

For obtaining the spatiotemporal data $u^{(1)}(t,x), u^{(2)}(t,x)$, Eq. (4.16) is solved numerically with Euler discretization in the spatial domain, with spatial length $L = 1$ spanning 160 spatial sites and $M = 40$ snapshots are stored at a time step $\Delta t = 0.1$ and with periodic boundary conditions $u^{(1)}(t,0) = u^{(1)}(t,L)$ and $u^{(2)}(t,0) = u^{(2)}(t,L)$ imposed. The initial conditions correspond to the stationary solution $u^{(1)}(0,x) = 1$ and $u^{(2)}(0,x) = 0$ except for a few central sites which are given a random perturbation to break the symmetry. On subjecting the spatiotemporal data to KL-decomposition the most significant empirical basis functions $\phi_1^{(1)}$ and $\phi_1^{(2)}$ corresponding to the variable $u^{(1)}$ and $u^{(2)}$ is shown in Figure 4.3(a) and (b) respectively. The eigenvalues λ_i of the correlation matrix indicating the importance of KL-modes is shown in Figure 4.3(c).

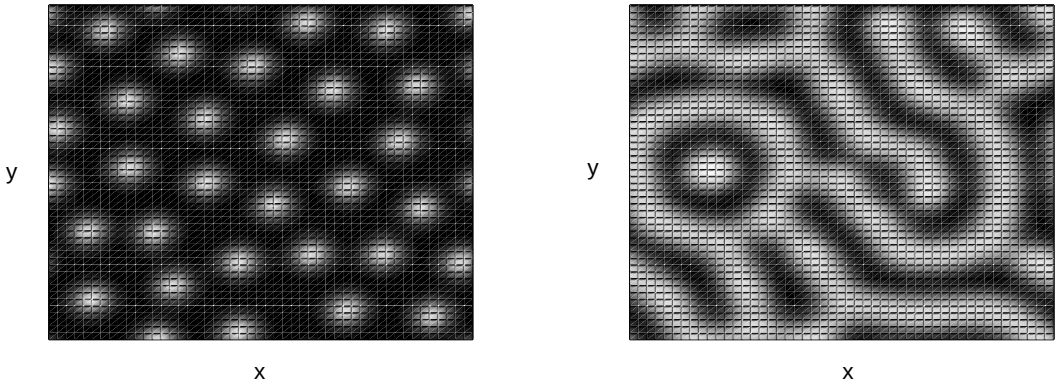

Figure 4.4: Patterns obtained on simulation of the two-dimensional activator-inhibitor model.

4.2.3 Two-dimensional Reaction-Diffusion System: Activator-Inhibitor Model

A most fascinating aspect of biological systems is the generation of complex features in each round of the life cycle. This involves the processes like cell differentiation, cell movement, change of shape of cells and tissues, region specific control of cell division and cell death. A crucial problem is that in spite of genetic information coded in each cell though same how spatial patterns are generated that specifies functionality of cells. Modeling of biological systems exhibiting complex patterns has been a subject of active research. Pattern formation is certainly based on the interaction of many components and interactions are expected to be nonlinear. Two features that play a crucial role in pattern formation are *local self-enhancement* and *long-range inhibition* [Koc81].

The patterns that can be generated are graded concentration profiles, local concentration maxima and stripe like distribution of substances. A possible interaction between an activator $u^{(1)}$ and its rapidly diffusing antagonist $u^{(2)}$ can be expressed

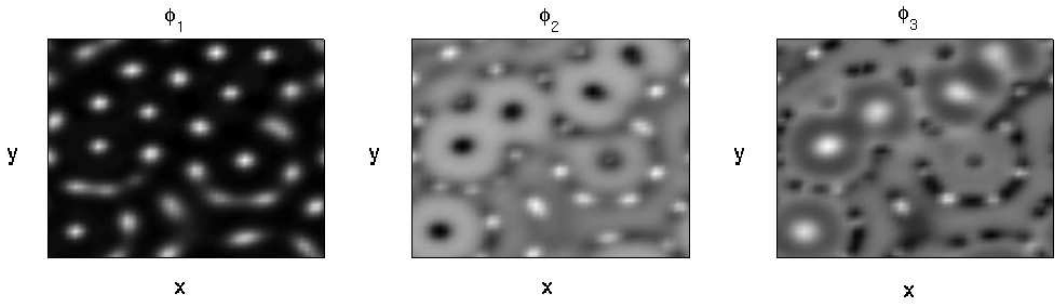

Figure 4.5: The first three significant spatial basis functions for the two-dimensional activator-inhibitor model.

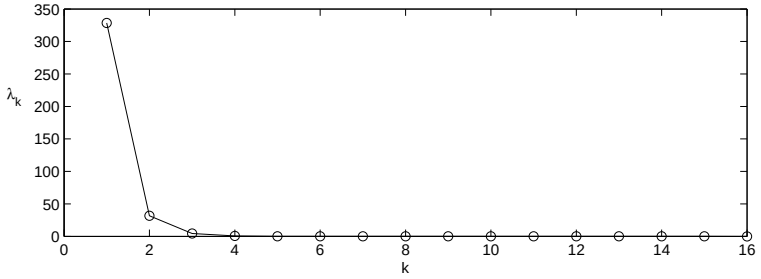

Figure 4.6: Eigenvalue spectra vs. the KL-modes for the two-dimensional activator-inhibitor model.

as:

$$\frac{\partial u^{(1)}}{\partial t} = D_1 \triangle u^{(1)} + \rho_1 \frac{u^{(1)} u^{(1)}}{(1 + \kappa_1 u^{(1)} u^{(1)}) u^{(2)}} - \mu_1 u^{(1)} + \sigma_1$$
$$\frac{\partial u^{(2)}}{\partial t} = D_2 \triangle u^{(2)} + \rho_2 u^{(2)} u^{(2)} - \mu_2 u^{(2)} + \sigma_2. \tag{4.17}$$

Here $\triangle = \partial^2/\partial x^2 + \partial^2/\partial y^2$ is the Laplace operator in a two-dimensional (x, y) orthonormal coordinate system. The parameters of the system are the diffusion constants D_1, D_2, removal rates μ_1, μ_2, cross-reaction terms ρ_1, ρ_2, basic production terms σ_1, σ_2 and the saturation constant κ_1.

The patterns on simulation are shown in Figure 4.4 which when subjected to the Karhunen-Loève decomposition yields the two-dimensional basis functions as shown in Figure 4.5.

4.3 Application of Karhunen-Loéve decomposition for Image Analysis

Two-dimensional images obtained from various sources are often found to be marred and noisy. As is the case of satellite images in the presence of cloud cover as a natural obstruction. Thus recovering a full image from a marred image when an ensemble of like images are provided is essential for further image analysis studies. Moreover, an even more demanding exercise is retrieving an image when the ensemble provided is itself marred and noisy. Here we utilize the methodology of Karhunen-Loève decomposition to identify an image by characterizing the significant coherent structures present in the data.

Let $\{\psi_n(\mathbf{x})\}$ be an ensemble of empirical eigenfunctions obtained from an ensemble of snapshots (images) given by $v_n\mathbf{x}$. Let an image $\phi(\mathbf{x})$ be represented as

$$\phi(\mathbf{x}) \approx \sum_{n=1}^{N} a_n \psi_n(\mathbf{x}) \tag{4.18}$$

where, the coefficients, a_n are obtained from the usual inner product,

$$a_n = (\phi, \psi_n) \tag{4.19}$$

and N represents the number of basis functions needed to reconstruct with sufficient accuracy. Let a masked image be described by

$$\tilde{\phi}(\mathbf{x}) = m(\mathbf{x})\phi(\mathbf{x}) \tag{4.20}$$

where, $m = 0$ on the mask and $m = 1$ elsewhere. Our aim is to write $\tilde{\phi}(\mathbf{x})$ as

$$\tilde{\phi}(\mathbf{x}) \approx m(\mathbf{x}) \sum_{n=1}^{N} \tilde{a}_n \psi_n(\mathbf{x}) \tag{4.21}$$

and determine the optimum set of coefficients $\tilde{a}_n$ which can no longer be evaluated via Eq. (4.19) since ψ_n are not necessarily orthogonal over the support of $\tilde{\phi}$, $s[\tilde{\phi}]$. We

intend to minimize the least square error defined as

$$E = \int_{s[\tilde{\phi}]} d\mathbf{x} \left(\tilde{\phi} - \sum_{n=1}^{N} \tilde{a}_n \psi_n \right)^2 \tag{4.22}$$

and the minimization of E requires

$$\left(\tilde{\phi} - \sum_{n=1}^{N} \tilde{a}_n \psi_n, \psi_k \right)_{s[\tilde{\phi}]} = 0 \tag{4.23}$$

which requires that the residual be orthogonal to ψ_k for $k = 1, \cdots, N$, and inner product is evaluated over the support of $\tilde{\phi}$, $s\tilde{\phi}$. The Hermitian matrix M is

$$M_{kn} = (\psi_k, \psi_n)_{s[\tilde{\phi}]} \tag{4.24}$$

is non-negative and we seek the unknown coefficients $\tilde{a}_k$ from

$$\mathbf{M}\tilde{\mathbf{a}} = \mathbf{f} \tag{4.25}$$

and we write

$$f_k = (\phi, \psi_k)_{s[\tilde{\phi}]}. \tag{4.26}$$

In the present case if we denote the eigenvalues by μ_n and corresponding eigenvectors by $\mathbf{v}_n$ and the solution is given by

$$\tilde{\mathbf{a}} = \sum_{k=1}^{N} \frac{1}{\mu_n} (\mathbf{v}_n, \mathbf{f}) \mathbf{v}_n. \tag{4.27}$$

In our study we have considered images obtained from the two-dimensional Gray-Scott model described in Eq. (4.16). To illustrate the nature of this construction we have considered an ensemble of $K = 35$ snapshots. Figure 4.7 shows the snapshot 1, 15 and 30 each having 100×100 pixels. This data set is subjected to KL decomposition and the corresponding ensemble of 35 eigenfunctions $\{\psi\}$ are obtained. The test/original image ϕ is masked by a randomly generated mask $m(\mathbf{x})$ and an

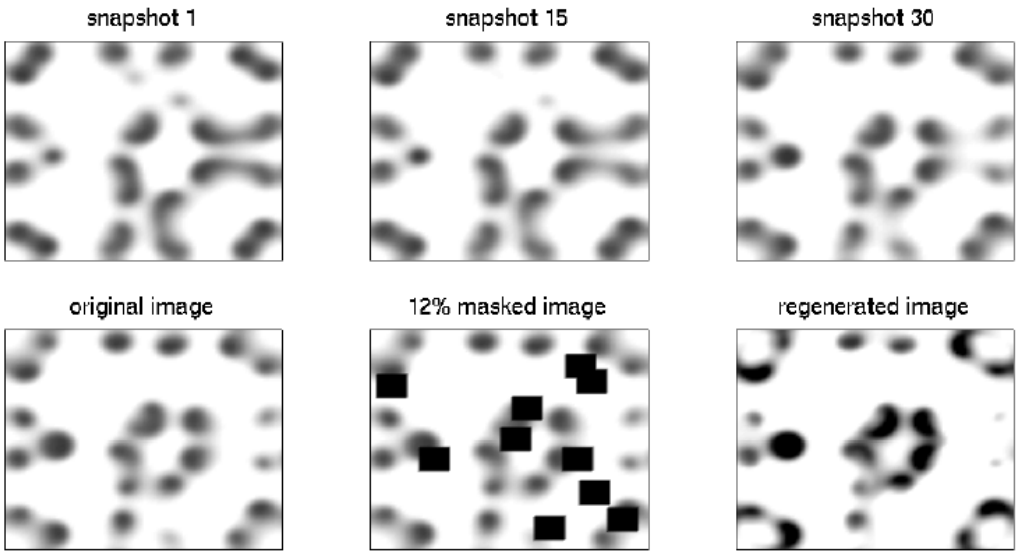

Figure 4.7: Reconstruction of a masked image using an ensemble of 35 images generated from the 2-D Gray-Scott model.

image with 12% mask is shown in Figure 4.7. It is to be noted that masked image is not an element in the set of snapshots considered for generating the eigenfunctions. We determine the coefficients $\tilde{\mathbf{a}}$ by the procedure described above and the image is reconstructed via Eq. (4.21) for a choice of $N = 10$ and the reconstructed image is shown in Figure 4.7.

The success of the above mentioned procedure owns to the fact that only a limited number of fitting functions are required in order to approximate the full image as the underlying empirical eigenspace is optimum. It is intuitively clear that an image with fairly high extent of masking cannot be reconstructed at finer scales. Since

eigenfunctions corresponding to higher KL-modes (*i.e.* increasing N) resolving at smaller scales using too many eigenfunctions can thus result in deterioration during reconstruction.

Now we explore the situation when the data set provided is obscured and hence the empirical eigenfunctions thus obtained from them are marred. Let the ensemble of marred faces be $\{\tilde{\phi}(\mathbf{x})\}$ and each of the marred face is of the form

$$\tilde{\phi}(\mathbf{x}) = m_n(\mathbf{x})\phi(\mathbf{x}) \tag{4.28}$$

where $\phi(\mathbf{x})$ is chosen from the original set of images. Here, we will numerically demonstrate the procedure of reconstructing images from the ensemble of marred images. Let us start by calculating the average value at pixel location $\mathbf{x}$ by

$$\langle\tilde{\phi}(\mathbf{x})\rangle = \frac{1}{M(\mathbf{x})}\sum_{n\in S[\mathbf{x}]}\tilde{\phi}_n(\mathbf{x}) \tag{4.29}$$

where, $S[\mathbf{x}]$ is the set of indices at which $m_n(\mathbf{x})$ is unity and $M(\mathbf{x})$ is the number of indices in this set at pixel location $\mathbf{x}$. We obtain the repaired ensemble $\{\tilde{\phi}_n^{(0)}(\mathbf{x})\}$ by missing values of $\tilde{\phi}_n(\mathbf{x})$ and subsequently apply Karhunen-Loéve decomposition on this repaired set to generate $\{\psi_n^{(0)}(\mathbf{x})\}$. Next we obtain $\{\tilde{\phi}_n^{(1)}(\mathbf{x})\}$ by a superposition of R eigenfunctions as

$$\hat{\phi}^{(1)} = \sum_{k=1}^{R} a_k^{(1)}\psi_k^{(0)}(\mathbf{x}) \tag{4.30}$$

and the set $\{a_k^{(1)}\}$ by minimization of the error function given by

$$\tilde{E}_n = \int(\tilde{\phi}_n - \hat{\phi}_n^{(1)})^2 m_n(\mathbf{x})d\mathbf{x}. \tag{4.31}$$

The repaired snapshot, is obtained by

$$\tilde{\phi}_n^{(1)}(\mathbf{x}) = \begin{cases} \tilde{\phi}_n\mathbf{x} & \text{if} \quad m_n(\mathbf{x}) = 1 \\ \hat{\phi}_n\mathbf{x} & \text{if} \quad m_n(\mathbf{x}) = 0 \end{cases} \tag{4.32}$$

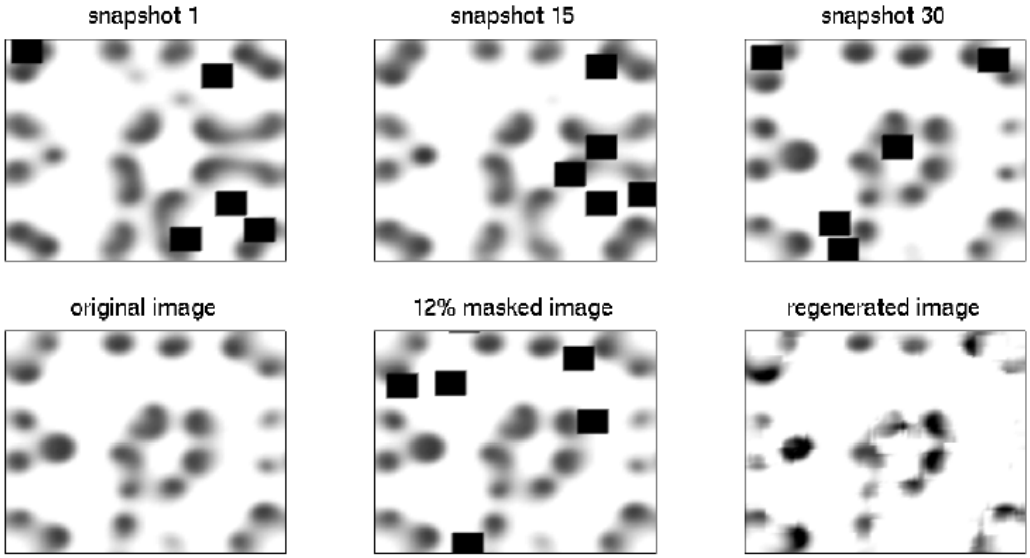

Figure 4.8: Reconstruction of a masked image using an ensemble of 35 masked images generated from the 2-D Gray-Scott model.

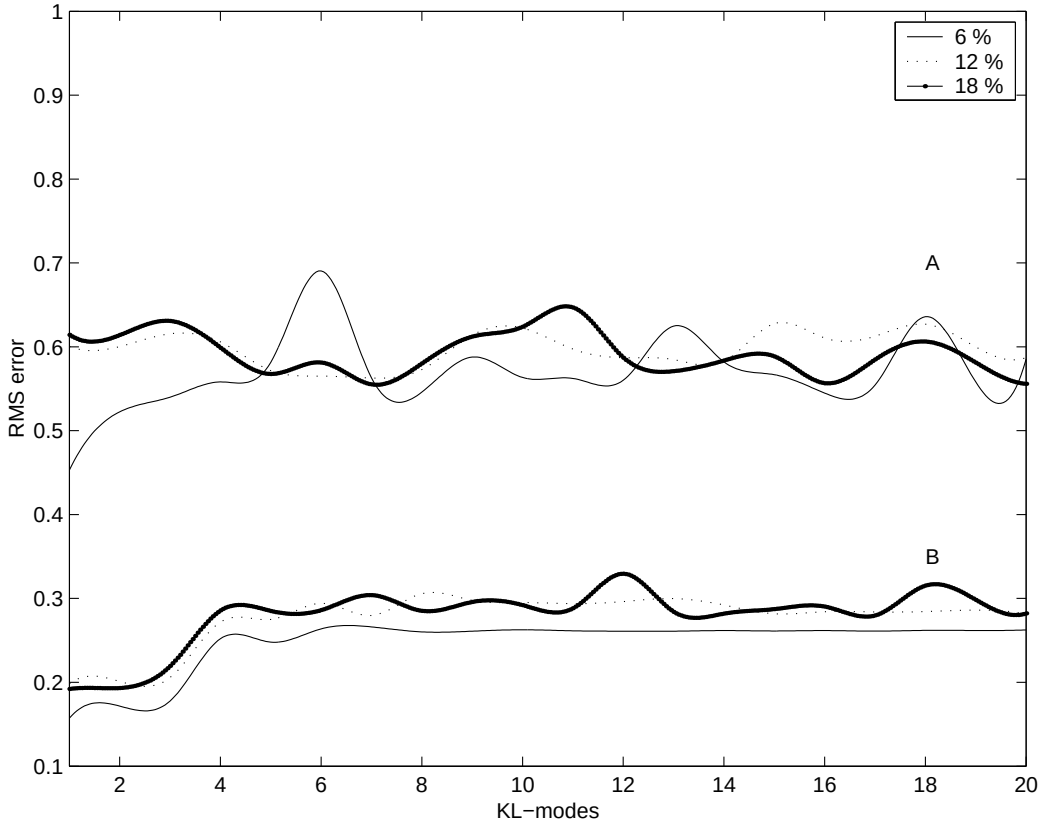

Figure 4.9: RMS error vs. KL-modes for masked image(100×100) using masked (A) and unmasked (B) ensemble of 35 snapshots for various percentage of masking.

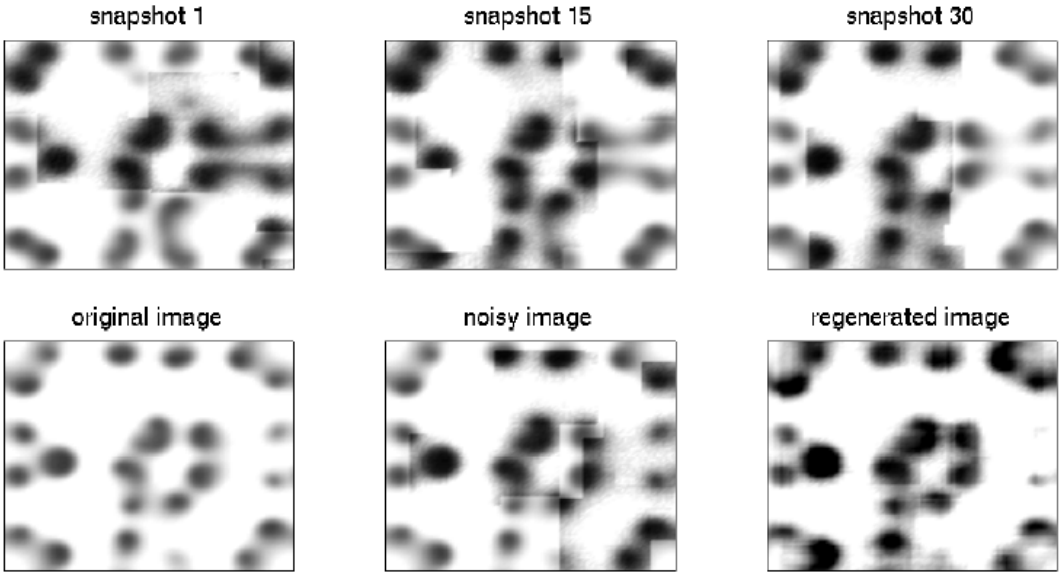

Figure 4.10: Reconstruction of a noisy image using an ensemble of 35 noisy images generated from the 2-D Gray-Scott model.

Thus the refined values of the eigenfunctions are obtained on an iterative basis and on reconstruction the image is retrieved. The results of this iterative scheme is exemplified for an ensemble of marred images as shown in Figure (4.8). The efficiency in reconstructing the images can be quantified by calculating the RMS error. The variation of RMS error with the number of KL-modes for masked images taken for analysis is shown in Figure (4.9). Another commonly encountered problem in surface characterization of various physical and chemical spatiotemporal systems is noisy images. The ensemble of snapshots considered for our study have been artificially made noisy by addition of randomly generated numbers. Extraction of information in the form of an cleaned image is also possible by the method outlined above. Here we take an ensemble of noisy images and try to extract the original image and the results are illustrated in Figure (4.10).

4.4 Conclusion

Introducing spatial coupling to simple logistic maps, a variety of dynamical features ranging from traveling wave to chaos can be seen. Even reaction diffusion systems modeling autocatalytic reaction or activation-inhibition in species have pattern forming capabilities for certain parameter ranges. By the Karhunen-Loève decomposition, we have demonstrated a methodology to extract the spatial features by identifying the coherent spatial structures in the data by suitable transformations to obtain a space-time separable form both for CMLSs and continuous time domain systems. This feature can be suitably used to obtain reduced description of high-dimensional systems as will be shown in Chapter 5. As a further application of this procedure we have addressed the problem of image analysis where marred or noisy images is encountered. We show that once the coherent structures are identified it is possible to extract the image within reasonable error bounds.

Chapter 5

Inverse Problem and Model Reduction for Reaction-Diffusion-Convective Systems

Once the "coherent structure" in a spatiotemporal data has been identified (Chapter 4) one would like to arrive at mathematical models, which are reduced descriptions of the original high-dimensional model, and address the inverse problem of parameter estimation (Chapter 3). This can be achieved by projecting the governing equations onto relevant modes by KL decomposition along with Galerkin projection (KLG). The use of empirical eigenfunctions as spatial basis functions are advantageous because of their orthogonal properties which lead to considerable simplification of the original high-dimensional model. We now show another profitable use of this approach for parameter estimation with reduced model descriptions of spatiotemporal systems and which advantageously uses subsystem data for the identification. For this purpose we develop the Karhunen-Loève and Galerkin Multiple Shooting approach (KLGMS) and exemplify it for a discrete time continuous variable coupled map lattice (CML) system, representative of reaction-diffusion-convective processes exhibiting turbulent dynamics, and a continuous time domain multi-variable system, such as the autocatalytic reaction-diffusion, exhibiting chaos discussed earlier in Chapter 4. The resulting

advantages in estimating parameters from small amounts of data from subsystems, availability of only scalar and noisy time series data, effects of space time parameter variations and in the presence of multiple time scales have been discussed. Apart from empirical eigenfunctions the use of wavelet basis functions have been studied because they are known to have superior space-time localization properties. The results of analysis show that wavelet basis functions can be used to further simplify the reduced model, whereby, the higher order derivatives can be estimated analytically using connection coefficients in conjunction with the wavelet transforms. The use of wavelet basis functions also is advantageous in terms of studying snapshots of system dynamics for long evolutions, synchronization properties of spatiotemporal dynamics, parameter estimation and multi-time scale features. Online estimates of parameters from processes would facilitate development of control strategies for highly complex dynamics.

The organization of the Chapter is as follows: In Section 5.1 we explain the procedure to obtain reduced model description of spatially extended systems described by set of partial differential equations. We incorporate the method of model reduction and parameter estimation by multiple shooting and formulate the KLGMS methodology in Section 5.2 and show its applicability to CML in Section 5.2.1 and continuous systems in one and two spatial dimensions in Section 5.2.2 and Section 5.2.3 respectively. In Section 5.3 the KLGMS methodology has been extended to situations where only scalar data is available and recovery of unmonitored data and estimation of parameters has been demonstrated.

5.1 Galerkin Projection

In numerical simulation of spatially extended reaction-diffusion-convection systems, one can integrate a finite set of differential equations, *i.e.* seek solutions on a finite

grid. One method that converts an infinite dimensional evolution equation or partial differential equation into a finite set of ordinary differential equations is that of Galerkin projection. In this procedure the functions defining the original equation are projected onto a finite-dimensional subspace of the full phase space. In deriving low-dimensional models we use subspaces spanned by the small sets of empirical eigenfunctions, as described in Chapter 4. However, Galerkin projection can be used in conjunction with any suitable set of basis functions as will be discussed later.

Let us suppose that the process is described by the following general model equation:

$$\frac{\partial v}{\partial t} = F(v, \mu) \tag{5.1}$$

where μ denotes the set of process parameters. Now let us truncate the KL-decomposition series Eq. (4.2) to the order $i = N$ (for $N < M$), so that,

$$v(t, \mathbf{x}) = \sum_{i=1}^{N} a_i(t)\phi_i(\mathbf{x}). \tag{5.2}$$

We next define the residual (or error due to truncation) as

$$r(t, \mathbf{x}) = \frac{\partial v(t, \mathbf{x})}{\partial t} - F(v(t, \mathbf{x}), \mu) \tag{5.3}$$

and shall attempt at minimizing this residual for the solution given in Eq. (5.2) by Galerkin projection. This may be carried out by forcing its projection on the subspace of truncated basis functions $\phi_i(\mathbf{x})$ to be zero at all time t, *i.e.*,

$$(r, \phi_i) = \int r(t, \mathbf{x})\phi_i(\mathbf{x})d\mathbf{x} = 0, \qquad i = 1, \cdots, N. \tag{5.4}$$

From Eq. (5.2) we get

$$\frac{\partial v}{\partial t} = \frac{\partial}{\partial t}\sum_{i=1}^{N} a_i(t)\phi_i(\mathbf{x}) = \sum_{i=1}^{N} \dot{a}_i(t)\phi_i(\mathbf{x}). \tag{5.5}$$

Eq. (5.3) may then be recast as,

$$r(t,\mathbf{x}) = \sum_{i=1}^{N} \dot{a}_i(t)\phi_i(\mathbf{x}) - F(\sum_{j=1}^{N} \dot{a}_j(t)\phi_j(\mathbf{x}), \mu), \tag{5.6}$$

and Eq. (5.5) as,

$$\begin{aligned}(r,\phi_i) &= \int \left[\sum_{j=1}^{N} \dot{a}_j(t)\phi_j(\mathbf{x}) - F(\sum_{k=1}^{N} a_k(t)\phi_k(\mathbf{x}), \mu)\right] \phi_i(\mathbf{x})d\mathbf{x} \\ &= \dot{a}_i(t) - \int F(\sum_{k=1}^{N} a_k(t)\phi_k(\mathbf{x}), \mu)\phi_i(\mathbf{x})d\mathbf{x} \end{aligned} \tag{5.7}$$

Thus, from Eq. (5.3) we obtain the equations that may be used for solving for the desired coefficients, *i.e.*, the a's, *viz.*

$$\dot{a}_i(t) = \int F(\sum_{k=1}^{N} a_k(t)\phi_k(\mathbf{x}), \mu)\phi_i(\mathbf{x})d\mathbf{x}, \qquad i = 1, \cdots, N. \tag{5.8}$$

It is to be noted that for known initial conditions $v^0(\mathbf{x})$, $a_i(0)$, for the above can be independently obtained by forcing the initial residue $I(\mathbf{x})$, given as $I(\mathbf{x}) = v^0(\mathbf{x}) - v(0,\mathbf{x})$, also to have zero projection on the space of ϕ_i:

$$\begin{aligned}(I,\phi_i) &= \int \left[v^0(\mathbf{x}) - v(0,\mathbf{x})\right] \phi_i(\mathbf{x})d\mathbf{x} \\ &= \int \left[\sum_{j=1}^{N} a_j(0)\phi_j(\mathbf{x}) - v(0,\mathbf{x})\right] \phi_i(\mathbf{x})\mathbf{dx} \\ &= 0 \\ \Rightarrow a_i(0) &= \int v(0,\mathbf{x})\phi_i(\mathbf{x})d\mathbf{x}. \end{aligned} \tag{5.9}$$

Thus the task is now reduced to solving (for $N < M$) a set of of ODE's in time t.

5.2 Karhunen-Loève Galerkin Multiple Shooting

In this section we use a reduced description of the spatiotemporal system (Eq.(5.8)) which can be used for the purpose of parameter estimation. Such a reduced description has been obtained by Galerkin's projection of the model in conjunction with the

KL decomposition [Eq. (4.2)] and we shall discuss the steps involved in this procedure separately for discrete CML type systems and for continuous systems modeled by PDEs.

A CML model with discrete space index j and time n may be written in a general form as

$$u^{(i)}(n+1,j) = g(u^{(1)}(n,j+j'), u^{(2)}(n,j+j'), \cdots, \mu), \tag{5.10}$$

where, $j' = \cdots, -2, -1, 0, 1, 2, \cdots$ and g any function with $\mu = \{\mu_1, \mu_2, \cdots, \mu_p\}$ the model parameters. The boundary conditions for Eq. (5.10) are generally dependent on the example being studied and we show cases involving periodic and open flow (as in convection) boundary conditions. In the KL-Galerkin's method we minimize the residual by forcing the projection of the model on the subspace of truncated basis functions $\phi_k^{(i)}(j)$ to be zero at all time n and obtain $N < M$ KL-Galerkin equations for the CML model described by Eq. (5.10) as

$$a_k^{(i)}(n+1) = \sum_{j=1}^{L} [g(\sum_{l=1}^{N} a_l^{(1)}(n)\phi_l^{(1)}(j) + \bar{u}^{(1)}(j), \cdots, \mu) - \bar{u}^{(i)}(j)]\phi_k^{(i)}(j) \tag{5.11}$$

where the use of the orthonormal property of the basis functions allows considerable simplification. The initial conditions for solving the map [Eq. (5.11)] can be obtained as in Eq.(5.9) by forcing the initial residual to have zero projection on the space of basis functions, *i.e.*, $a_k^{(i)}(0) = \sum_{j=1}^{L} v^{(i)}(0,j)\phi_k^{(i)}(j)$.

For continuous systems in both space x and time t, the mathematical model can be written in general form as PDE's with appropriate boundary conditions, *viz.*,

$$\dot{u}^{(i)}(t,x) = h(u^{(1)}(t,x), u^{(2)}(t,x), \cdots, \mu) \tag{5.12}$$

and the corresponding KL-Galerkin equations are obtained by projection as

$$\dot{a}_k^{(i)}(t) = \int h(\sum_{l=1}^{N} a_l^{(1)}(t)\phi_l^{(1)}(x) + \bar{u}^{(1)}(x), \cdots, \mu)\phi_k^{(i)}(x)dx. \tag{5.13}$$

Here again $N < M$ equations form a simpler and reduced model incorporating system parameters μ. Note that the summation in Eq. (5.11) for discrete systems becomes an integral for continuous ones, *i.e.*, $(\phi_l^{(i)}, \phi_m^{(i)}) = \int_0^1 \phi_l^{(i)}(x)\phi_m^{(i)}(x)dx$ with the $(\cdot,\cdot)$ now denoting the usual $\mathbf{L}^2([0,1])$ inner product space [Hol96] defined in spatial domain $0 \leq x \leq 1$. The initial conditions for solving Eq. (5.13) may again be independently obtained by $a_l^{(i)}(0) = \int v^{(i)}(0,x)\phi_l^{(i)}(x)dx$.

We next discuss the use of the simpler KL-Galerkin models in the time-dependent coefficients $a_k^{(i)}(n)$ [*i.e.*, [Eq. (5.11) for CML or Eq. (5.13) for a continuous system], along with the known coefficient values $b_k^{(i)}(n)$ obtained from the data by $b_k^{(i)}(n) = a_k^{(i)}(n) = (v^{(i)}(n,j), \phi_k^{(i)}(j))$ for the estimation of parameters μ for the respective spatiotemporal dynamics [*i.e.*, Eq. (5.10) or Eq. (5.12)]. We show that this is possible by using an effective algorithm in parameter estimation for low-dimensional nonlinear dynamical systems, *viz.*, the multiple shooting algorithm formulated as a multipoint boundary value problem with nonlinear constraints for optimization [Baa92] and illustrated earlier in Section 3.1. The algorithm curtails error propagation observed in chaotic dynamics and offers advantages in terms of number of data points required, negating effects of noise, handling missing data situations, and stopping at local minima during optimization [Tim98, Tim00].

For the CML model [Eq. (5.10)], the observations in the discrete time interval $[n_1, n_M]$ may be chosen to form a grid for M multiple shooting-points at $n_1 < n_2 < \cdots < n_l < \cdots < n_M$ nodes forming $(M-1)$ sets of initial value problems in the form of [Eq. (5.11)] for each of the shooting nodes n_l with $1 \leq l \leq M-1$. That is, on considering $k = 1, 2, \cdots, N$ spatial basis modes for $N < M$, we obtain for a i^{th} variable $N(M-1)$ maps to be solved

$$a_k^{(i)}(n+1) = \mathcal{G}(a_k^{(i)}(n), \phi_k^{(i)}(j), \bar{u}^{(i)}(j), \mu) \qquad a_k^{(i)}(n_l) = s_k^{(i)}(l), \tag{5.14}$$

for an incremental time-step $n \to n+1$. Here, $s_k^{(i)}(l)$ denotes the value of the i^{th}

variable at the l^{th} shooting-point for k^{th} basis mode and initial guesses for solving $N(M-1)$ maps of Eq. (5.14) are taken to be the known values of $b_k^{(i)}(l)$. It may be noted that for the system governed by PDEs and data available at shooting points $\tau_1 < \tau_2 \cdots < \tau_l < \cdots < \tau_M$ and which are monitored at time $n\Delta t$, the corresponding set of $N(M-1)$ initial value problems may be written as

$$\dot{a}_k^{(i)}(t) = \mathcal{H}(a_k^{(i)}(t), \phi_k^{(i)}(x), \bar{u}^{(i)}(x), \mu), \qquad a_k^{(i)}(\tau_l) = s_k^{(i)}(l). \tag{5.15}$$

We can construct an augmented vector of initial values s and parameters μ for either model Eq. (5.10) or Eq. (5.12), *viz.*,

$$\mathbf{z} = (s_1^{(1)}(1), s_1^{(1)}(2), \cdots, s_1^{(1)}(M), s_1^{(2)}(1), s_1^{(2)}(2), \cdots, \mu_1, \mu_2, \cdots, \mu_p) \tag{5.16}$$

and attempt to minimize a least square cost function $\mathcal{L}_2(\mathbf{z})$ in Eq. (3.31) now assuming the form

$$\mathcal{L}_2(\mathbf{z}) = \sum_{i=1,2,\cdots} \sum_{k=1}^{N} \sum_{n=1}^{M} \frac{1}{\sigma_{kn}^{(i)}} [b_k^{(i)}(n) - \mathcal{F}_k^{(i)}(a(n), \mu)]^2, \tag{5.17}$$

where, $\mathcal{F}_k^{(i)}$ is a function relating components of $\mathcal{G}$ in Eq. (5.14) or $\mathcal{H}$ in Eq. (5.15) and comparing to the known $b_k^{(i)}(n)$ with $\sigma_{kn}^{(i)}$ the square of the standard deviation. The minimization in Eq. (5.17) is carried out subject to satisfying

$$a^{(i)}(n_{l+1}) - s^{(i)}(l+1) \to 0 \tag{5.18}$$

so that the trajectories in the coefficients $a^{(i)}(n_{l+1})$ become continuous. Alternatively stated, by identifying $\mathbf{y}_1(\mathbf{z}) = r(s_1^{(i)}(1), s_2^{(i)}(2), \cdots, s_N^{(i)}(M), \mu_1, \mu_2, \cdots, \mu_p)$ and $\mathbf{y}_2(\mathbf{z}) = a^{(i)}(n_{l+1}) - s^{(i)}(l+1)$ we obtain, a standard nonlinear minimization problem [Pow78] of the type

$$\min_{\mathbf{z}} \{ \| \mathbf{y}_1(\mathbf{z}) \|_2^2 \mid \mathbf{y}_2(\mathbf{z}) \to 0 \} \tag{5.19}$$

where the minimization of $\mathbf{y}_1(\mathbf{z})$ corresponds to minimizing the cost function Eq. (5.17) while that for $\mathbf{y}_1(\mathbf{z})$ implies satisfying the constraints imposed by Eq. (5.18). The

minimization of Eq. (5.19) can be carried out by starting with initial guess values $\mathbf{z}^{(0)}$ and iterating for $\mathbf{z}$ using $\mathbf{z}^{(q+1)} = \mathbf{z}^{(q)} + \omega^{(q)}\Delta\mathbf{z}^{(q)}$ where, $\omega^{(q)} \in [0, 1]$ are damping factors. In doing so corrections to the augmented vector $\mathbf{z}$, *viz.*, $\Delta\mathbf{z}^{(q)}$ are obtained by solving the linearized problem

$$\min_{\mathbf{z}}\{\| \mathbf{y}_1(\mathbf{z}^{(q)}) + \frac{\partial \mathbf{y}_1(\mathbf{z}^{(q)})}{\partial \mathbf{z}}\Delta\mathbf{z}^{(q)} \|_2^2 \quad | \quad \mathbf{y}_2(\mathbf{z}^{(q)}) + \frac{\partial \mathbf{y}_2(\mathbf{z}^{(q)})}{\partial \mathbf{z}}\Delta\mathbf{z}^{(q)} \to 0\} \tag{5.20}$$

The above Eq. (5.20) may be solved by a suitable nonlinear optimization technique in the optimization variables, $\mathbf{z}$ [Eq. (5.16] for arbitrary guess values for the parameters μ and initial states $s_k^{(i)}(l) = b_k^{(i)}(l)$. In the coding of the above KLGMS approach, we have employed the successive quadratic programming algorithm [Sch86] coupled with numerical differentiation for the sensitivity matrices. For illustration, we have retained simplicity in the cost function [Eq. (5.17)] but more effective functionals [Mcs99] may be adopted in optimizing for the parameters μ. It is to be noted that the methodology also allows optimizing for the $s_k^{(i)}(l)$ even when some values of $b_k^{(i)}(l)$ are initially not available and arising due to missing snapshot data in say some i^{th} variable.

The KLGMS methodology can be schematically represented as:

$$\underbrace{\begin{array}{l} \textit{Step}.1 \text{ Model :} \\ \frac{\partial v}{\partial t} = F(v, \mu) \rightarrow \end{array} \left[\begin{array}{c} \textit{Step}.2 \\ \text{Spatiotemporal data } v(t, \mathbf{x}) \\ \\ \textit{Step}.3 \text{ Basis functions} \\ C \text{ matrix} \rightarrow \phi_k(\mathbf{x}) \end{array}\right]}_{\textit{Step}.5 \text{ Galerkin projection :}\ \dot{a}_i(t) = \int F(\sum_{k=1}^{N} a_k(t)\phi_k(\mathbf{x}), \mu)\phi_i(\mathbf{x})d\mathbf{x}} \longrightarrow \begin{array}{l} \textit{Step}.4 \text{ Observations :} \\ b_k(t) = (v(t, \mathbf{x}), \phi_k(\mathbf{x})) \\ \\ \downarrow \\ \\ \textit{Step}.6 \text{ Multiple Shooting} \\ \\ \downarrow \\ \\ \text{Estimated parameters } \mu \end{array}$$

Table 5.1: Parameter estimation for the CML with varying dynamics. Error bounds for arbitrary initial guesses are shown.

case		F	D_d
(a)	Weakly chaotic	1.73 ± 0.01	0.40 ± 0.02
	with noise	1.74 ± 0.03	0.39 ± 0.02
(b)	Traveling wave	1.50 ± 0.01	0.50 ± 0.01
	with noise	1.54 ± 0.03	0.53 ± 0.04
(c)	Fully chaotic	1.99 ± 0.01	0.40 ± 0.01
	with noise	2.03 ± 0.04	0.38 ± 0.03

5.2.1 Discrete System: Coupled Map Lattice

Studies with KL-Galerkin Eq. (5.11) for the CML Eq. (4.15) using the KLGMS approach did accurately and simultaneously estimate the unknown parameters (F, D_d, D_c) from a few snapshots of the data. The results of convergence for arbitrary and different initial guesses for the parameters shown in Table 5.1 for the *(a)* weakly chaotic, *(b)* traveling wave and *(c)* fully developed chaos cases.

The robustness is seen when parameters were successfully estimated even for noisy spatiotemporal data sets [Table 5.1] obtained by additive noise $\hat{u}(n,j) = u(n,j) + \eta$ with Gaussian distribution noise $\eta \in N[0, \varepsilon^2]$. The strength of the noise level used was determined by $\sigma_{noise}/\sigma_{data}$ and chosen to be 0.01. It may be observed that noise in the data enters through the "coefficient trajectories" $b_k(l)$ that are obtained by the convolutions of the fluctuating data $v(n,j) = u(n,j) - \bar{u}(j)$ with the basis functions $\phi_k^{(i)}(j)$. It is to be noted that although the functional form of the CML in the form of Eq. (4.15) is single dimensional and single variable the procedure may be extended to situations involving multi-variable mappings Eq. (5.10) and higher spatial dimensions. The effects of considering higher spatial dimensions do not change the methodology because the KL decomposition yields two or three-dimensional spatial basis functions $\phi(i,j,k)$ but the Galerkin equation still retains the mapping form of Eq. (5.11) in the time-dependent coefficients $a_k(n)$.

The presence of scaling relationships in Lyapunov exponents as a function of subsystem size have been studied [Bau91, Par98, Car99]. For KL decomposition modes, using the spatial correlation matrix, a linear relationship in KL dimension [Zol97] has also been seen. Our studies for subsystem scaling with the temporal correlation matrix, C_{lm}, showed some interesting features. We observe that $\mathcal{D}_T = \max\{N : \eta_N \leq f\}$ required to capture a fraction f of the total variance showed scaling behavior after an optimum subsystem size before saturation. The saturation occurs either due to the dynamics being not complicated enough to warrant all modes to be included as a function of subsystem size or alternatively when the dynamics is sufficiently complex that all KL modes (limited by the number of snapshots M) are required. Therefore, depending on the complexity of the pattern and number of snapshots, M, an optimum subsystem size exists beyond which only system features can be extracted reliably. The feasibility of estimating parameters by relaxing the need for data from the entire spatial domain was then considered. Thus, on computing $\mathcal{D}_T$ for the convective CML data as a function of subsystem size j for $L = 80$ we observed that beyond $j = 30$ there is linear scaling and this determines the optimum subsystem size. For this subsystem size even with a lower number of modes($\approx N = 15$), parameter values could be estimated, while for larger subsystem size all KL modes need to be considered.

Figure 5.1*(a)* shows the subsystem data for the central 31 lattice sites and used for parameter estimation purposes for $N = 15$. The accurate convergence of the estimated parameters F, D_d and D_c with search iterations is shown in Figure 5.1*(b-d)* and reported as the homogeneous case *(a)* in Table 5.2. These studies suggest that when reliability of data is poor from certain regions, considerable information may be gained by using only authentic data available from other subsystems in the spatial domain.

A number of real situations have inhomogeneous distribution of parameter values

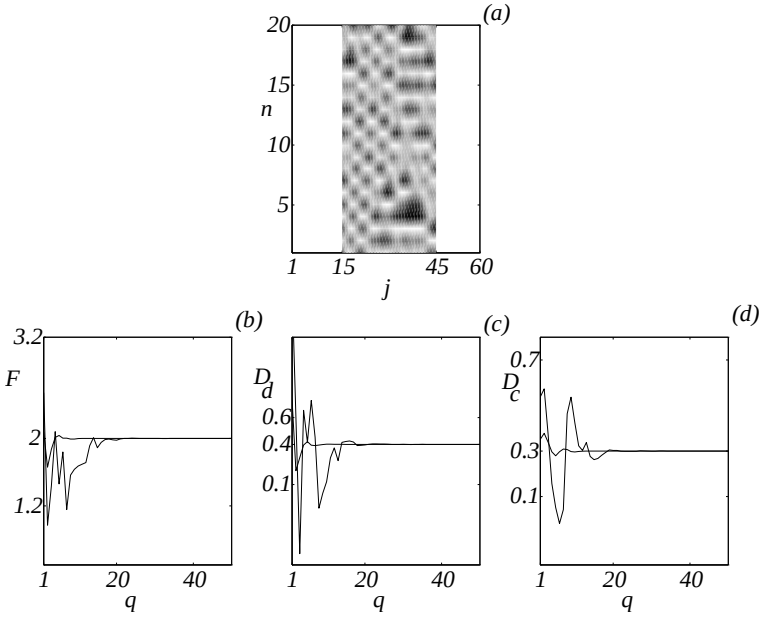

Figure 5.1: Parameter estimation for convective turbulence. *(a)* Subsystem data for the central 31 lattice sites; *(b,c,d)* Simultaneous convergence to parameter estimates for F, D_d and D_c for arbitrary initial guesses (shown as y-axis labels) as iterations q proceed for minimizing the least square functional.

Table 5.2: Parameter estimation from subsystem CML data for convective turbulence. Error bounds for arbitrary initial guesses are shown.

case		F	D_d	D_c
(a)	Homogeneous	1.99 ± 0.02	0.41 ± 0.03	0.32 ± 0.03
(b)	Inhomogeneous left	1.99 ± 0.03	0.39 ± 0.02	0.29 ± 0.04
(c)	Inhomogeneous right	1.88 ± 0.03	0.42 ± 0.04	0.28 ± 0.04

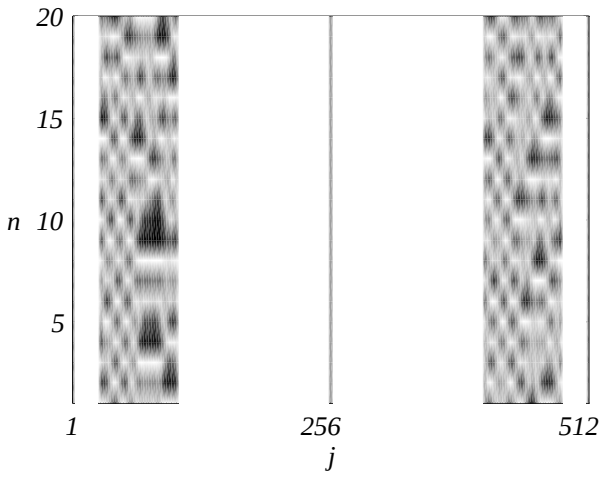

Figure 5.2: Data from the left ($F = 2.0$) and the right ($F = 1.9$) subsystems for the inhomogeneous CML. The vertical line at $j = 256$ marks the boundary; Other parameter values $D_d = 0.4$, $D_c = 0.3$.

in space and/or slowly varying in time domain [Mex00]. Studies in this context for parameter estimation were carried out and the analysis of a simple example is discussed here. We evolve a CML such that the sites in the left half (*i.e.*, $1 \leq j \leq 256$) have $F = 2.0$ while the right half (*i.e.*, $257 \leq j \leq 512$) evolve data with $F = 1.9$ for $L = 512$.

Subsystem data from each half [Figure 5.2] was used for parameter estimation. Since the local dynamics propagate in space, the data obtained form both subsystems had composite features leading to inconsistent and unreliable parameter estimates. To overcome this difficulty we recorded data immediately after a giving a perturbation at time n (*i.e.*, noise of strength 0.01) to the variable $u(n, j)$ and then carried out KLGMS parameter estimation for each of the subsystems (left and right). The results presented in Table 5.2 cases *b,c* show that parameter estimation is now possible. Studies were also carried out for situations modeling F as a slowly varying parameter in time. The need to record subsystem data at optimum time gaps was found necessary to monitor the slow parametric changes. In real situations, repeated parameter

estimations at sufficient time intervals can help in establishing relationships in the nature of parametric variations and this can considerably aid system analysis.

5.2.2 One-dimensional Reaction-Diffusion system: Gray-Scott Model

For our study of parameter estimation we shall illustrate the methodology for a prototype reaction-diffusion model where one chemical species grows autocatalytically on another species [Gra90, Maz96]. This model is a simplification of the model of glycolysis proposed by Selkov [Sel68] and it follows the reaction mechanism $U + 2V \rightarrow 3V$; $V \rightarrow P$ with a continuous supply of the reactant U and removal of product P. The model has been extensively studied from the point-of-view of pattern formation and comparisons with features observed in experimental data have also been attempted [Lee94].

Here we will also consider situations where only scalar data in a single variable $u^{(1)}(t,x)$ is monitored. Because the data in the $u^{(2)}(t,x)$ is not available we need to use basis functions other than empirical. In the present study, we choose to exemplify KLGMS using Fourier basis functions defined as

$$\phi_k^{(i)}(x) = \sqrt{2}\sin(2\pi k x) \tag{5.21}$$

with temporal coefficients obtained by

$$b_k^{(i)}(t) = a_k^{(i)}(t) = \int_0^L v^{(i)}(t,x)\phi_k^{(i)}(x)dx \tag{5.22}$$

and use the $b_k^{(i)}(t)$ as observable in evaluating the least square functional in Eq.(5.17). For the model Eq. (4.16) the KL Galerkin projection equations for the time-dependent coefficients *i.e.,* Eq. (5.13), for modes $k = 1, 2, \cdots, N$ can be written as (suppressing (x) and (t)):

$$\dot{a}_i^{(1)} = \int_0^L [D_u \nabla^2 (\sum_{k=1}^{N} a_k^{(1)}\phi_k^{(1)} + \bar{u}^{(1)}) - (\sum_{k=1}^{N} a_k^{(1)}\phi_k^{(1)} + \bar{u}^{(1)})(\sum_{k=1}^{N} a_k^{(2)}\phi_k^{(2)} + \bar{u}^{(2)})^2$$

$$+f(1-\sum_{k=1}^{N} a_k^{(1)}\phi_k^{(1)} - \bar{u}^{(1)})]\phi_i^{(1)}dx$$

$$\dot{a}_i^{(2)} = \int_0^L [D_v\nabla^2(\sum_{k=1}^{N} a_k^{(2)}\phi_k^{(2)} + \bar{u}^{(2)}) + (\sum_{k=1}^{N} a_k^{(1)}\phi_k^{(1)} + \bar{u}^{(1)})(\sum_{k=1}^{N} a_k^{(2)}\phi_k^{(2)} + \bar{u}^{(2)})^2$$
$$-(f+k)(\sum_{k=1}^{N} a_k^{(2)}\phi_k^{(2)} + \bar{u}^{(2)})]\phi_i^{(2)}dx \quad (5.23)$$

and a reduced $N < M$ set of ODEs solved by integrating using the initial conditions discussed for Eq. (5.13).

Our studies with the set of Galerkin equations Eq. (5.23) with KLGMS for estimating system parameters using the spatiotemporally chaotic data showed two interesting features described below. Firstly, accurate parameter estimation of the diffusion coefficients (D_u, D_v) did not particularly depend on the choice of (k, f) when initial transient data was chosen as snapshots with the diffusion mechanism playing a significant role. It was also observed that similar results in estimating (k, f) were obtained using snapshots after giving perturbation to the system state $u^{(1)}(t, x)$ at any time t. The second feature was that having evaluated (D_u, D_v) in the above fashion the other two parameters (f, k) could be successfully estimated using post-transient data. These observations suggest that diffusion rates and reaction rates occur at differing time-scales and clearly point to the need for suitable data sampling strategies. It may be noted that the values of diffusion coefficients employed here lie in typical ranges. The multiple time-scale features discussed above may therefore be expected to be frequently present in the dynamics of spatiotemporal systems. Any methodology seeking model identification would need to consider this relevant aspect for parameter estimation.

Without any ambiguity, we discuss other features of the KLGMS with reference to evaluating f and k from monitored post-transient data. The KL decomposition of the data set using Fourier modes for 40 snapshots showed that a single Fourier basis mode

Table 5.3: Parameter estimation for the autocatalytic reaction-diffusion system. Error bounds for arbitrary initial guesses are shown.

case	data used	noise level	f	k
(a)	$u^{(1)}(x,t)$	0.00	0.0290 ± 0.0001	0.0535 ± 0.0001
	$u^{(2)}(x,t)$	0.02	0.0291 ± 0.0001	0.0537 ± 0.0001
		0.05	0.0296 ± 0.0003	0.0540 ± 0.0003
(b)	$u^{(1)}(x,t)$	0.00	0.0291 ± 0.0002	0.0538 ± 0.0003
		0.02	0.0296 ± 0.0005	0.0565 ± 0.0003
		0.05	0.0303 ± 0.0008	0.0610 ± 0.0003
(c)	$u^{(1)}(x,t)$	0.00	0.0295 ± 0.0002	0.0540 ± 0.0002
	$0.25 < x < 0.75$	0.02	0.0307 ± 0.0008	0.0578 ± 0.0002
		0.05	0.0321 ± 0.0008	0.0614 ± 0.0003

could reconstruct the data snapshots accurately ($> 99.8\%$). Results of parameter estimation with this single mode considered showed that accurate convergence was consistently possible even when the data was corrupted with noise of the order of 5% and are summarized in Table 5.3 case *a*.

For the present reaction-diffusion system we have observed that the use of Fourier basis functions allows tolerance for higher noise levels when compared to empirical basis functions (using correlation matrices). A more practical problem arises in multi-variable systems when only one dynamical variable is monitored. We assume that $u^{(2)}(t,x)$ is not monitored and assign initial guesses for the temporal coefficients $a^{(2)}(t) = 0.2$ and $\bar{u}^{(2)} = 0$ for the multiple shooting algorithm. The least square functional Eq. (5.17) and equality constraints are suitably modified so as to take into account only terms in variables $u^{(1)}(t,x)$. Results of the study presented in Table 5.3 case *b* showing accurate parameter estimation is again possible for both f, k although with a small decrease in noise tolerance. It may be seen that the parameter estimation of k present only in the $u^{(2)}$ equation of the PDE model Eq. (4.16) is also possible. Importantly, we have recovered the unmonitored variable $u^{(2)}(t,x)$ using Eq. (4.2) and the estimated values of $a^{(2)}(t)$ by multiple shooting.

Similar to the studies using CML we attempted to evaluate parameters using sub-

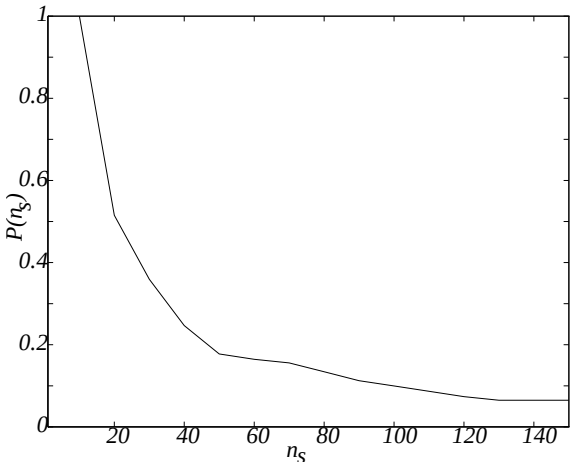

Figure 5.3: Power $P(n_s)$ in the first mode of the temporal coefficients, normalized to the maximum, is plotted as a function of subsystem size n_s.

system data with only scalar variable data in $u^{(2)}(t,x)$ available. An indication of the optimum subsystem size in this study using Fourier basis functions was suggested on evaluating the normalized power $P(n_s) = \int [a_1^{(1)}(t)]_{n_s}^2 dt$ as a function of the subsystem size n_s and is shown in Figure 5.3.

The results indicate a near saturation beyond $n_s = 80$. The results of KLGMS carried out with subsystem scalar data available only in $u^{(1)}$ and with noise (Table 5.3 case c) shows that parameter estimation within reasonable error bounds is still possible.

5.2.3 Two-dimensional Reaction-Diffusion System: Activator-Inhibitor Model

The KLGMS methodology for parameter estimation is shown for the snapshot data obtained on integrating the activator-inhibitor model Eq.(4.17), for the parameter values given in Table 5.4. In the simulation, periodic boundary conditions are assumed and initial conditions are given by the homogeneous steady state of the system. The fields of spatial dimension are taken as 64×64 and 16 snapshots are stored at time-

Table 5.4: Parameter values for simulating the activator-inhibitor model.

α	D_α	ρ_α	μ_α	σ_α	κ_α
1	0.005	0.01	0.01	0.0	0.0
2	0.2	0.02	0.02	-	-

Table 5.5: Converged values and error in parameter estimation for the activator-inhibitor model.

	α	D_α	ρ_α	μ_α
(a)without noise	1	0.0052 ± 0.0003	0.0103 ± 0.0007	0.0102 ± 0.0007
	2	0.2000 ± 0.0008	0.0207 ± 0.0014	0.0201 ± 0.0010
(b)with noise	1	0.0046 ± 0.0004	0.0106 ± 0.0011	0.0105 ± 0.0009
	2	0.2010 ± 0.0013	0.0206 ± 0.0019	0.0203 ± 0.0020

interval of 0.1 after discarding 10000 transients. The results of parameter estimation using KLGMS are shown in Table 5.5(a). The robustness of the methodology is shown for data frames is corrupted with noise (5%) and the results of the parameter estimation in this situation are shown in Table 5.5(b).

5.3 Wavelet Based Multiple Shooting: Synchronization and Parameter Estimation

A frequently encountered practical problem in multi-variable systems is that all process variables cannot be monitored simultaneously in the spatial domain. Determination of empirical basis functions (Section 4.1) of the unmonitored variables is not possible. An alternative approach would be to write Eq. (4.2) in terms of other suitable mathematical orthogonal functions such as Chebyshev polynomials, Fourier modes or wavelet functions [Hol96, Wit98]. The potential difficulty in using Fourier basis functions is that they are spatially localized and therefore is not a convenient choice for extracting features of the dynamics which arise due to spatially localized interactions. Wavelet basis functions, on the other hand, due to their superior space time localization properties [Dau92] provide a better alternative. In contrast to KLD

methods outlined in Section 4.1 wavelet basis functions, however, do not form an *optimized* basis. But they can still be used advantageously for accurately characterizing coherent structures as seen by definite peaks being formed in the power spectrum at respective wavelet scales [Wit98a].

We assume that any spatiotemporal data can be expanded in terms of wavelet functions Ψ_{jk} (Section 2.2), in a separable form in the following way

$$v(t,x) = \sum_{j=0}^{J} \sum_{k=0}^{2^j-1} a_{jk}\Psi_{jk}(x) = \sum_{\alpha=0}^{K-1} a_\alpha(t)\Psi_\alpha(x). \tag{5.24}$$

The index α is a multi-index for (j,k) and a notation equivalence is given by $\alpha = 2^j + k$. Here $J < p$ is a small-scale cutoff required to obtain a finite decomposition such that accurate representation of $v(t,x)$ is possible for $K = 2^J$ while $K = 2^p$ corresponds to the maximum value of the number spatial grid points N. Here $\Psi(x)$ are the coherent structures present in the system and $a(t)$ are the time dependent coefficients. Keeping in mind the fact that experimental measurements yield only a discrete and finite set of data, from now on $v(t,x)$ will be represented as an ensemble of snapshots $\{v_n(x)\}$ where $n = 1, 2, \cdots, M$, for M number of snapshots.

The time dependent coefficients $a_\alpha(t)$ in Eq.(5.24) are determined by

$$a_\alpha(t) = \int v_n(x)\Psi_\alpha(x)dx. \tag{5.25}$$

In the present study we have chosen Daubechies wavelet with four filter coefficients [Pre92] and the wavelet functions for the index α taking values 5, 9 and 23 is shown in Figure 5.4 (a), (c) and (e) respectively and the corresponding time dependent coefficients are shown in Figure 5.4 (b), (d) and (f) for the reaction-diffusion system given by Eq.(4.16).

The coherent structures if present in a particular wavelet scale is revealed by a definite peak forming in the wavelet power spectrum calculated as $P_j(t) = \sum_k a_{jk}^2(t)$. The choice of the small scale cutoff J can now be inferred from the power spectrum

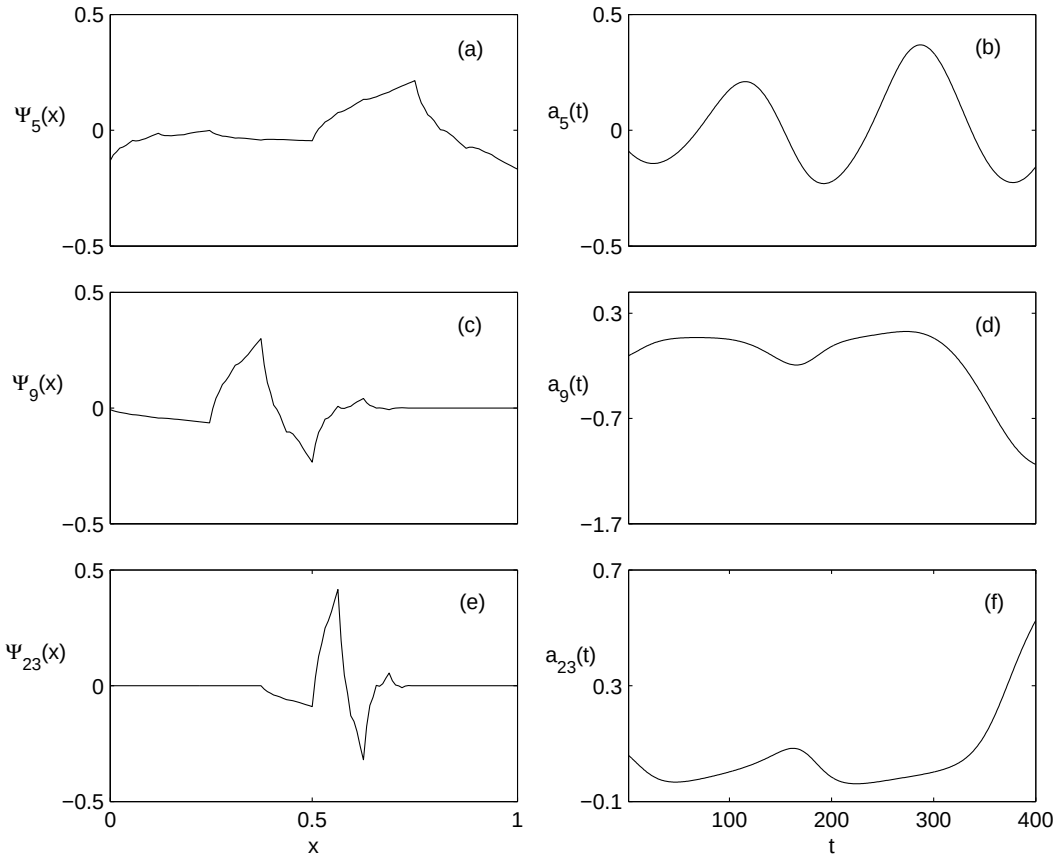

Figure 5.4: (a), (c), (e) The wavelet functions (Daubechies-4) for the index α taking values 5, 9 and 23. (b), (d), (f) The time dependent coefficients for the index α taking values 5, 9 and 23.

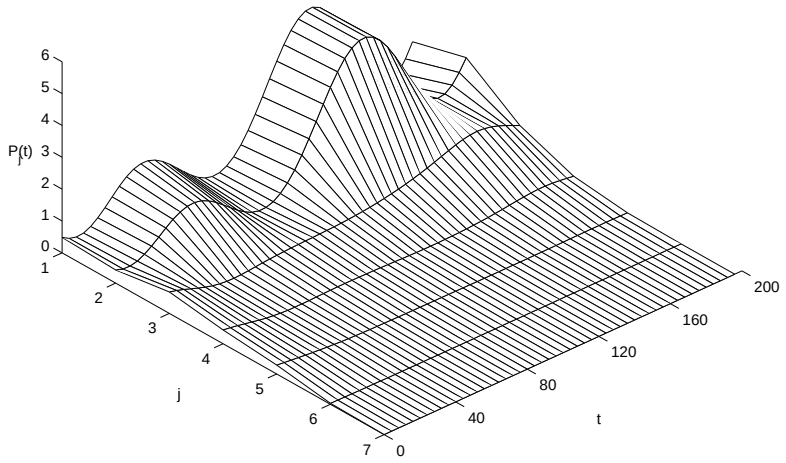

Figure 5.5: The power spectrum $P_j(t)$ with time t is shown for wavelet scales j computed for the spatiotemporal data shown in Figure 4.2.

properties at each wavelet scale j. The power spectrum $P_j(t)$ computed for the spatiotemporal data over snapshots M for the wavelet scales j is shown in Figure 5.5 and indicate that most of the power is present in lower scales. We choose $J = 3$, implying that $K = 8$ is assured of capturing all the dynamical features in the spatiotemporal dynamics. Thus, using the series expansion Eq. (5.24) in terms of wavelet basis functions the Galerkin equation again assumes the general form

$$\dot{a}_i(t) = \int F(\sum_{k=1}^{N} a_k(t)\Psi_k(\mathbf{x}), \mu)\Psi_i(\mathbf{x})d\mathbf{x}, \qquad i = 1, \cdots, N. \tag{5.26}$$

given in Eq. (5.8) using empirical basis functions.

For solving the reaction-diffusion equations Eq.(4.16) we require the evaluation of the derivative of the basis functions Ψ in the spatial domain. Estimation of numerical derivatives can be computationally exhaustive and prone to errors. Wavelet basis functions, however, provides significant advantages in this respect because it becomes possible to approximate the derivative of the spatial terms incorporating the wavelet

transform coefficients by using a parallel set of coefficients termed as connection coefficients [Qia93, Lat96] which may be readily evaluated as follows. A connection coefficient is an integral of products of wavelet basis functions and their derivatives and translates. Let wavelet transform of any function $f(x)$ be

$$f(x) = \sum_l c_l \Psi_l(x) \tag{5.27}$$

and we assume the Galerkin approximation of a derivative of $f(x)$ as,

$$f^d(x) = \sum_l c_l \Psi_l^d(x) \tag{5.28}$$

Now we approximate $\Psi_l^d(x)$ in terms of $\Psi_l(x)$ by forming,

$$\Psi_l^d(x) = \sum_m \lambda_m \Psi_m^d(x) \tag{5.29}$$

where

$$\lambda_m = \int_{-\infty}^{\infty} \Psi_l^d(x) \Psi_m(x) dx \tag{5.30}$$

Thus the coefficient λ_m can be called a 2-term connection coefficient because it connects up a wavelet basis with its required higher order derivative. The connection coefficients may be written in a general form for applications as

$$\Lambda_{l_1,l_2}^{d_1,d_2} = \int_{\infty}^{\infty} \Psi_{l_1}^{d_1} \Psi_{l_2}^{d_2} dx. \tag{5.31}$$

Thus for the present problem Eq. (5.23) the diffusion term in the Galerkin equations can now be written in terms of 2-term connection coefficients as

$$\int D_u \nabla^2 \sum_{\alpha=0}^{K-1} a_\alpha \Psi_\alpha \Psi_i dx = D_u \sum_{\alpha=0}^{K-1} a_\alpha \Lambda_{\alpha,i}^{2,0} \tag{5.32}$$

The connection coefficient values for Daubechies-4 wavelet function for various resolutions can be readily used in evaluating the above diffusion term without resorting

to numerical differentiation and appropriately substituted while solving the Galerkin equations. The above procedure due to its analytical nature reduces the computer time involved by a fair measure.

For our purpose the reduced model description suitably formulated in terms of wavelet basis functions has been used to estimate all the parameters of the system and at the same time recover the dynamics of the unmonitored variable $v_1(t,x)$ of the process. To do so we additionally introduce notions of synchronization principles for chaotic processes while carrying out the parameter estimation. Chaotic processes under identifiable conditions exhibit interesting properties which permit synchronization of its dynamics with a second unit called the *response system*. Without any ambiguity the response system in our case is chosen to be the mathematical model used for parameter estimation and is henceforth referred to as such. The response system (Eq.(5.26)) is therefore *driven* by monitored data and we study conditions leading to the response system dynamics synchronizing with the process data.

Let, the monitored data be $v_2(t,x)$ which can be expressed in terms of wavelet basis functions as

$$v_2(t,x) = \sum_{\alpha=0}^{K-1} b'_\alpha(t)\Psi_\alpha(x) \tag{5.33}$$

where the series is suitably truncated at $K = 2^J = 8$ which is sufficient for capturing the complexity in the data as discussed above in Figure 4.2 The time dependent coefficients $b'_\alpha(t)$ for wavelet scale $\alpha = 0, \cdots, K-1$ can now be considered as the driving data to drive the response system written in terms of wavelet basis functions $\Psi_\alpha(x)$ as

$$\begin{aligned}
\dot{a}_i &= \int [D_u \nabla^2 \sum_{\alpha=0}^{K-1} a_\alpha \Psi_\alpha - \sum_{\alpha=0}^{K-1} a_\alpha \Psi_\alpha (\sum_{\alpha=0}^{K-1} b'_\alpha \Psi_\alpha)^2 + f(1 - \sum_{\alpha=1}^{K-1} a_\alpha \Psi_\alpha)]\Psi_i dx \\
\dot{b}_i &= \int [D_v \nabla^2 \sum_{\alpha=0}^{K-1} b'_\alpha \Psi_\alpha + \sum_{\alpha=0}^{K-1} a_\alpha \Psi_\alpha (\sum_{\alpha=0}^{K-1} b'_\alpha \Psi_\alpha)^2 - (f+k) \sum_{\alpha=0}^{K-1} b'_\alpha \Psi_\alpha]\Psi_i dx
\end{aligned} \tag{5.34}$$

We intend to synchronize by driving the response system, with unknown parameters, reformulated as a set of wavelet Galerkin equations Eq.(5.34) with $v_2(t,x)$ as a monitored variable transformed in the form of time dependent coefficients and calculated by $b'_\alpha(t) = \int v_2(t,x)\Psi_\alpha(x)dx$. Let, $b'_\alpha(t)$ be the driving variable and the respective error in the driving and response system variables be

$$e_\alpha^{(1)}(t) = a'_\alpha(t) - a_\alpha(t) \tag{5.35}$$

$$e_\alpha^{(2)}(t) = b'_\alpha(t) - b_\alpha(t). \tag{5.36}$$

We now confirm that synchronization of the drive and the response system dynamics is indeed possible for this system for the above conditions by Lyapunov stability analysis. Any dynamical system is defined to be stable by Lyapunov stability analysis if any continuously positive definite function, L, called the Lyapunov functional can be defined along the trajectory such that its time derivative, $\dot{L} \leq 0$, is guaranteed as $t \to \infty$ [Ton90]. We now construct a suitable Lyapunov functional in terms of the error variables as

$$L = \sum_i \sum_{\alpha=0}^{K-1} [e_\alpha^{(i)}(t)]^2 \tag{5.37}$$

which is guaranteed to be positive definite and whose derivative is then given by

$$\frac{1}{2}\dot{L} = \sum_i \sum_{\alpha=0}^{K-1} e_\alpha^{(i)}(t)\dot{e}_\alpha^{(i)}(t). \tag{5.38}$$

Substituting Eq. 5.36 in Eq. 5.34 and using the orthogonal properties of the wavelet basis functions we can obtain the derivative $b_i(t)$ of temporal coefficients in the time and the stability condition then reduces to

$$\dot{L} = D_u \sum_{\alpha=0}^{K-1} [e_\alpha^{(1)}(t)]^2 \Lambda_{\alpha,1}^{2,0} - \sum_{\alpha=0}^{K-1} \text{const}[e_\alpha^{(1)}(t)]^2. \tag{5.39}$$

Thus synchronization is possible on driving the response system by $b'_\alpha(t)$ as long as $D_u \sum_{\alpha=0}^{K-1} [e_\alpha^{(1)}(t)]^2 \Lambda_{\alpha,1}^{2,0}$ is less than $\sum_{\alpha=0}^{K-1} \text{const}[e_\alpha^{(1)}(t)]^2$. For the present simulation

Table 5.6: Convergence and error in parameter estimation for Gray-Scott model for different noise intensity Σ.

Σ	$D_u(\times 10^{-5})$	$D_v(\times 10^{-5})$	f	k
0.000	1.9864 ± 0.0020	1.0103 ± 0.0010	0.0292 ± 0.0001	0.0554 ± 0.0001
0.005	2.0371 ± 0.0076	0.9945 ± 0.0095	0.0294 ± 0.0008	0.0576 ± 0.0007
0.010	1.9682 ± 0.0196	0.9436 ± 0.0143	0.0301 ± 0.0010	0.0583 ± 0.0012
0.015	2.0611 ± 0.0282	0.9527 ± 0.0188	0.0336 ± 0.0085	0.0492 ± 0.0096
0.020	1.8750 ± 0.0624	0.9393 ± 0.0664	0.0342 ± 0.0173	0.0424 ± 0.0182

with the choice of parameters it is ensured that $\dot{L} < 0$ *i.e.* synchronization is with respect to the monitored spatiotemporal data $v_2(t, x)$.

The Wavelet Galerkin Multiple Shooting (WGMS) methodology with synchronization can be schematically represented as:

$$\underbrace{\begin{array}{ccc} & (A) & \\ & \text{Driving data } v'(t,\mathbf{x}) & \\ (B)\ \text{Response system} & & (C)\ \text{Wavelet functions} \\ \frac{\partial v}{\partial t} = F(v,\mu) & & \Psi_k(\mathbf{x}) \end{array}}_{\textit{Step}.2\ \text{Galerkin projection :}\ \dot{a}_i(t) = \int F(\sum_{k=1}^{N} a_k(t)\Psi_k(\mathbf{x}),\mu)\Psi_i(\mathbf{x})d\mathbf{x} \longrightarrow} \quad \left.\begin{array}{c} \textit{Step}.1\ \text{Observations :} \\ b'_k(t) = (v'(t,\mathbf{x}), \Psi_k(\mathbf{x})) \\ \downarrow \\ \textit{Step}.3\ \text{Multiple Shooting} \\ \text{alongwith} \\ \text{Synchronization} \\ \downarrow \\ \text{Estimated parameters } \mu \end{array}\right\}$$

The response system is integrated and M snapshots are obtained in time where $b_\alpha(M)$ is driven with known $b'_\alpha(M)$ via Eq. (5.34). The results of synchronization is shown in Figure 5.6 (a) for the time dependent component corresponding to $a_1(t)$.

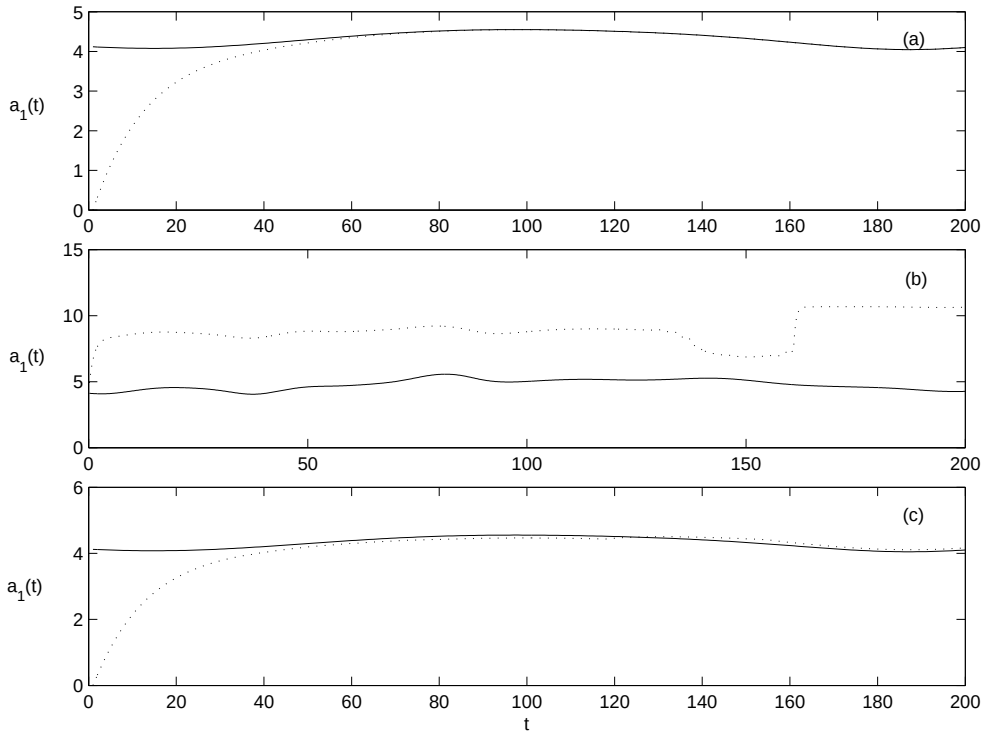

Figure 5.6: The results of synchronization with wavelet basis functions. (a) known parameters (b) inaccurate parameters (c) inaccurate parameters but are simultaneously estimated with synchronization.

The incorporation of the parameter estimation procedure is mandatory when the response system has initially wrong set of parameter values. The Figure 5.6(b) clearly shows that synchronization is not achieved if the parameters are inaccurately set when compared to the true values of $D_u = 0.00002$, $D_v = 0.00001$, $f = 0.029$ and $k = 0.0535$. On the other hand if we incorporate the multiple shooting parameter estimation procedure by minimizing the least square functional the inaccurate parameters are auto-tuned to the their correct values as shown in Table 5.6. Synchronization with parameter estimation was also possible using noisy spatiotemporal data. This is because the optimization procedure using the least square functional Eq. 5.17 minimizes the errors arising due to noise present in the data simultaneously.

5.4 Conclusion

The results obtained using the KLGMS show that this basic framework has the necessary robustness for parameter estimation for spatiotemporal dynamics. We have exemplified the method for simultaneously estimating all parameters of a CML and reaction diffusion systems. Importantly, for complex dynamics and noise in the data we show that accurate parameter estimates are possible even from small data sets obtained from subsystems of optimal size. We show ways of adapting the methodology for inhomogeneous situations when parameters vary in space and time and by using transient data soon after perturbing the system dynamics. The algorithm has been extended to situations when only scalar data is available and by using wavelet basis functions in the Galerkin multiple shooting framework (WGMS). Here, principles of synchronization and the capability to recover the dynamics of the unmonitored variable with simultaneous estimation of the parameters has been shown to be possible.

Chapter 6

Conclusion and Future Scope

Studies in chaos theory have enhanced the scope of studying irregular time series data obtained from experiments. The studies in this area provide deep connections between empirical observations and theory as typically shown in Chapter 2 where using experimental time series observations of stress measurements in an aqueous polymer solution (N-isopropyl acrylamide) and a biopolymer (Carrageenan) showed irregularity for identifiable steady shear regions. A way to efficiently preprocess the data by noise reduction for enhancing systemic features using wavelet transform was also developed. The noise reduction was carried out efficiently by differentiating the stress measurement data and subjecting this differentiated data to wavelet transform. The process of carrying out the wavelet transform shifts the power due to noise to the lower wavelet scales and these could be automatically identified from the power spectrum of the wavelet coefficients at the different scales. Noise free and feature enhanced time series data could be obtained by setting the wavelet coefficients in these lower wavelet scales to zero before inverse wavelet transform and integration. The noise free data was subsequently used for characterization of the dynamical properties of the systems under consideration. Interesting theoretical conclusions about the nature of the experimental systems being studied have thus been presented. The analysis of the denoised rheological data using phase-space reconstruction techniques, in fact, revealed

the presence of low-dimensional attractors as can be obtained from studies with two model reacting systems, namely, endo-exothermic and autocatalytic reactions taking place in a CSTR and exhibiting chaotic dynamics. The presence of chaotic dynamics was established by studying invariant properties of the observed dynamics with respect to the mutual information, correlation dimension, Lyapunov exponents and entropy. Lyapunov dimension for these low dimensional systems turned out to be less than 3 which suggested the presence of a strongly contracting flow and that valuable information about the chaotic dynamics could be gained by additionally carrying out a topological analysis of the observed attractors. The topological analysis required the identification of periodic orbits from the first return map on the Poincarè section and the method to achieve this has been described. A topological study of the extracted periodic orbits showed global characterization and classification of dynamics was indeed possible using topological invariants, namely, linking numbers and relative rotation rates. The topological entropy was also calculated and it converged to a value comparable to entropy estimated from Lyapunov spectrum showing the robustness in the methodologies used for topological characterization. Analysis of these invariants also yielded the template and the Markov transition matrix that contained in them the basic nature of the flow. It was observed that the template could be deduced by topological characterization of only the period-1, 2 and 3 orbits. Interestingly, results of analysis showed that both the experimental and the model system considered followed the Horseshoe mechanism in terms of stretching and folding associated with chaotic dynamics. The results show how properties of systems in interdisciplinary areas are related due to existence of universal properties and that systems of interest in many physical and chemical systems exhibiting chaotic dynamics may be classified and studied on common grounds.

Reaction-diffusion-convection systems are particularly interesting and may be modeled with optimum dimensionality by Galerkin projection of the original high-

dimensional model as shown in Section 5.1. It is interesting to note that reduced models of spatiotemporal systems exhibit features like synchronization properties of low-dimensional chaotic systems as seen in Section 5.3. Characterization and quantification of spatiotemporal chaos can be further pursued by analyzing these finite-dimensional systems. However, topological analysis discussed in Section 2.3.2 holds good for dynamical systems for the Lyapunov dimension $d_L < 3$. Locating periodic orbits and their surrogates for high-dimensional system is also difficult because the unstable periodic orbits fall apart when embedding dimension $m > 3$. This suggest topological invariants need new formalisms like consideration of subsystems for high-dimensionality. Extending the topological analysis to high-dimensional system will throw some light in understanding transition routes to spatiotemporal chaos, pattern formation, intermittency, turbulence, etc. It is hoped that with the methodologies presented here, these topics may be addressed with success in the near future.

The invariant measures analyzed above depend upon the parameter values of the system. A knowledge of these parameter values is essential for studying system properties and the behavior of the models with respect to stability, bifurcation, control, etc. Thus, it is important to estimate the values of unknown parameters of the system by auto tuning an appropriate nonlinear model to fit the observed chaotic data. Chapter 3 considered the simple situation of a well-mixed system whose dynamics is described by a set of coupled nonlinear ordinary differential equations. Developing boundary value multiple shooting approach to parameter estimation, was chosen so that its logical extension for applications in high-dimensional systems could be carried out. It may be emphasized that for chaotic dynamics, estimating parameters and system states is not a trivial task even for simple model descriptions. The results presented focus on this practically important aspect of modeling and bring out the advantages gained by applying the boundary value multiple shooting approach to stringent nonlinear situations when the system exhibits low-dimensional chaotic

dynamics. The aim here, therefore, was to simultaneously estimate all values of the unknown parameters and non-monitored system states from available transient data. Further exemplification of the analysis was carried out by adapting the method to tune empirical mathematical models using scalar time series with noisy data. The results of estimating all intrinsic kinetic parameters and operational system parameters even with small data sets show the robustness and usefulness of the methodology.

Chapters 4 and 5 study the class of complex systems, that show not only temporal variability but also spatial. The variability in these spatially extended systems are brought about by reaction-diffusion-convection mechanisms operating in the process. Unlike temporal systems that could be modeled as ordinary differential equations as in Chapters 2 and 3, reaction-diffusion-convection systems need to be modeled by partial differential equations due to the introduction of the spatial domain. Spatiotemporal systems can be studied using CML models which show the necessary complex spatiotemporal features like chaos, traveling wave, etc. They are popularly used in studies because the ease in computation affords methodologies and analysis of complex system dynamics to be well developed before applying them to continuous time domain systems which are less tractable. All the same, studies with CML's is not easy due to the high-dimensionality introduced by the spatial domain and the nonlinear mechanisms operating. In this scenario, it was found advantageous to identify the coherent spatial structures present in the space-time data so that a separable form of the CML model amenable to dimensionality reduction (*i.e.* model reduction) could be obtained. The identification of coherent structures could be carried out by calculating empirical eigenfunctions from the correlation matrix obtained from the space-time data and using Karhunen-Loève (KL) decomposition. The results obtained for the representative systems, namely, CML, an autocatalytic and an activator-inhibitor systems for different types of complex dynamics showed when and to what extent model reduction is possible. These results are discussed in detail in

Chapter 4. Importantly, we also studied situations when incomplete spatiotemporal information is only available due to partial monitoring. Here, the aim was to reconstruct masked portions of the data while carrying out the projection. The method when applied to situations where snapshots in time are marred with noise successfully yielded unbiased estimates of the missing information using the evaluated empirical eigenfunctions.

Importantly, it was possible to design ways of applying the low-dimensional methodologies discussed in Chapters 2 and 3 for the high-dimensional spatiotemporal systems that have been considered. This was made possible by model projection techniques using Galerkin's method on the separable model obtained by KL decomposition. The profitable use of this approach is seen when the methodology of multiple shooting studied in Chapter 3 can be reformulated to estimate all parameters of the high dimensional system using KL reduced model descriptions with Galerkin projection. In Chapter 5 we have developed the Karhunen-Loève and Galerkin multiple shooting (KLGMS) approach and have exemplified it for both coupled map lattice (CML) systems and the two reacting systems. The resulting advantages in estimating parameters from small amounts of data from subsystems (*i.e.* local regions/channels), availability of only scalar and noisy time series data, effects of space time parameter variations and in the presence of multiple time scales was significantly demonstrated. Apart from empirical eigenfunctions, the use of wavelet basis functions as a complementary alternative was studied because the latter are known to have excellent space-time localization properties with significant advantages in data handling capability. The study carried out here showed that wavelet basis functions can be used to estimate accurately in an analytical fashion the diffusion term (with the higher order derivative) using connection coefficients evaluated from wavelet coefficients by suitably combining with the Galerkin multiple shooting formalism. Furthermore, the use of wavelet basis functions affords studying long time evolution of spatiotemporal

dynamics, its synchronization properties and multi-time scale features in a fashion much easier than empirical basis functions. The resulting advantages in estimating system parameters when only some variables are monitored using the devised multiple shooting algorithm for spatiotemporal systems has been clearly brought out. Online estimates of parameters from processes is an important goal in realizing practical applications, that would facilitate accurate model building from data, along with development of control and optimization strategies for highly complex dynamics.

Bibliography

[Aba93] Abarbanel, H. D. I., Brown, R., Sidorowich, J. J., and Tsimiring, L. Sh., "The analysis of observed chaotic data in physical systems", *Rev. Mod. Phys.* **65**, 1331 [1993].

[Are91] Arecchi, F. T., "Space-time complexity in nonlinear optics", *Physica D* **51**, 450 [1991].

[Arg94] Argyris, J., Faust, G. and Haase, M., *An exploration of chaos*, North-Holland, Amsterdam [1994].

[Baa92] Baake, E., Baake, M., Bock, H. G. and Briggs, K. M., "Fitting ordinary differential equations to chaotic data", *Phys. Rev. A* **45**(8), 5524 [1992].

[Bal01] Balkovsky, E., Fouxon, A. and Lebedev, V., "Turbulence in polymer solutions", *Phys. Rev. E* **64**, 056301 [2001].

[Ban93] Bandyopadhay, J. K., Ravi Kumar, V. and Kulkarni, B. D., "On altering the conversion selectivity behaviour for a CSTR exhibiting chaotic dynamics", *Ind. Engg. Chem. Res.* **32**, 2953 [1993].

[Bar94] Bär, M., Gottschalk, N., Eiswirth, M. and Ertl, G., "Spiral waves in a surface reaction: Model calculations", *J. Chem. Phys.* **100**(2), 1202 [1994].

[Bar99] Bär, M., Hegger, R. and Kantz, H., "Fitting partial differential equations to space-time dynamics", *Phys. Rev. E* **59**, 337 [1999].

[Bau91] Bauer, M. and Martienssen, W., "Lyapunov exponents and dimensions of chaotic neural networks", *J. Phys. A.* **24**, 4557 [1991].

[Bel58] Belousov, B. P., "A periodic reaction and its mechanism", *Sb. Ref. Radiat. Med.*, Medzig, Moscow [1958].

[Bha98] Bhaumik, A, Mukerjee, P. and Kumar, R., "Triphase catalysis over Titanium Silicate molecular sieves under solvent free conditions 1. direct hydroxylation of Benzene", *J. Catal.* **178**, 101 [1998].

[Bir83] Birman, J. and Williams, R., "Knotted periodic orbits in dynamical systems I: Lorenz's equations", *Topology* **22**, 47 [1983].

[Boc83] Bock, H. G., "Recent advances in parameter identification techniques for ODE", *Numerical treatment of inverse problems in differential and integral equations*, Birkhäuser, Boston [1983].

[Boc84] Bock, H. G. and Plitt, K. J., *A multiple shooting algorithm for direct solution of optimal control problems*, International federation of automatic control, 9^{th} World congress, Budapest [1984].

[Boc84a] Bocko, M. F., Douglas, D. H. and Fruchty, H. H., "Bounded regions of chaotic behavior in the control parameter space of a driven nonlinear resonator", *Phys. Lett. A* **104**, 388 [1984].

[Bou97] Boulant, G., Lefranc, M., Bielawski, S. and Derozier, D., "Horseshoe templates with global torsion in a driven laser", *Phys. Rev. E* **55**, 5082 [1997].

[Car99] Carreto-González, R., Ørstavik, S., Huke, J., Broomhead, D. S. and Stark, J., "Scaling and interleaving of sub-system Lyapunov exponents for spatio-temporal systems", *Chaos* **9**, 466 [1999]

[Cha95] Chaikin, P. M. and Lubensky, T. C., *Principles of condensed matter physics*, Cambridge University Press [1995].

[Cha90] Chan, C. K., and Lin, L., "Effects of shear on the phase transition of binary mixtures", *Europhys. Lett.* **11**, 13 [1990].

[Chen93] Chen, C. J., *Introduction to scanning tunneling microscopy*, Oxford University Press, New York [1993].

[Chr64] Christensen, O., "Carrageenan, a useful food additive", *Food Manuf.* **39**, 49 [1964].

[Coh95] Cohen, L., *Time frequency analysis*, Cambridge University Press [1995].

[Con87] Constantinides, A., *Applied numerical methods with personal computers*, McGraw-Hill Book Company [1987].

[Cro93] Cross, M. C. and Hohenberg, P. C., "Pattern formation outside of equilibrium", *Rev. Mod. Phys.* **65**, 851 [1993].

[Cru87] Crutchfield, J. P. and Kaneko, K., *Directions in chaos*, World Scientific, Singapore [1987].

[Dau92] Daubechies, I., *Ten lectures on wavelets*, CBMS-NSF regional conference series in applied mathematics, Philadelphia [1992].

[Dip81] DiPrima, R. C. and Swinney, H. L., "Instabilities and transition in flow between concentric rotating cylinders", in *Hydrodynamic instabilities and transition to turbulence* edited by Swinney, H. L. and Gollub, J. P., Springer-Verlag, Berlin [1981].

[Eli62] Eliassaf, J. and Silberberg, A., "The gelation of aqueous solutions of polymethacrylic acid", *Polymer* **3**, 555 [1962].

[Eli78] Eliassaf, J., "Aqueous solutions of poly (*N*-isopropylacrylamide)", *J. Appl. Polym. Sci.* **22**, 873 [1978].

[Far82] Farmer, J. D., "Information dimension and the probabilistic nature of chaos", *Zietschrift fuer Naturforsch* **37**, 1304 [1982].

[Far83] Farmer, J. D., Ott, E. and Yorke, J. A., "The dimension of chaotic attractors", *Physica D* **7**, 153 [1983].

[Fie85] Field, R. J. and Burger, M., *Oscillations and traveling waves in chemical systems*, John Wiley, New York [1985].

[Fra86] Fraser, A. M., and Swinney, H. L., "Independent coordinates for strange attractors from mutual information", *Phys. Rev. A* **33**, 1134 [1986].

[Fuj87] Fujishige, S., "Intrinsic viscosity-molecular weight relationships for Poly (*N*-isopropylacrylamide) solutions", *Polym. J.* **19**, 297 [1987].

[Gal95] Galaev, I. Yu., "Smart polymers in biotechnology and medicine", *Russ. Chem. Rev.* **64**(5), 471 [1995].

[Gea71] Gear, C.W., *Numerical initial-value problems in ordinary differential equations*, Prentice-Hall, Englewood Cliffs, New Jersey [1971].

[Gen79] DeGennes, P. G., *Scaling concepts in polymer physics*, Cornell, Ithaca, New York [1979].

[Gil98] Gilmore, R., "Topological analysis of chaotic dynamical systems", *Rev. Mod. Phys.* **70**, 1455 [1998].

[Gra99] Graham, M.D., "The sharkskin instability of polymer melt flows", *Chaos* **9**, 154 [1999].

[Gra83a] Grassberger, P. and Procaccia, I., "Measuring the strangeness of strange attractors", *Physica D* **9**, 189 [1983].

[Gra83b] Grassberger, P. and Procaccia, I., "Characterization of strange attractors", *Phys. Rev. Lett.* **50**, 346 [1983].

[Gra84] Grassberger, P., and Procaccia, I., "Dimensions and entropies of strange attractors from a fluctuating dynamics approach", *Physica D* **13**, 13 [1984].

[Gra90] Gray, P. and Scott, S. K., *Chemical oscillations and instabilities*, Oxford University Press [1990].

[Gro00] Grossmann, S., "The onset of shear flow turbulence", *Rev. Mod. Phys.* **72**, 603 [2000].

[Guc83] Guckenheimer, J. and Holmes, P., *Nonlinear oscillations, dynamical systems, and bifurcations of vector fields*, Springer-Verlag, New York [1983].

[Hil99] Hilgers, A. and Beck, C., "Hierarchical coupled map lattices as cascade models for hydrodynamical turbulence", *Europhys. Lett.* **45**, 552 [1999].

[Hof95] Hoffman, A. S., "Intelligent polymers in medicine and biotechnology", *Macromol. Symp.* **98**, 645 [1995].

[Hol96] Holmes, P., Lumley. J. L. and Berkooz, G., *Turbulence, coherent structures, dynamical systems and symmetry*, Cambridge University Press, Cambridge [1996].

[Hol95] Holschneider, M., *Wavelets: An analysis tool*, Clarendon Press, Oxford [1995].

[Hub89] Hübner, U., Abraham, N. B. and Weiss, C. O., "Dimensions and entropies of chaotic intensity pulsations in a single mode far infra red NH_3 laser", *Phys. Rev. A* **40**, 6354 [1989].

[Jaz70] Jazwinski, A. H., *Stochastic processes and filtering theory*, Academic Press, New York [1970].

[Kah81] Kahlert, C., Rôssler, O. E. and Varma, A., "Chaos in a CSTR with two consecutive first order reactions", *Springer Ser. Chem. Phys.* **18**, 355 [1981].

[Kap79] Kaplan, J. L. and Yorke, J. A., in Walter, H. O. and Peitgen, H. O. (Eds.), "Function differential equations and approximations of fixed points", **730** 204, Berlin: Springer [1979].

[Kap95] Kapral, R. and Showalter, K., Eds. *Chemical waves and patterns*, Kluwer, Dordrecht [1995].

[Kan89] Kaneko, K., "Pattern dynamics in spatiotemporal chaos", *Physica D* **34**, 1 [1989].

[Kan93] Kaneko, K., ed., *Theory and applications of coupled map lattices*, John Wiley & Sons Ltd., West Sussex [1993].

[Kan97] Kantz, H. and Schreiber, T., *Nonlinear time series analysis*, Cambridge University Press, Cambridge [1997].

[Kar46] Karhunen, K., "Zur spektraltheorie stochastischer prozesse", *Ann. Acad. Sci. Fennicae* Ser. A, **1**, 34 [1946].

[Kau93] Kauffman, S. A., *The origins of order*, Oxford University Press, New York [1993].

[Kau91] Kaufmann, L. H., *Knots and physics*, World Scientific, Singapore [1991].

[Koc81] Koch, A. J. and Meinhardt, H., "Biological pattern formation: from basic mechanisms to complex structures", *Rev. Mod. Phys.* **66**(4), 1481 [1981].

[Kri84] Krinsky, V. I., Ed. *Self-organization autowaves and structures far from equilibrium*, Springer-Verlag, Berlin [1984].

[Kur84] Kuramoto, Y., *Chemical oscillations, waves and turbulence*, Springer, Berlin [1984].

[Kur84a] Kuramoto, Y., "Phase dynamics of weakly unstable periodic structures", *Prog. Theor. Phys. Suppl.*, **71**, 1182 [1984].

[Lai65] Laidler, K. J. *Chemical kinetics*, Tata McGraw-Hill Publishing Co. Ltd., New Delhi [1965].

[Lar92] Larson, R. G., "Instabilities in viscoelastic fluids", *Rheol. Acta* **31**, 213 [1992].

[Lat89] Lathrop, D. P. and Kostelich, E. J., "Characterization of an experimental strange attractor by periodic orbits", *Phys. Rev. A* **40**, 4028 [1989].

[Lat96] Latto, A., Resinikoff, H. L. and Tenenbaum, E., "The evaluation of connection coeffcients of compactly supported wavelets", http://www2.appmath.com:8080/site/con3_5.html [1996].

[Lee94] Lee, K, J., McCormick, W. D., Pearson, J. E. and Swinney, H. L., "Experimental observation of self-replicating spots in a reaction-diffusion system", *Nature* **369**, 215 [1994].

[Let98] Letellier, C., Maquet, J., Labro, H., Le Sceller, L., Gouesbet, G., Argoul, F. and Arneodo, A., "Analyzing chaotic behavior in a Belousov-Zhabotinsky

reaction by using a global vector field reconstruction", *J. Phys. Chem. A* **102**, 10256 [1998].

[Loe55] Loéve, M. M., *Probability theory*, Van Nostrand, New York [1955].

[Lop00] López, C., Álvarez, A. and Hernández-García, E., "Forecasting confined spatiotemporal chaos with genetic algorithms", *Phys. Rev. Lett.* **85**, 2300 [2000].

[Lum71] Lumley, J. L., *Stochastic tools in turbulence*, Academic Press, New York [1971].

[Maz96] Mazin, W., Rasmussen, K. E., Mosekilde, E., Borckmans, P. and Dewel, G., "Pattern formation in the bistable Gray-Scott model ", *Maths. Comp. Simul.* **40**, 371 [1996].

[Mcs99] McSharry, P. E. and Smith, L. A., "Better nonlinear models from noisy data: attractors with maximum likelihood", *Phys. Rev. Lett.* **83**, 4285 [1999].

[Mex00] Meixner, M., Zoldi, S. M., Bose, S. and Schöll, E., "Karhunen-Loève local characterization of spatio-temporal chaos in a reaction-diffusion system", *Phys. Rev. E.* **61**, 1382 [2000].

[Min90] Mindlin, G. B., Hou, X. J., Solari, H. G., Gilmore, R. and Tufillaro, N. B., "Classification of strange attractors by integers", *Phys. Rev. Lett.* **64**(20), 2350 [1990].

[Mun00] Münstedt, H., Schimdt, M. and Wassner, E., "Stick and slip phenomenon during extrusion of polyethylene melts as invesigated by laser-Doppler velocimetry", *J. Rheol.* **44**(2), 413 [2000].

[Naf84] Nafaile, C. R., Metzner, A. B. and Wissbrun, K. F., "Analysis of stress induced phase speration in polymer solutions", *Macromolecules* **17**, 1187 [1984].

[New88] Newell, A. C., "The dynamics of patterns: a survey", in *Propagation in systems far from equilibrium*, Edited by Wesfreid, J. E., Brand, H. R., Manneville, P., Albinet, G. and Boccara, N., Springer-Verlag, Berlin [1988].

[Ott93] Ott, E., *Chaos in dynamical systems*, Cambridge University Press [1993].

[Par98] Parekh, N., RaviKumar, V. and Kulkarni, B. D., "Synchronization and control of spatiotemporal chaos using time series data from local regions", *Chaos* **8**, 300 [1998].

[Par00] Parlitz, V. and Merkwirth, C., "Prediction of spatiotemporal time series based on reconstructed local states", *Phys. Rev. Lett.* **84**, 1890 [2000].

[Per00] Percival, D. B. and Walden, A. T., *Wavelet methods for time series analysis*, Cambridge University Press [2000].

[Pes00] Peskov, N. V., "Spatiotemporal patterns in a model of heterogeneous reaction in a porous catalyst particle", *Physica D* **137**, 316 [2000].

[Pow78] Powell, M. J. D., Lecture notes in maths, **630**, Springer, Berlin [1978].

[Pre92] Press, W. H., Teukolsky, S. A., Vetterling, W. T, and Flannery, B. P., *Numerical recipes in fortran*, Cambridge University Press [1992].

[Qia93] Qian, S. and Weiss, J., "Wavelets and numerical solution of partial differential equations", *J. Comp. Phys.* **106**(1), 155 [1993].

[Reh88] Rehage, H. and Hoffmann, H., "Rheological properties of viscoelastic surfactants", *J. Phys. Chem.*, **92** 4712 [1988].

[Roy99] Roy, M., Ravi Kumar, V., Kulkarni, B. D., Sanderson, J., Rhodes, M., and Vander Stappen, M., "Simple denoising algorithm using wavelet transform", *AIChE Journal* **45**, 2461 [1999].

[Saa92] van Saarloos, W. and Hohenberg, P. C., "Fronts, pulses, sources and sinks in generalized Ginzburg-Landau equations", *Phys. Rev. Lett.* **56**, 303 [1992].

[Sch86] Schittkowski, K., "NLPQL: A FORTRAN subroutine solving constrained nonlinear programming problems ", *Annals of Operation Res.* **5**, 485 [1986].

[Sco91] Scott, S. K., *Chemical chaos*, Clarendon Press, Oxford [1991].

[Sel68] Selkov, E. E., "Self-oscillations in glycolysis: 1. A simple kinetic model", *Eur. J. Biochem.* **4**, 79 [1968].

[Sha81] Shaw, R., "Strange attractors, chaotic behavior, and information flow", *Zietschrift fuer Naturforsch* **36**, 80 [1981].

[Shr92] Shraiman, B. I., Pumir, A., van Saarloos, W., Hohenberg, P. C., Chate, H. and Holen, M., "Spatiotemporal chaos in the one-dimensional complex Ginzburg-Landau equation", *Physica D* **57**, 325 [1992].

[Sir87] Sirovich, L., "Turbulence and dynamics of coherent structures: I,II,III", *Quart. Appl. Math.* **45**, 561 [1987].

[Sli94] Slinko, M. M. and Jaeger, N. I., "Oscillating heterogeneous catalytic systems", *Studies in surface science and catalysis* **86** Elsevier, Amsterdam [1994].

[Sli01] Slinko, M. M., Ukharskii, A. A., Peskov, N. N. and Jaeger, N. I., "Chaos and synchronization in heterogeneous catalytic systems: CO oxidation over Pd zeolite catalysts", *Catalysis Today* **70**, 341 [2001].

[Sma91] Smale, S., "Dynamics retrospective: great problems, attempts that failed", *Physica D* **51**, 267 [1991].

[Sno93] Snowden, M. J., Thomas, D. and Vincent, B., "Use of colloidal microgels for the absorption of heavy metal and other ions form aqueous solution", *Analyst* **118**, 1367 [1993].

[Sno94] Snowden, M. J., Marston, N. J. and Vincent, B., "The effect of surface modification on the stability characteristics of poly (*N*-isopropylacrylamide) lattices under Brownian motion and flow conditions", *Coll. Polym. Sci.* **272**, 1273 [1994].

[Sno95] Snowden, M. J. and Chowdhary, B. Z., "Small sponges with big appetites", *Chem. Brit.* **31**, 943 [1995].

[Som91] Sompolinsky, H., Golomb, D. and Kleinfeld, D., " Cooperative dynamics in visual processing", *Phys. Rev. A* **43**, 6990 [1991].

[Sol88] Solari, H. G. and Gilmore, R., "Relative rotation rates for driven dynamical systems", *Phys. Rev. A* **38**(3), 3096 [1988].

[Sto85] Stoer, J., "Principles of sequential quadratic programming methods for solving nonlinear problems", *Computational mathematical programming*, ed. Schittkowski, K. NATO ASI Ser. **15**, Springer-Verlag [1985].

[Str95] Strogatz, S. H., *Nonlinear dynamics and chaos*, Addison-Wesley Publishing Company, Reading [1995].

[Str88] Strogatz, S. H. and Mirollo, R. E., "Phase locking and critical phenomena in lattices of coupled nonlinear oscillators with random intrinsic frequencies", *Physica D* **31**, 143 [1988].

[Tam92] Tam, K. C., Wu, X. Y. and Pelton R. H., "Viscometry - a useful tool for studying conformational changes of poly (*N*-isopropylacrylamide) in solutions", *Polymer* **33**, 436 [1992].

[Tak81] Takens, F., "Detecting strange attractors in turbulence", in *Dynamical systems and turbulence*, Rand, D. A. and Young, L. S. eds., Lecture notes in mathematics **898**, 366, Springer, Berlin [1981].

[Tem88] Teman, R., *Infinite-dimensional dynamical systems in mechanics and physics*, Springer, New York [1988].

[The86] Theiler, J., "Spurious dimension from correlation algorithms applied to limited time series data", *Phys. Rev. A* **34**, 2427 [1986].

[Tim98] Timmer, J., "Modeling noisy time series: Physiological tremor", *Int. J. Bif. Chaos.* **8**, 1505 [1998].

[Tim00] Timmer, J., Rust, H., Horbelt, W. and Voss, H. V., "Parametric, nonparametric and parametric modeling of a chaotic circuit time series", *Phys. Lett. A* **274**, 123 [2000].

[Ton90] Tong, H., *Nonlinear time series: A dynamical system approach*, Clarendon Press, Oxford [1990].

[Tuf92] Tufillaro, N. B., Abbott, T. A. and Reilly, J. P., *An experimental approach to nonlinear dynamics and chaos*, Addison-Wesley, Reading [1992].

[Vos98] Voss, H., Bünner, M. J. and Abel, M., "Identification of continuous spatiotemporal systems", *Phys. Rev. E* **57**, 2820 [1998].

[Vos00] Voss, H., *Nonlinear dynamics and statistics*, Ed. A. Mees, Birkhaüser, Boston [2000].

[Wed84] Wedding, B., Gasch, A. and Jaeger, D., "Chaos observed in a Fabry-Perot interferometer with quadratic nonlinear medium", *Phys. Lett. A* **105**, 105 [1984].

[Whi73] Whistler, R. L., *ed. Industrial gums*, 2^{nd} edition, Academic Press [1973].

[Wil95] Willeboordse, F. H. and Kaneko, K., "Pattern dynamics of a coupled map lattice for open flow", *Physica D* **86**, 428 [1995].

[Wit98] Witten, T. A., "Polymer solutions: A geometric introduction", *Rev. Mod. Phys.* **70** (4), 1531 [1998].

[Wit98a] Wittenberg, R. W., *PhD Thesis* "Local dynamics and spatiotemporal chaos. The Kuramoto-Sivashinsky equation: A case study", Princeton University [1998].

[Wit99] Wittenberg, R. W. and Holmes, P., "Scale and space localisation in the Kuramoto-Sivashinsky equation", *Chaos* **9**, 452 [1999].

[Zen98] Zeng, F., Zheng, X. and Tong, Z., "Network formation in poly (*N*-isopropyl - acrylamide) / water solutions during phase separation", *Polymer* **39**(5), 1249 [1998].

[Zha87] Zhabotinskii, A. M. and Rovinsky, A. B., "Mechanism and nonlinear dynamics of an oscillating chemical reaction", *J. Stat. Phys.* **48**, 959 [1987].

[Zol97] Zoldi, S. M. and Greenside, H. S., "Karhunen-Loève decomposition of extensive chaos", *Phys. Rev. Lett.* **78**, 1687 [1997].

List of Publications

Ghosh, A., Badiger, M. V., Ravi Kumar, V. and Kulkarni, B. D., "Characterization of chaotic dynamics-I: dynamical invariants of sheared polymer solutions", *Chem. Engg. Sci.* **56**, 5635 [2001].

Deshmukh, S., Ghosh, A., Badiger, M. V., Ravi Kumar, V. and Kulkarni, B. D., "Characterization of chaotic dynamics-II: topological invariants and their equivalence for an autocatalytic model system and an experimental sheared polymer solution", *Chem. Engg. Sci.* **56**, 5643 [2001].

Ghosh, Anandamohan, Ravi Kumar, V. and Kulkarni, B. D., "Paremeter estimation in spatially extended systems: The Karhunen-Loève and Galerkin multiple shooting approach", *Phys. Rev. E* **64** 056222 [2001].

Ghosh, Anandamohan, Ravi Kumar, V. and Kulkarni, B. D., "Analysis of wavelet basis functions for characterization and inverse problems in spatially extended systems", *Phys. Lett. A* [2002] (submitted).

Halligudi, S. B., Devassay, B. M., Ghosh, A. and Ravi Kumar, V., "Kinetic study of vapor phase hydrodechlorination of halons by Pd supported catalysts", *J. of Mol. Cat. A: Chemical*, **184**, 175 [2002].

Symposium and Conferences

Dutta, B., Ghosh, A., Ravi Kumar, V. and Kulkarni, B. D., "Parametric identification of nonlinear reacting systems: Applications of multiple shooting boundary value approach", CHEMCON, *Indian Chemical Engineering Congress* REC-37 [2000].

Ghosh, A., Bharadwaj, M., Anand, G., Ravi Kumar, V. and Kulkarni, B. D., "Topological analysis of an endo-exothermic CSTR", CHEMCON, *Indian Chemical Engineering Congress* TSM-212 [2001].

Ghosh, A., Ravi Kumar, V. and Kulkarni, B. D., "Parameter estimation in pattern forming systems with multiple spatial and temporal scales", Poster presentation, STATPHYS, Kolkata [2002].